DISSERTATION

THREE-DIMENSIONAL COMPUTATIONAL MODELING OF CURVED CHANNEL FLOW

Submitted by

Kyung-Seop Sin

Department of Civil and Environmental Engineering

In partial fulfillment of the requirements

For the Degree of Doctor of Philosophy

Colorado State University

Fort Collins, Colorado

Fall 2014

Doctoral Committee:

Advisor: Subhas K. Venayagamoorthy
Co-Advisor: Christopher I. Thornton

Steven R. Abt
Pierre Y. Julien
Lakshmi P. Dasi

ABSTRACT

THREE-DIMENSIONAL COMPUTATIONAL MODELING OF CURVED CHANNEL FLOW

Investigating flow dynamics in curved channels is a challenging problem due to its complex three-dimensional flow structure. Despite the numerous investigations that have been performed on this important topic over the last several decades, there remains much to be understood. The focus of this dissertation is on flow around curved channel bends with an emphasis on the use of three-dimensional numerical simulations to provide insights on the flow dynamics in channel bends. In particular, the answers to the following two main questions are sought: 1) when is it appropriate to use the rigid lid assumption for simulating flow around bends?; and 2) what is (are) the most relevant parameters for quantifying the enhanced shear stress in channel bends from a practical standpoint? A computational fluid dynamics framework was developed using the ANSYS Fluent code and validated using experimental flume data. Following the validation study, a total of 26 simulations were performed and the results analysed in an attempt to answer the two main questions.

In an attempt to answer the first question, a broad parametric study was conducted using both free surface resolving simulations as well as simulations that make use of the rigid lid assumption. It is shown that the two main parameters that appear to control the flow dynamics in a bend are the maximum bend angle, expressed as the ratio of the length of the channel bend L_c to its radius of curvature R_c, and the upstream Froude number. Analysis reveal when that $L_c/R_c \geq \pi/2$, the curvature effects begin to dominate the dynamics and the error between the free surface model and the rigid lid model dramatically increases regardless of the value of the Froude

number. The study calls for caution to be used when using the rigid lid assumption and indicates that this assumption should not be used for simulating flows when $L_c/R_c \geq \pi/2$, especially for sharply curved channels with a radius of curvature to top width ratio $R_c/T_w < 2$.

The increase in shear stress is commonly expressed as a K_b value, which is simply the ratio of shear stress in a bend of the channel to the averaged approach shear stress in a straight channel. The results from the parametric study show that the conventional approach for parameterizing K_b as a function of R_c/T_w, where R_c is the radius of curvature and T_w is the channel top width, appears to be inadequate because the distributions in the K_b values exhibit significant scatter for small changes in R_c/T_w i.e. for flow around sharply curved bends. Dimensional analysis reveals that for a given channel cross-section, constant flow rate, bed slope and channel bed roughness, K_b depends on both L_c/R_c and R_c/T_w. In this study, the combined effects of these two parameters were investigated. It is shown from the parametric study that the magnitude of the shear stress increases as a function of L_c/R_c and reaches an asymptotic limit as $L_c/R_c > \pi/2$, for $R_c/T_w < 2$. The study also highlights that the location of the maximum shear stress occurs in the inner (convex) side of the bend for $R_c/T_w < 2$ but shifts towards the outer bend for $R_c/T_w > 2$. While the emphasis (and in a sense a limitation) of this study has been mainly on sharp curved bends ($R_c/T_w < 2$), the analysis can be readily extended to curved bends with $R_c/T_w > 2$. It is envisaged that such an analysis will lead to a framework for parameterizing K_b in a comprehensive manner that would be useful for practical design guidelines.

ACKNOWLEDGEMENTS

I want to express my sincere appreciation to my academic advisor, Dr Subhas Karan Venayagamoorthy and my academic co-advisor, Dr. Christopher I. Thornton. They have both supported my graduate work and continuously provided me with encouragement and passionate academic guidance throughout my Ph.D. studies.

Also, I want to express my appreciations to my committee members, Dr. Steven R. Abt, Dr. Pierre Julien, and Dr. Lakshmi Dasi for their valuable suggestions for my research. I would like to also especially thank Dr. David Mclean who encouraged and guided me during my undergraduate studies in civil engineering at Washington State University from 2002-2005.

I also want to thank the staff members of ENS (Engineering Network Service) at CSU especially Ryan Medhurst and Shaila Parashar who provided me assistance with computational resources. In addition, I wish to show my best appreciation to past and current hydraulic engineering graduate students at CSU who provided with me useful suggestions and encouragement.

This dissertation would have never become a reality without the unending patience, support and encouragement of my family members who I deeply value namely: my father (Young-ho Shin), my mother (Young-Hee Kim), my wife (Yongbin Lee), my son (Luke Jinwoo Shin), and my younger sister (Shin, Jung-Hye). I hereby express my heartfelt thanks to all of them.

TABLE OF CONTENTS

LIST OF TABLES

LIST OF FIGURES

LIST OF SYMBOLS

A = flow area

A_b= the unit area

C_α = the curvature coefficient (dimensionless)

C_u = the ratio of thalweg velocity to mean flow velocity (dimensionless)

d = the spacing of flood-plain ridges

d = the spacing of flood-plain ridges

D = the hydraulic radius of the channel cross-section

DH = hydraulic diameter

dp = the differential pressure

F = simulation results from free surface model

F = the force that applies on the channel bank

F_c = the centrifugal force

g_x = acceleration of gravity in x- axis direction

Δh = free surface elevation

I = turbulent intensity

K_b = the ratio of maximum shear stress in a bend to the averaged shear stress in a straight channel (dimensionless)

L_c = arc length of the curved channel using the maximum bend angle of the channel

M = the rate of migration rate

M = the length of the channel meandering

M_v = the ratio of maximum flow velocity in bend to the averaged flow velocity (dimensionless)

m = the mass of the moving object

n = the number of the data samples

P = wetted perimeter

P_a = atmospheric pressure

$\overline{p}$ = the average pressure

Δp = the dynamic pressure ft of H_2O

P_f = pressure at surface

r = the value of radius of curvature

R = hydraulic radius

R = simulation results from rigid lid model.

R_c = radius of curvature of the bend to the channel centerline

Re_{DH} = Reynolds number at the depth of hydraulic diameter (dimensionless)

S_f = friction slope

T_w = channel top (water surface) width

U = flow velocity

u = the x-axis velocity

$\overline{u_i}$ = the time-averaged velocity field

$\overline{u_i' u_j'}$ = the Reynolds stress tensor.

u_* = shear velocity

v = the moving velocity of the object

v = y-axis velocity

w = z-axis velocity

w_m= the stream width

y = the distance normal to the plane of the channel bottom

Greek Symbols

γ = the specific gravity of water

θ = the bend angle of a channel

κ = the constant of Von Karman (dimensionless)

ρ = the mass density of water

τ_o = the boundary shear stress

ν = kinematic viscosity of water

ϕ = the direction angle obtained from the original and final location between two points in a meandering channel

ω = the maximum angle the path generates from the averaged downstream direction

Chapter 1. Introduction

1.1 Motivation and Background

Flow around curved channel bends has garnered a lot of interest over the last century. This is mainly due to the importance of flow in curved open channels in many applications ranging from river meandering and associated control of erosion and sedimentation to design of hydropower plants. Hence, understanding the flow dynamics in curved open channel bends is critical for developing appropriate engineering designs and mitigation strategies. To this end, numerous studies ranging from field observations to laboratory experiments and (relatively recently) to numerical simulations have been performed over the last few decades to investigate the flow characteristics in bends, in particular the secondary (transverse) circulation and its effect on the geomorphology of the channel bed (Zeng et al. 2010).

Despite the vast body of work in this field, there are many outstanding questions that require further investigation. One such question of particular importance is to quantify the increase in shear stress in the channel bend compared to average shear stress in an equivalent straight channel under similar flow conditions. The increase in shear stress is commonly expressed as a K_b value, which is simply the ratio of shear stress in a bend of the channel to the averaged approach shear stress in a straight channel. An accurate estimation of K_b is an important consideration for developing appropriate design guidelines for meandering channels. It is well known that the enhanced shear stress in channel bends can lead to massive failures of channel banks, resulting in floods that pose significant risk to natural and manmade habitats.

Most of the studies on flow in curved bends have been done using laboratory flume experiments. Some of the classical flume studies (see figure 1.1) include the study by Ippen et al. (1962a) and the United States Department of the Interior Bureau of Reclamation (USBR) (1964). Datasets of flow velocity, water depth, and shear stress have been documented for these studies. At Colorado State University (CSU), a 1:12 Froude scale physical model of a meandering reach of the Rio Grande River was constructed at the Engineering Research Center (ERC) to study flow physics in a double reverse bend. Sin (2010) performed an analysis of the dataset collected from the CSU study. A design guideline for meandering channel flow based on the composite datasets of CSU and those of Ippen et al. (1962a), USBR (1964), and Yen (1965) was proposed (Sin 2010). Figure 1.2 shows the plot of the K_b values as a function of R_c/T_w, where R_c is the radius of the curvature of the bend (measured to the channel centerline) and T_w is the top width of the water surface. However, the results shown in Figure 1.2 indicate that R_c/T_w might not be the most relevant parameter for quantifying K_b. The results presented show that K_b values exhibit a scatter of up to a factor of 2 to 3 for low values of R_c/T_w (i.e. for strongly curved flows). This suggests that perhaps an additional (independent) parameter that takes into account the change in momentum flux that occurs in sharp bends i.e., the length over which the curved flow occurs might be required. From a practical standpoint, a robust (and simple) parameterization of the shear stress in a channel bend as a function of the bend geometry and upstream flow conditions is required. These important and practical questions underscore the motivation for the study presented in this dissertation

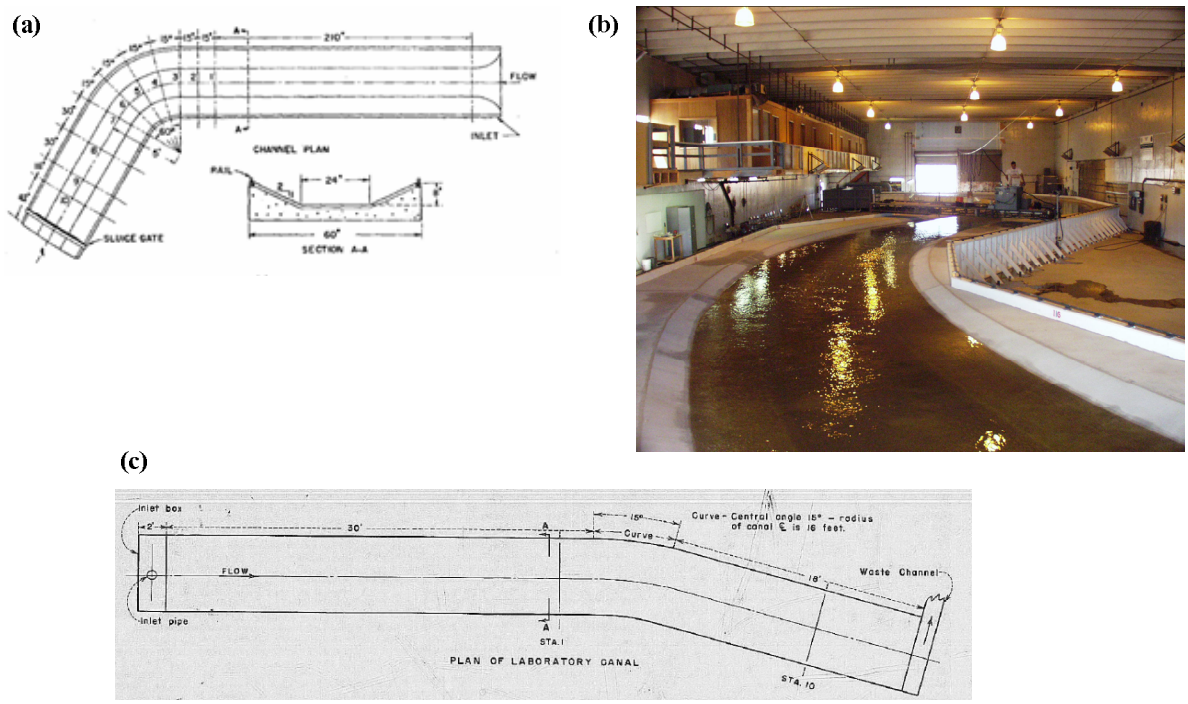

Figure 1.1 Examples of experimental study of meandering flow ((a) Ippen et al. (1962a), (b) S-shaped meandering flume constructed by CSU, and (c) Curved flume study performed by USBR (1964)).

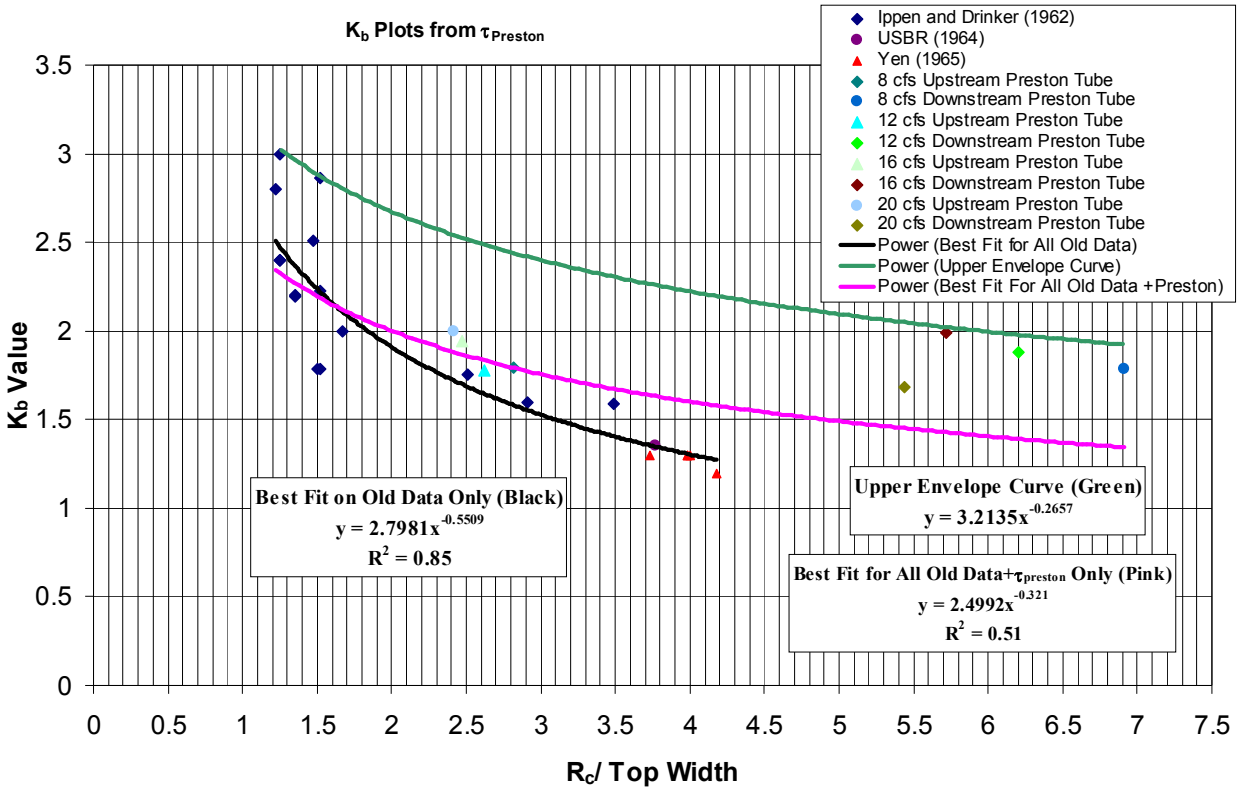

Figure 1.2 Plot of K_b values for a trapezoidal channel (Sin 2010).

Recently, there has been a proliferation in the use of computational fluid dynamics (CFD) techniques to investigate flow around curved bends and for many other applications in open channel flow. This can be attributed to the significant potential for CFD techniques to provide better perspective on the complex three-dimensional turbulent flow characteristics in open channel flow which can help improve engineering design of river restoration measures (Sturm 2009). However, there are a myriad of techniques that are used in CFD to simulate open channel flow, each with its own assumptions and simplifications. For example, the rigid-lid assumption is often employed to simulate flow around bends based on arguments that the free-surface effect is negligible and also considering that CFD simulations using this assumption are computationally less expensive. While the rigid-lid assumption may be valid for mildly curved bends at low Froude numbers, it is likely to break down for strongly curved bends at higher Froude number (subcritical) flows. One of the main goals of this dissertation is to investigate the applicability of the rigid-lid assumption to simulate flow around bends for different flow and bend properties.

1.2 Research Objectives

The overarching goal of this research is towards improved understanding of flow in channel bends with an eye toward practical design guidelines. Numerical simulations of flow in channel bends is the primary tool employed in this study. Laboratory experimental data will be mainly used for validation. The main objectives are:

- To perform three-dimensional numerical simulation of a previous laboratory scale channel bend flume experiment in order to validate the use of the CFD framework that will be used for the next two objectives.

- To investigate the three-dimensional flow dynamics in meandering channels using CFD. In particular, the focus is to elucidate the effect of the free surface in a curved channel and highlight the drawback of using the rigid-lid assumption in CFD simulations.
- To perform a parametric study using CFD to determine an alternative parameter (s) for quantifying K_b in channel bends.

1.3 Dissertation Layout

The work presented in this dissertation is organized into five further chapters. The contents of chapters 4 and 5 have been written up for possible publication in hydraulic engineering journals, hence they are relatively self-contained and as such some redundancy exists.

Chapter 2 provides a literature review on the mechanism of meandering flow and the methodologies used for studying such flows experimentally as well as numerically. Chapter 3 presents a description of the numerical framework used in this study together with validation results with an experimental dataset. Chapter 4 presents a parametric study of meandering flow physics with an emphasis on the consequences of neglecting free surface effects in CFD simulations of flow in curved channel bends. Using a broad parametric study, results are presented to determine suitable thresholds values of relevant flow and geometric parameters beyond which neglecting free surface effects in CFD simulations may lead to erroneous results. Chapter 5 presents a parametric study to determine the most relevant parameters for quantifying K_b. Finally, the conclusions and recommendations for further work are discussed in Chapter 6.

Chapter 2. Literature Review

Meanders and curved bends are common features in natural rivers. The associated flows in curved and meandering channels are complex and very different from flow encountered in straight channels. These differences include curvature-induced secondary currents and their interaction with the main flow. Hence one-dimensional numerical models are not capable of reproducing the physical phenomena observed in meandering channel flow such as the secondary circulation. In particular, an in depth understanding of the complex interaction between streamwise and spanwise flow in such a system is yet to emerge. As such, three-dimensional numerical simulations are being increasingly used to study meandering channel flow. In this chapter, the goal is to provide an overview of the basic principles of meandering flow as well as an overview of the different approaches used to study them both experimentally and numerically.

2.1 Mechanism of Meandering Flow

This section will describe the basic geometric characteristics, physical phenomena, and geomorphic change of a meandering channel.

2.1.1 Geometry in a Meandering Channel

A simplified schematic of a channel meander is shown in Figure 2.1. A common parameter to describe degree of meandering is sinuosity (Watson et al. 2005). Sinuosity is defined as the ratio of stream length to valley. A channel with a sinuosity greater than 3 is considered to be highly meandered. Langbein and Leopold (1966) argue that the formation of the channel meandering can be described using the random-walk model developed by Von Schelling (1951, 1964). The model developed by Von Schelling (1951, 1964) is presented in Equation 2.1;

$$s = \frac{1}{\sigma}\int \frac{d\phi}{\sqrt{2(\alpha - cos\phi)}}, \tag{2.1}$$

where, ϕ is the direction angle obtained from the original and final location between two points in a meandering channel; and α is the constant of the integration. Langbein and Leopold (1966) recast Equation 2.1 as:

$$\alpha = \cos\omega, \tag{2.2}$$

where, ω = the maximum angle the path generates from the averaged downstream direction. They went on to suggest that planimetric geometry of river meanders may be expressed as:

$$\phi = \omega \times \sin\frac{s}{M}2\pi, \tag{2.3}$$

where, ϕ = the flow direction at the points and M = the length of the channel meandering. A sine-generated curve is commonly used to model a single meandering channel as shown in Equation 2.1. Figure 2.2 shows the sketch of sine-generated curve.

$$\theta = \omega \sin kx, \tag{2.4}$$

where, θ = channel direction; and x is flow distance along the reach and k is meander wavenumber.

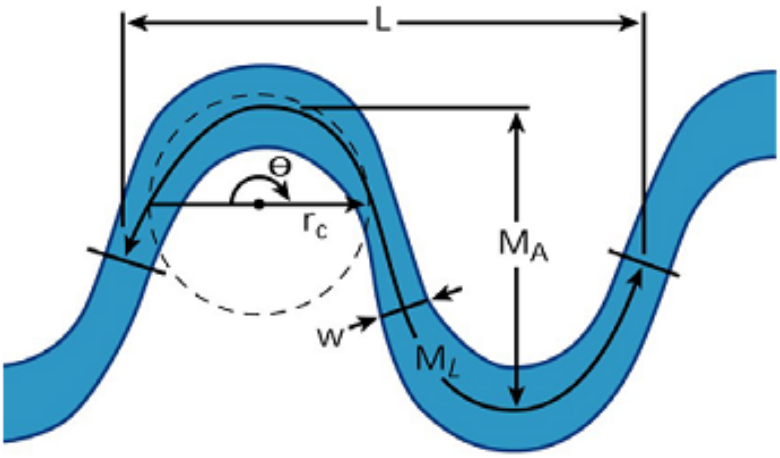

L meander wavelength
M_L meander arc length
w average width at bankfull discharge
M_A meander amplitude
r_c radius of curvature
Θ arc angle

Figure 2.1 Geometry of meandering channel (from Watson et al. 2005).

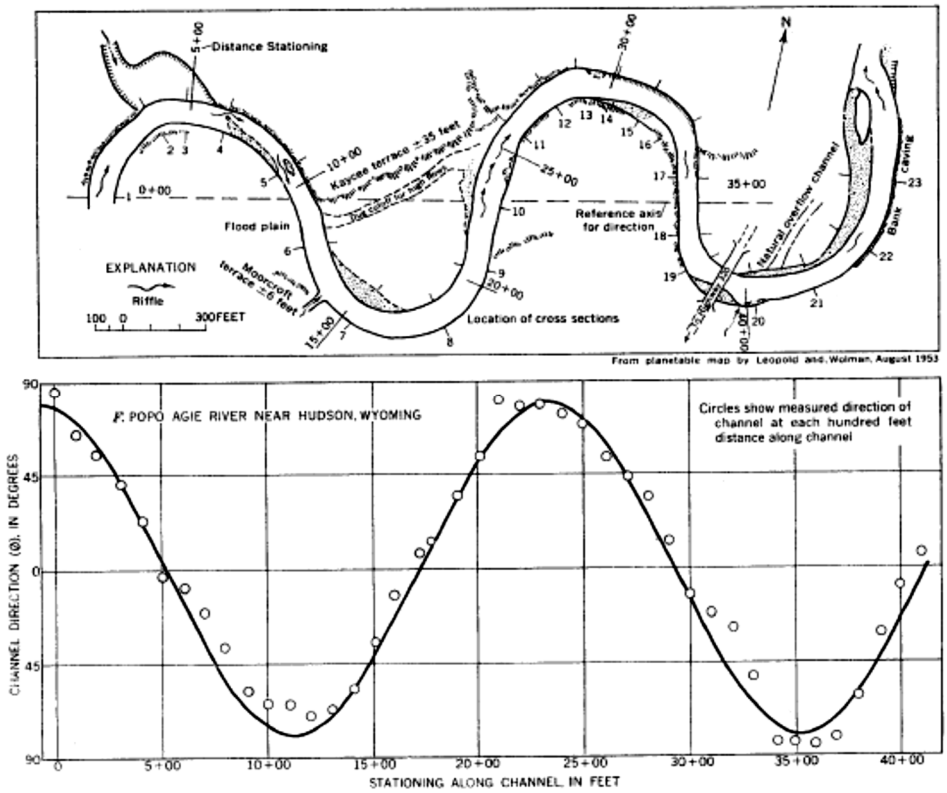

Figure 2.2 Description of sine-generated curve function (from Langbein and Leopold 1966).

2.1.2 Flow Patterns in a Meandering Flow

In typical meandering channels, secondary flow is generated in channel bends. A pictorial description of secondary flow is shown in Figure 2.3. Secondary flow is caused from the imbalance between centrifugal force and differential hydrostatic force, γdz. Centrifugal force in river bends can be calculated using Equation 2.5 (FHWA 2001).

$$F_c = \frac{mv^2}{r}, \tag{2.5}$$

where, $F_{c\,is}$ the centrifugal force; r is the value of radius of curvature; m is the mass of the moving object; and v is the moving velocity of the object. The imbalance between centrifugal force and hydrostatic force is presented in Figure 2.4. The net force between centrifugal force and hydrostatic force is higher at the bed of the channel and lower close to the water surface. As a result, a across channel circulation is generated in channel bends. The secondary (circular) flow in river bends causes geomorphic change in order to maintain channel equilibrium. Figure 2.5 shows erosion and sedimentation in a river bend for equilibrium. Due to secondary flow characteristics, the channel bed has the strongest secondary flow and inner bank of the channel has the weakest secondary flow. Therefore, coarse material will be located at channel bed and erosion will occur at the outer bank of the channel. At the same time, sedimentation will occur at the inner bank of the channel and a point bar will be generated.

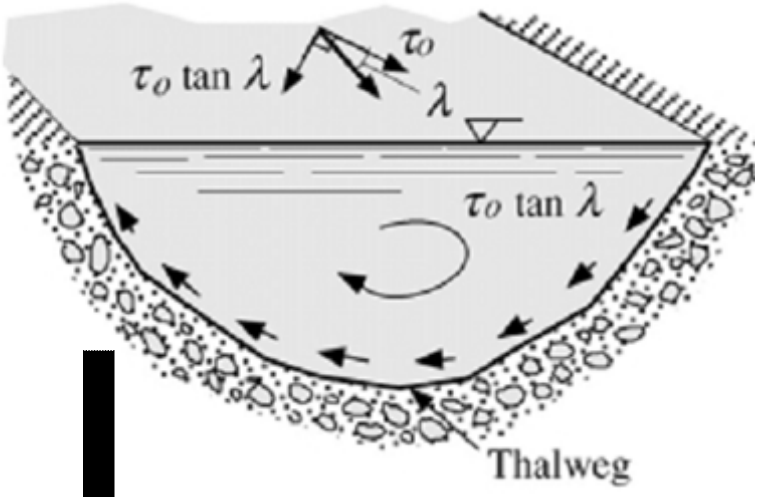

Figure 2.3 Secondary flow in river bends (from Julien 2002).

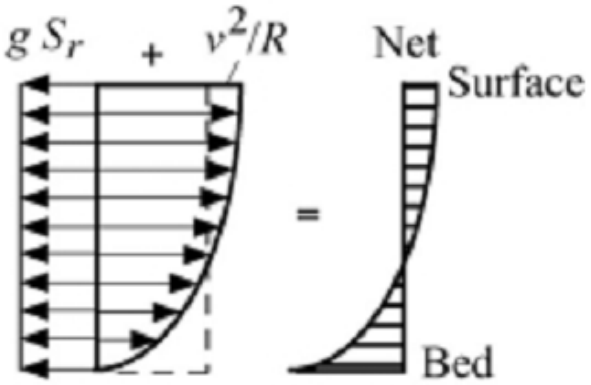

Figure 2.4 Imbalance between centrifugal force and hydrostatic force (from Julien 2002).

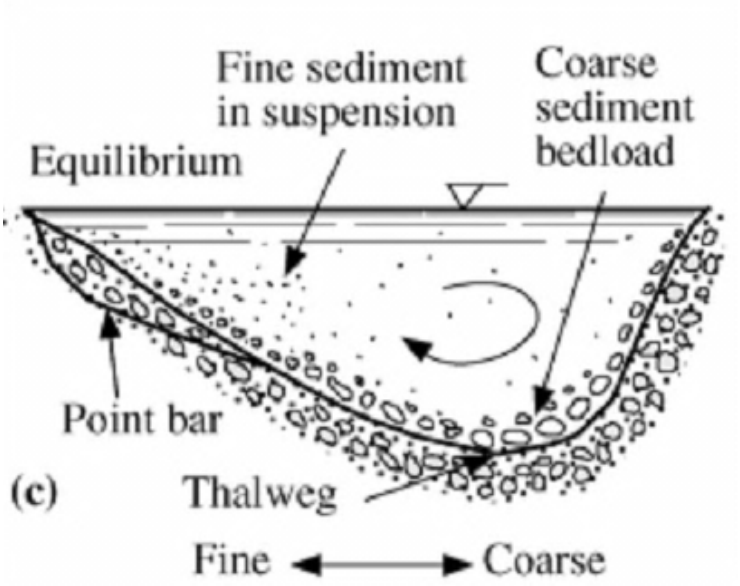

Figure 2.5 Erosion and sedimentation in a river bend (from Julien 2002).

2.1.3 Channel Erosion Rate in Meandering Channels

A major problem caused by the flow in channel bends is erosion. As mentioned in Chapter 1, the K_b is used as measure of the increase in shear stress in a channel bend and is often expressed as function of the radius of curvature to top width. Numerous studies have been conducted to investigate the channel migration rate as function of the ratio of the radius of curvature to top width. Hickin et al. (1975) developed equations for estimating meandering channel migration rate as shown in Equation 2.6 and Equation 2.7 based on the field data obtained from Beatton River located in British Columbia, Canada.

$$\mathbf{M = 0.05 \times \left(\frac{R_c}{w_m}\right)^{2.05} + 0.00035d^{2.63}} \ (1.3 < \frac{R_c}{w_m} < 2.9) \ , \tag{2.6}$$

$$\mathbf{M = \frac{2.75}{\left(\frac{R_c}{w_m}\right)^{1.73}} + 0.00035d^{2.63}} \ (2.9 < \frac{R_c}{w_m} < 7.0) \ , \tag{2.7}$$

where M is the rate of migration (meters/year); $\frac{R_c}{w_m}$ is the ratio of radius of curvature to stream width; and d is the spacing of flood-plain ridges.

Begin (1981) used momentum equation approach to study the relationship between the ratio radius of curvature of the bend to channel width and the force exerted at the outer bank of a meandering channel. He developed an equation for the force exerted per unit area by using momentum equation applied in both horizontal and vertical directions. The derived equation that describes the force per unit area at the outer bank of the meandering channel is given by;

$$\frac{F}{A_b} = C_u C_\alpha \times \frac{\sqrt{2(1-\cos\theta)}}{\theta} \times \rho U^2, \tag{2.8}$$

where $\frac{F}{A_b}$ is the force that is applied on the channel bank per unit area; C_u is the ratio of thalweg velocity to mean flow velocity; and C_α is the curvature coefficient. He argued that R_c/T_w is highly correlated with the change of curvature coefficient, C_α in Equation 2.8. He also showed

that the C_α value correlated well with the meandering channel migration rate which indicates that the value of R_c/T_w value is related with the migration rate.

2.2 Previous Researches Relevant to This Study

In this section, summaries of previous research on meandering flow will be described. Analysis of meandering flow has been performed using experimental and numerical methods. This section will provide overview of both methods to highlight relevant work in literature.

2.2.1 Experimental Methods

Ippen et al. (1962) conducted experimental studies to measure shear stress in a meandering channel. The shear stress contour map is portrayed in Figure 2.6. The shape of the channel cress-section was trapezoidal with side slope of 1:2 (vertical: horizontal). The bed shear stress data was collected using a Preston tube. They showed that the bed shear stress is one of the important parameters to predict geomorphic change in a meandering channel. The work of Ippen et al. (1962) concluded that a curved channel with a larger radius of curvature will cause higher shear stresses.

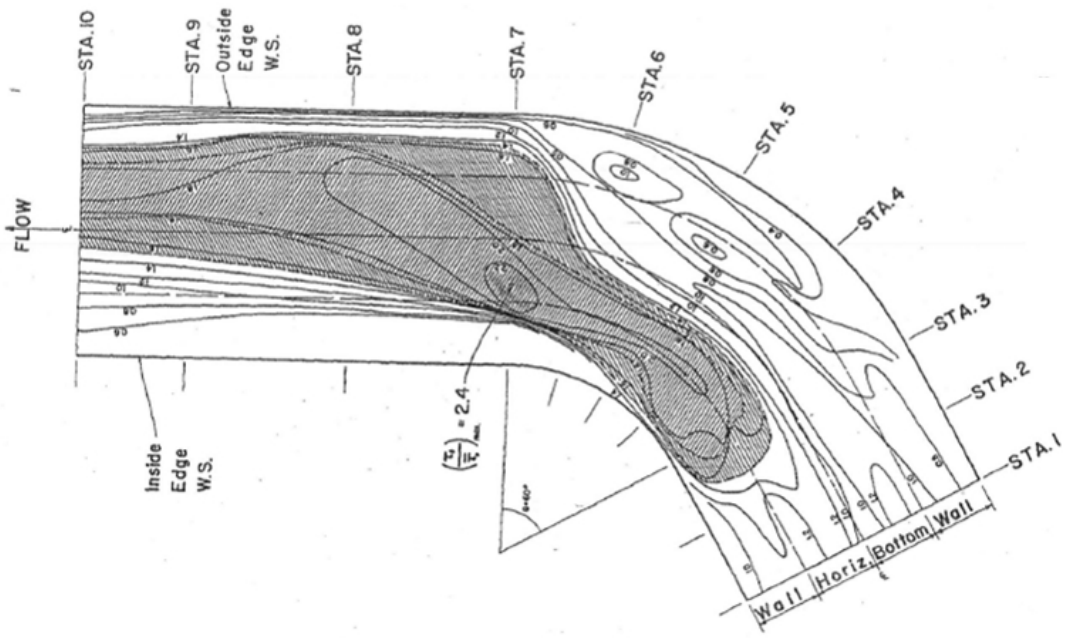

Figure 2.6 Contour plot of shear stress distribution in a curved channel (from Ippen et al. 1962a).

USBR (1964) conducted a flume study to collect data from flow in a curved channel. The data of USBR (1964) was selected because the flume constructed by USBR (1964) had very similar flow geometry to that used in the study by Ippen et al. (1962a) but with lower curvature and bed slope. USBR (1964) collected data of velocity, water surface elevation and shear stress data. For instrumentation, USBR (1964) used 3/16 inch Prandtl tube for flow velocity measurements. For water surface measurements, USBR (1964) used a point gauge. The results of shear stress measurements were taken with Preston tube with similar instrumentation methodology to that of Ippen et al. (1962a).

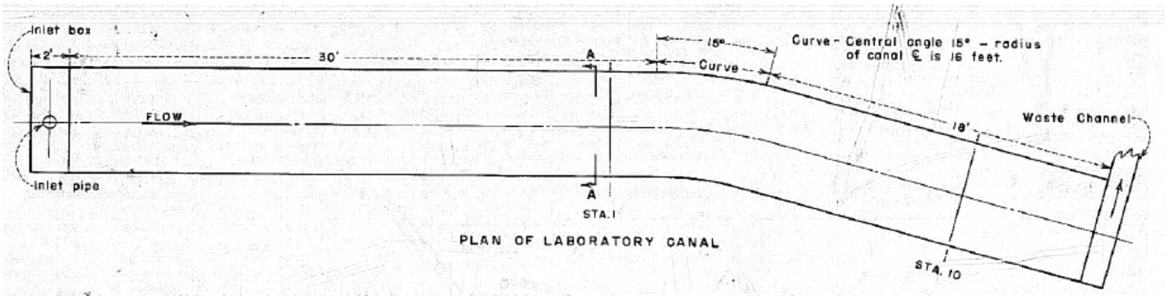

Figure 2.7 Schematic view of the curved flume (from USBR 1964) (flow: from left to right).

Yen (1965) performed a flume study to investigate the characteristics of subcritical flow in an S-shaped curved channel. The instrumentation technique was similar to those used in the studies done by Ippen et al. (1962a) and USBR (1964). Yen (1965) also parameterized the shear stress in bend by expressing the K_b value, as a function of the radius of curvature to top width.

Bathurst et al. (1979) performed field measurements and an experimental study. The location of the field measurement site is the River Severn in Wales. The bed material of the river is composed of cobble while the bank material was composed of fine alluvium coarse gravel. Table 2.1 presents the information of the study reach.

Table 2.1 Field measurements (from Bathurst, et al. 1979)

Site	Radius of Curvature (m)	Rotation Angle (Degrees)	Median axis of sediment bigger than or equal to n % of median axes by count (mm)	
			n = 84	n = 50
Llandinam	70.5	62	60	40
Rickety Bridge	44	50	93	63
Maes Mawr	95	38	50	31.5
Penstrowed	75	105	38	22

The electromagnetic flow meter was used for velocity data collection in the experiments (Bathurst, et al. 1979). The device was used to measure two mutually perpendicular velocity components at once. From the velocity components, boundary shear stress was calculated from the following equations:

$$u = \frac{2.303}{\kappa} \times u_* \times \log(y) + C, \tag{2.9}$$

$$u_* = \sqrt{\frac{\tau_o}{\rho}}, \tag{2.10}$$

where, κ is the constant of Von Karman; u_* is shear velocity (ft/sec); y is the distance normal to the plane of the channel bottom (ft); τ_o is the boundary shear stress (psf) and ρ is the mass density of water (slug/ft^3). Bathurst et al. (1979) observed the occurrence of secondary flow in their field study. From their field data, they found out the location of the maximum boundary shear stress, i.e. the point was located at the junction of main flow and outer bank secondary flow. In addition, they concluded that the Reynolds number and secondary flow were the main factors that influenced the shear stress distribution.

Blanckaert and Graf (2004) performed a laboratory study of meandering channel flow to investigate the characteristics of secondary flow. Laboratory experiments were conducted in a 0.4 m wide, 60º bend angle, plexiglass flume. The schematic sketch of the flume is shown in Figure 2.8. The ADVP (Acoustic Doppler Velocity Profiler) was used to measure the velocity field. The ADVP measures the 3 components of flow velocity (u, v, and w) from which the six components of turbulent shear stress; τ_{xy}, τ_{yx}, τ_{xz}, τ_{zx}, τ_{yz}, and τ_{zy} can be calculated.

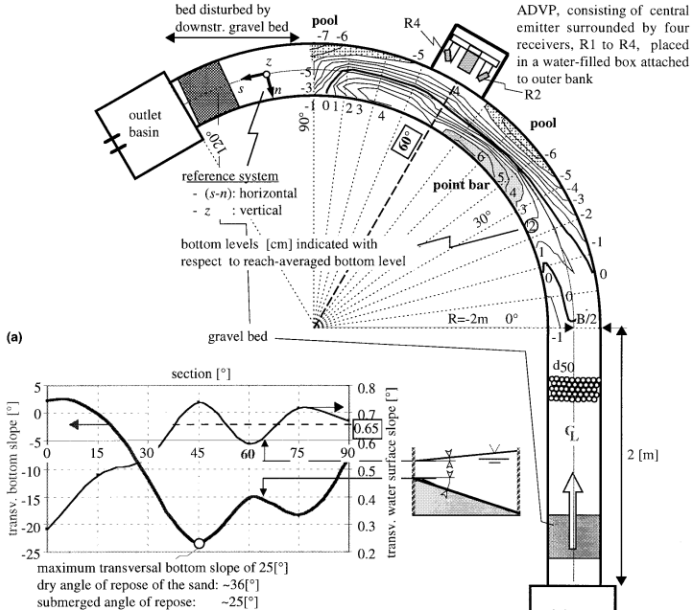

Figure 2.8 Detail sketch of flume (from Blanckaert and Graf 2004).

From their experimental study, Blanckaert and Graf (2004) noticed the existence of two-celled secondary flow in the bend. In case of inner bank, the circulation of water is clockwise and at the outer bank, the flow is counterclockwise. Figure 2.9 shows the secondary flow in the bend. They also observed a reduced degree of turbulence in the outer bend region that results in a weaker outer bank shear stress.

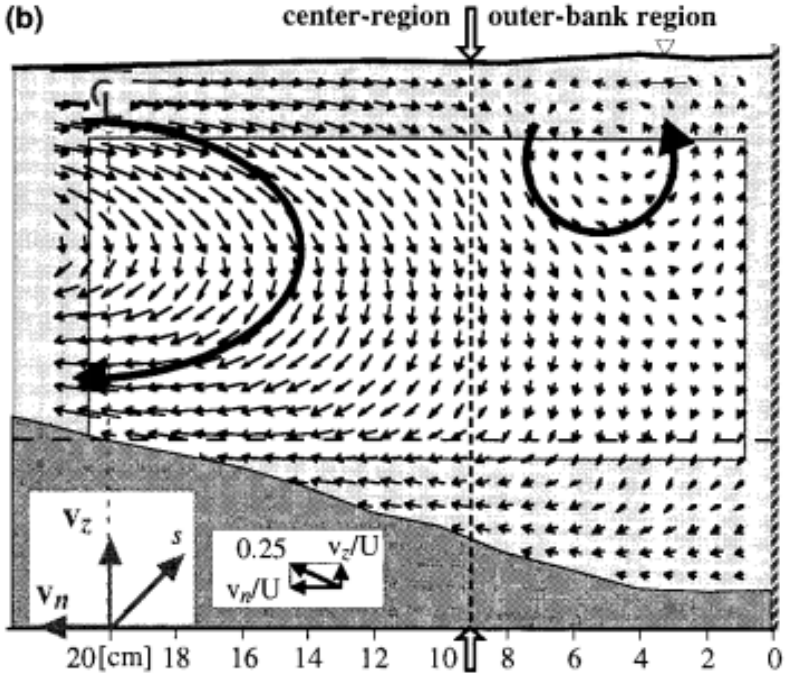

Figure 2.9 Two celled secondary flow in bend (from Blanckaert and Graf 2004).

Blanckaert and Graf (2004) observed the fact that the flow velocity distribution is not the only factor to determine secondary flow characteristic in meandering channel. They concluded that turbulence of flow is another important factor that produces the outer bank circulation flow. In addition, they argued that their results are applicable for studying transport of sediment in meandering channels.

Heintz (2002) performed an experimental study of a meandering channel flow using trapezoidal channel geometry at CSU. Flow velocity, flow depth and shear stress were measured. An ADV was used for velocity data collection and a point gage was used for measuring flow

depth. A pressure transducer and Preston tube were used to measure shear stress (Heintz 2002). Figure 2.10 shows a Preston tube and a pressure transducer. Equation 2.11 shows the relationship between dynamic pressure and shear stress that was obtained from Preston tube calibration.

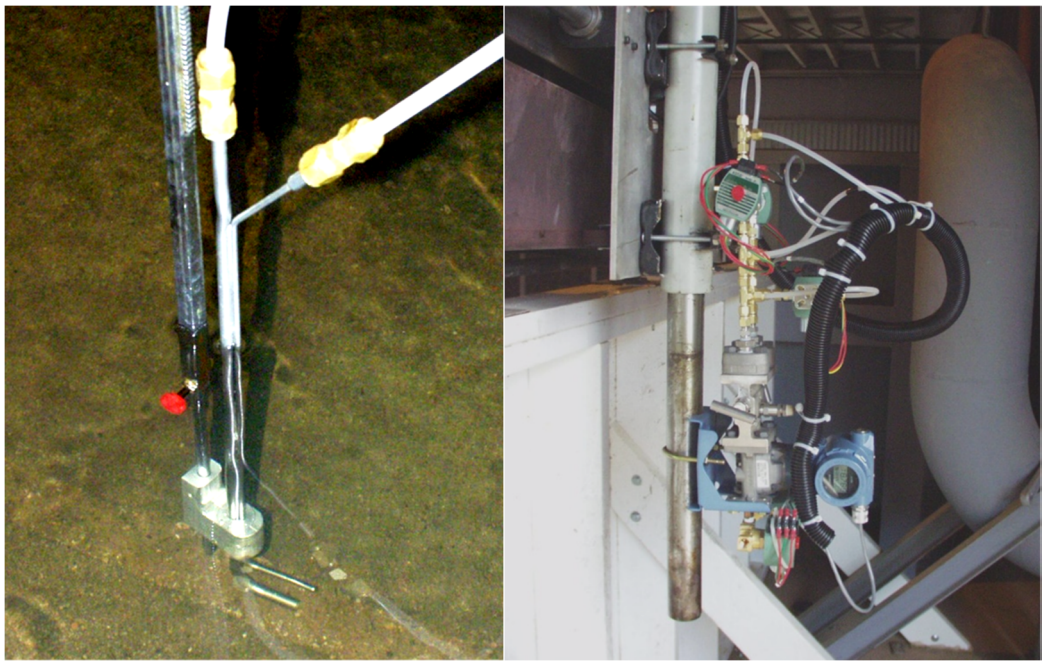

Figure 2.10 Preston tube for shear stress measurement (at left) and pressure transducer (at right) (from Heintz 2002).

$$\tau = 0.02788 \times \gamma \times \Delta p\,, \tag{2.11}$$

where, τ is the shear stress (psf); γ is the specific gravity of water (lb/ft^3); and Δp is the dynamic pressure in ft of H_2O.

Booij (2003) conducted an experimental study of a shallow (width to depth ratio was about 10.) mildly meandering flow (radius of curvature to depth ratio was about 80.) in the laboratory. Figure 2.11 shows the sketch of the curved flume that was used in the study of Booij (2003). As shown in Figure 2.11, the flume was composed of two straight channels and one semi-circular bend. The shape of the channel cross section was rectangular, with a width of 0.5 m and a flow depth of 0.052 m respectively (Booij 2003). The average flow velocity was 0.2 m/s. The LDV

(Laser Doppler Velocimetry) was used to measure the flow velocity. The experimental study of Booij (2003) also revealed the existence of secondary flow in a channel bend. The measured secondary flow is shown in Figure 2.12.

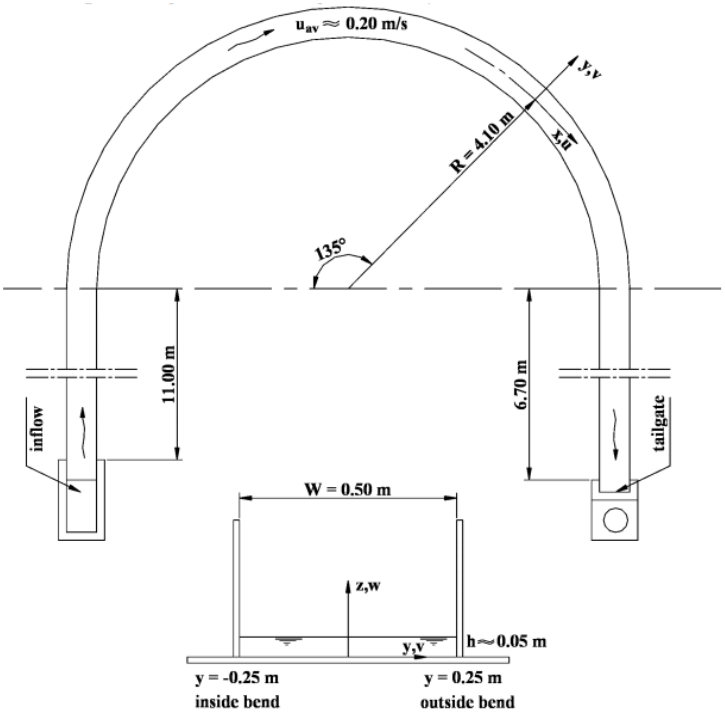

Figure 2.11 Curved flume at Delft University of Technology (from Booij 2003).

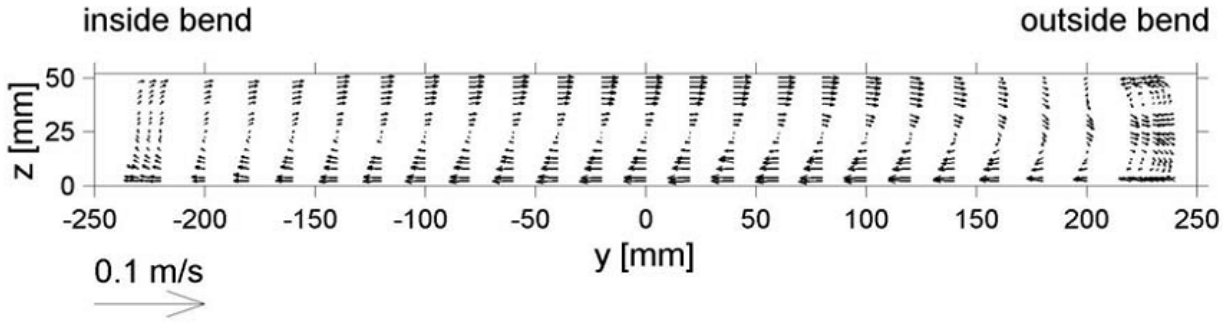

Figure 2.12 Measured secondary flow (from Booij 2003).

Sclafani (2008) also carried out another Preston tube calibration at CSU to overcome the limitation of meandering geometry. This experimental study was performed in a 60-foot long, 4-foot wide, 2.5-foot tall flume. Equation 2.12 describes the relationship between the shear stress and the differential pressure that was obtained from this study.

$$\tau = 0.1644 \times dp \,, \tag{2.12}$$

where, τ is the shear stress (psf); and dp is the differential pressure (in).

Sin (2010) performed an experimental study at CSU to determine the best way to calculate shear stress in a meandering channel. The shear stress calculation methods that were used include: 1) Reynolds shear stress extrapolation; 2) the Rozovskii (1961) method; 3) linear regression of flow velocity profile; and 4) Preston tube measurements. According to the results from data analysis, Reynolds shear stress extrapolation and linear regression of flow velocity profile underestimate the shear stress because these methods were based on a one-dimensional moment balance approach. In case of the Rozovskii (1961) method, only the lateral shear stress is computed. Therefore, the shear stress from Rozovskii (1961) method was significantly less than any other shear stress calculation methods. Finally, the shear stress obtained from Preston tube calibration was determined as the most appropriate shear stress calculation method because the Preston tube calibration did not show any of the limitations that were discussed above. For applications in real world situations, plots of ratios of maximum shear stress in the bend obtained from Preston tube calibration to averaged shear stress, K_b, were generated and presented in Figure 1.2, Chapter 1. As a follow up to the study of Sin (2010), Ursic (2011) performed experimental study for K_b values in natural shaped channel geometry. Again, an ADV and a Preston tube calibration were used to measure shear stress. The K_b values from Ursic (2011) showed much higher values than other previous experimental studies.

2.2.2 Numerical Studies

This section will provide an overview of relevant numerical studies that were performed prior to this study.

2.2.2.1 Previous Numerical Works

Odgaard (1989) published theoretical background and application of a numerical modeling to study meandering channel flow. To develop the numerical model, Odgaard (1989) used the following assumptions;

a) A prismatic channel;

b) Radius of curvature is significantly larger than the channel width;

c) Flow depth is smaller than channel width;

d) Longitudinal flow velocity of the channel is dominant; and

e) The turbulence is isotropic.

The numerical model was used to investigate the characteristics of the flow and bed profile in a meandering channel. Flow conditions were assumed to be steady, subcritical and turbulent. Through interpretation of the analysis results, Odgaard (1986) recognized that the channel radius was a major factor that determines the flow characteristics in a numerical channel. For the verification of the mathematical model, observation was performed by using field data of Fall River and Muddy Creek. This data came from Thorne (1986) and Dietrich and Smith (1983). Comparisons between the field data and the numerical model result were found to be in a good agreement. The numerical model made it possible to predict the trend of secondary flow component and the transverse bed slope in meandering channel.

Jin and Steffler (1993) also performed numerical simulation study using a depth-averaged model. To simplify the irregular channel geometry, the finite element method was used. To

validate the numerical model, experimental data of DeVriend (1976) and Steffler (1984) were used. Figure 2.13 and Figure 2.14 show that the numerical model results were in good agreement with experimental data.

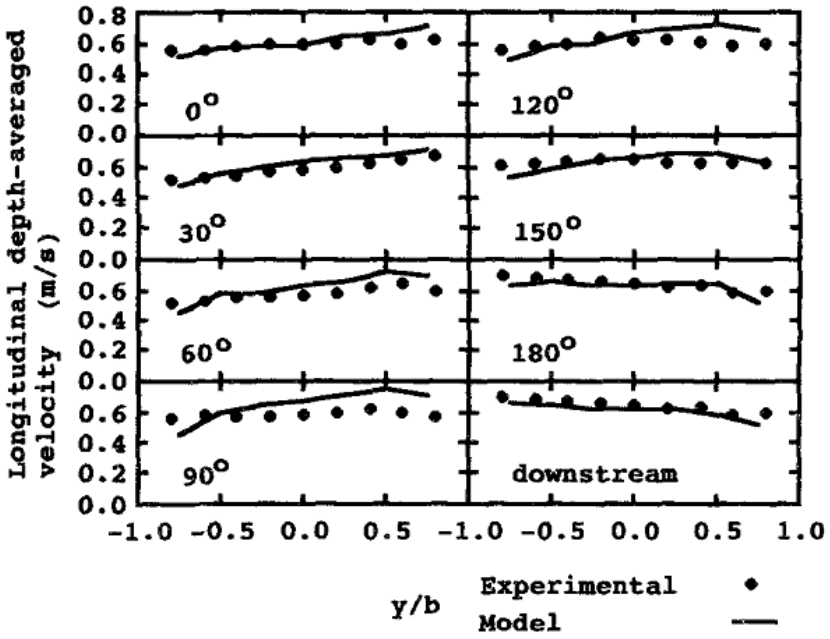

Figure 2.13 Validation of numerical modeling comparing with data of DeVriend (1976) (from Jin and Steffler 1993).

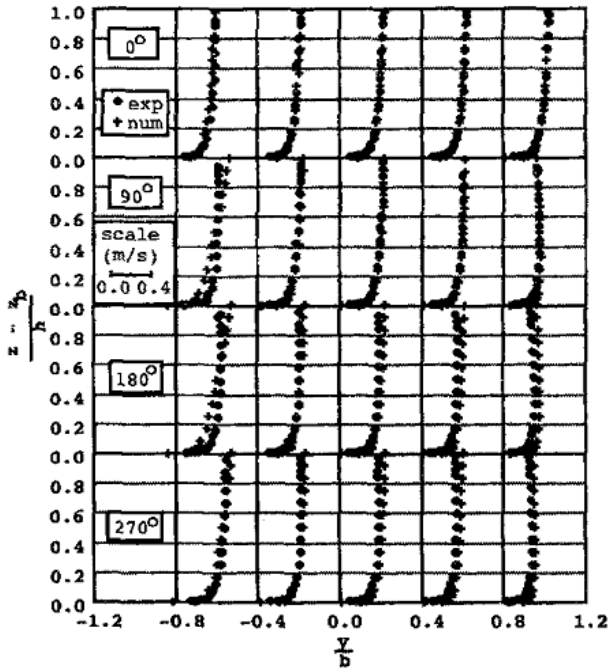

Figure 2.14 Validation of numerical modeling comparing with data of Steffler (1984) (from Jin and Steffler 1993).

Hodskinson and Ferguson (1998) simulated separated flow in a sharply curved meandering channel. For the three-dimensional numerical modeling, Fluent CFD code was used. They recognized the problem of deposition of fine-grained sediment due to flow separation that results from channel meandering. To simulate the flow separation in a meandering channel, Hodskinson and Ferguson (1998) selected RNG (renormalization group theory) k-ε turbulence model due to its higher accuracy than the standard k-ε turbulence model.

Figure 2.15 portrays the field site of the numerical simulation. Figure 2.16 presents the comparison of simulation results and measured data in the sharp channel bend in River Dean. The solid line is the near-surface data and the dash line represents the near-bed data. They found that the simulation result for cross section 11 was in good agreement with the measured data but discrepancies of velocity vectors were observed in cross section 4. For a detailed comparison of CFD model results with the measured data set, they compared the velocity magnitude and the streamwise component (U) as shown in Figure 2.17.

Additionally, Hodskinson and Ferguson (1998) simulated flow separation at the outer bank of a bend by performing idealized meandering flume study. The plan view of the flume is presented in Figure 2.18 and the simulation result by Fluent is presented in Figure 2.19. Based on the idealized meandering simulation results, they concluded that flow separation is influence by the curvature and the formation of the point bar in the channel.

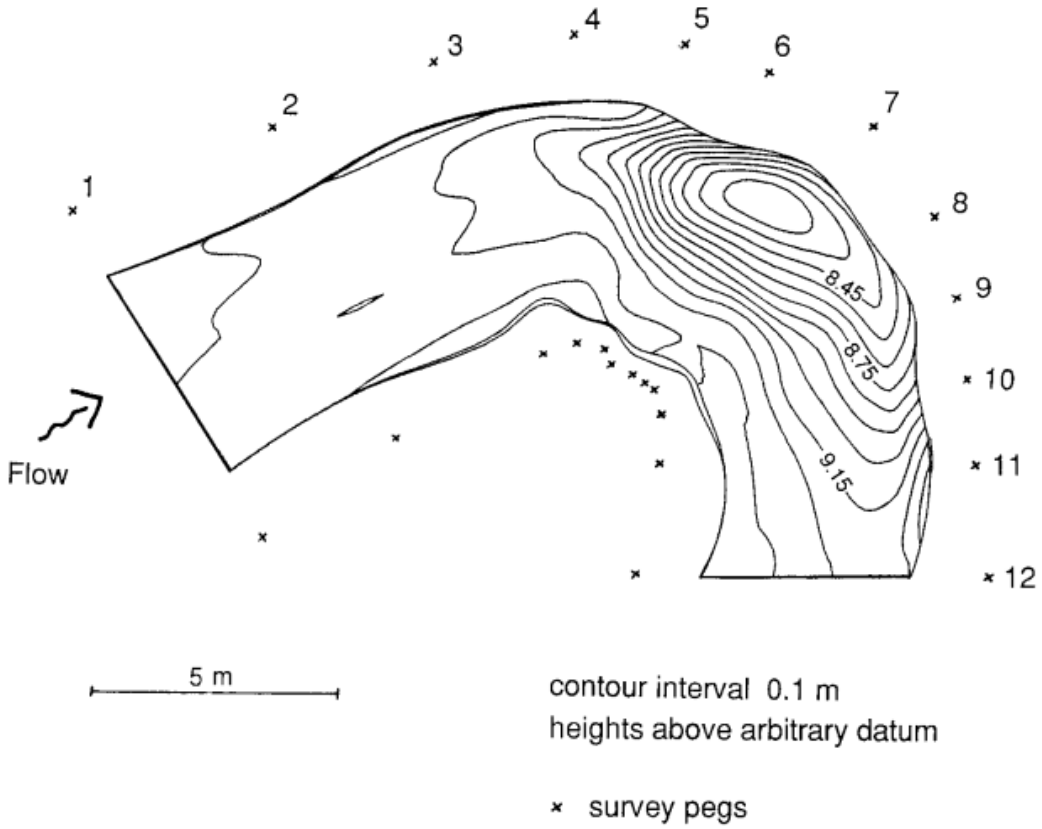

Figure 2.15 Plan view of the field site, River Dean UK (from Hodskinson and Ferguson 1998).

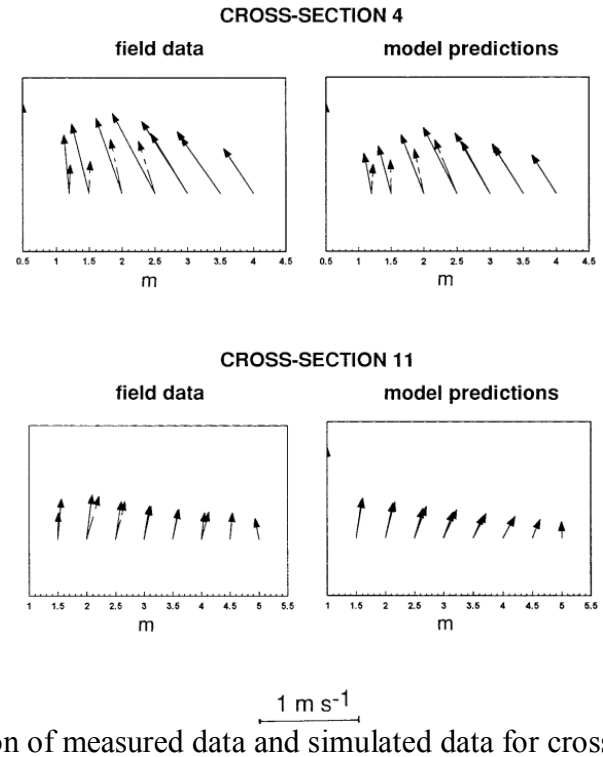

Figure 2.16 Comparison of measured data and simulated data for cross section 4 and 11 (from Hodskinson and Ferguson 1998).

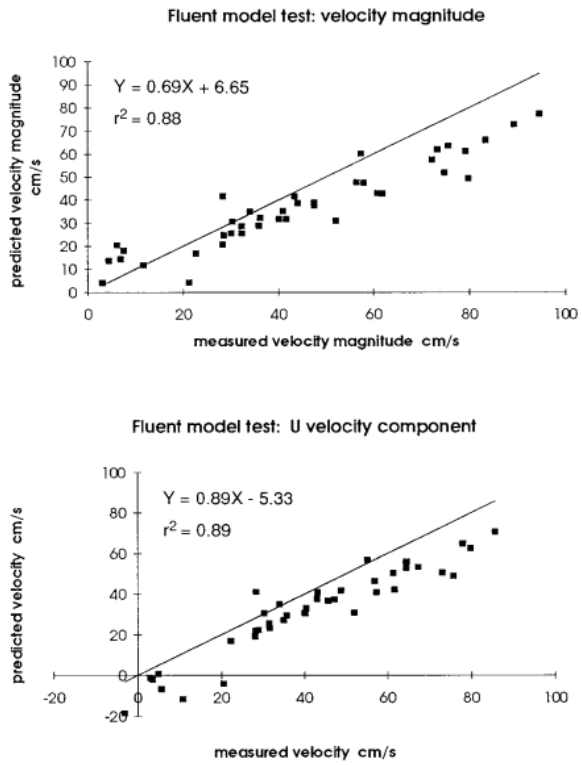

Figure 2.17 Comparisons between measured and observed data regarding flow velocity (from Hodskinson and Ferguson 1998).

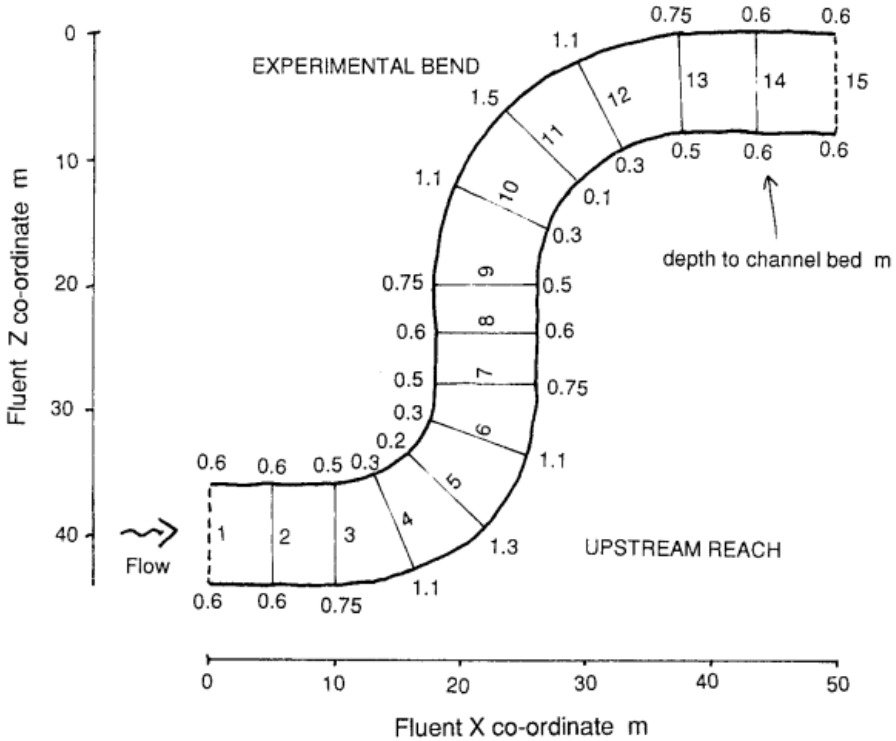

Figure 2.18 Plan view of the flume to simulate idealized meandering (from Hodskinson and Ferguson 1998).

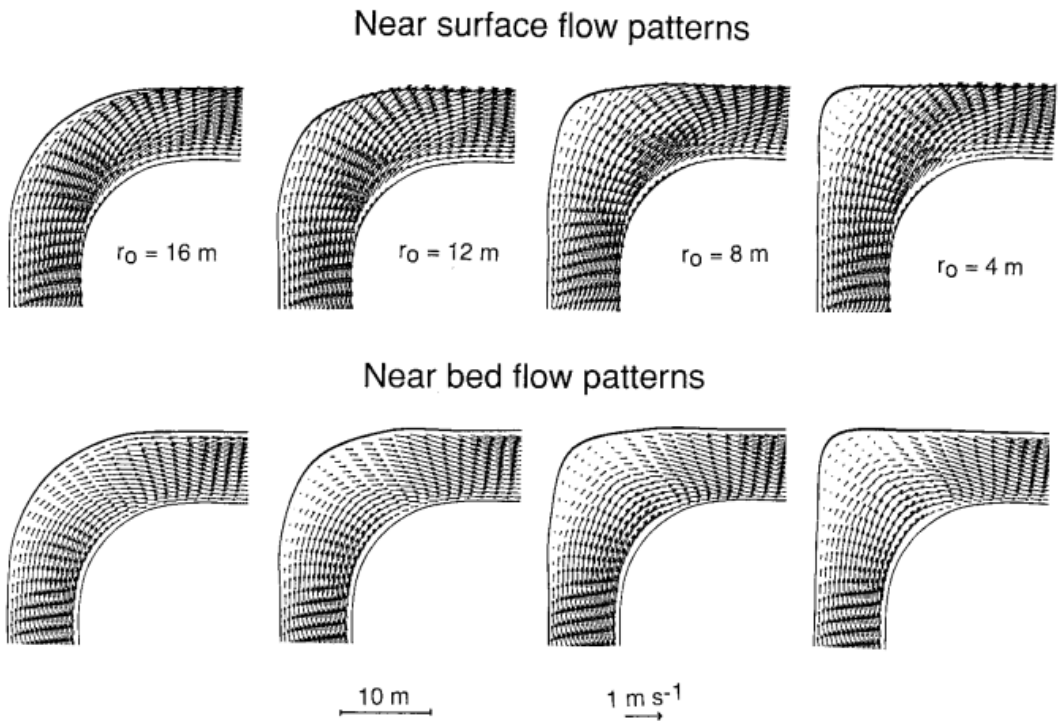

Figure 2.19 Simulation result in idealized meandering by changing outer bank curvature and apex width (from Hodskinson and Ferguson 1998).

Lien et al. (1999) performed numerical analysis using a two-dimensional depth-averaged model. The depth-averaged equations were obtained from an integration of the Navier-Stokes equations from channel bed to the water surface. The equations are based on orthogonal curvilinear coordinates. To validate the numerical model, they used two experimental data sets; 1) from a mildly curved channel; and 2) from a sharply curved channel. For the mildly curved channel, they used data of DeVriend and Koch (1977). For the sharply curved channel, the data set of Rozovskii (1961) was used. Figure 2.20 and Figure 2.21 shows the comparison of numerical simulation results with experimental data sets.

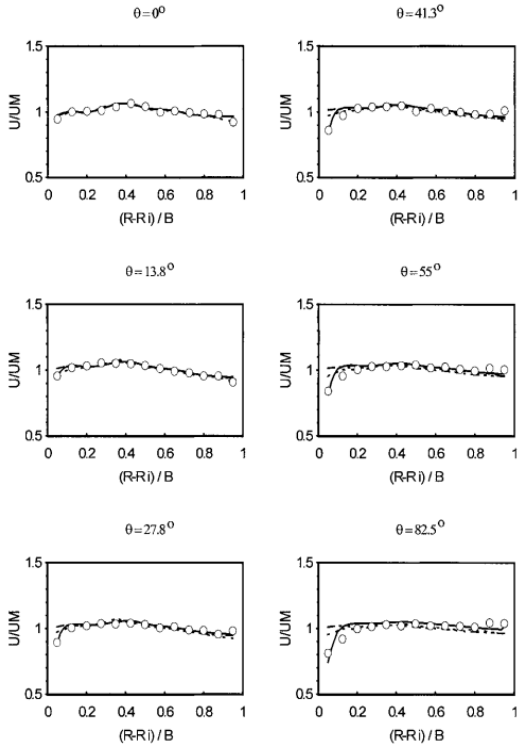

Figure 2.20 Velocity ratio across dimensionless channel width for DeVriend and Koch (1977) (from Lien et al. 1999).

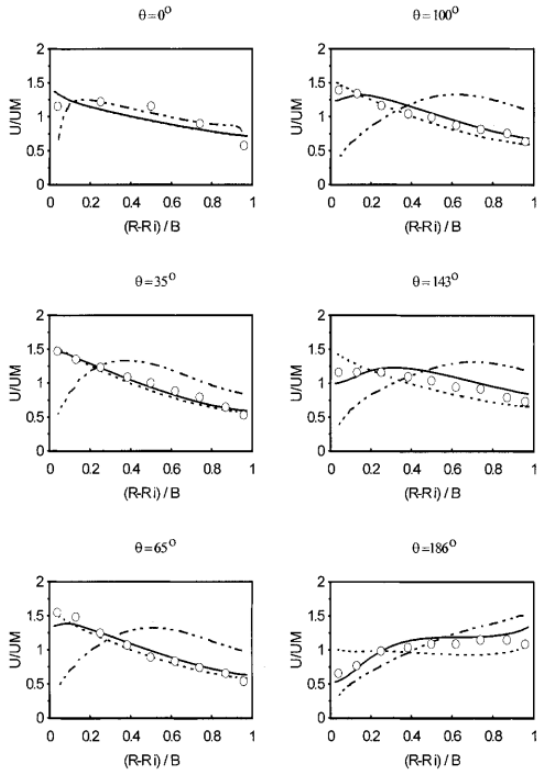

Figure 2.21 Velocity ratio across dimensionless channel width for Rozovskii (1961) (from Lien et al. 1999).

They found that the numerical simulation results were in good agreement with experimental data for the case of the mildly curved channel but significant differences were observed for the sharply curved channel. Despite these variations, they weakly concluded that the numerical model properly simulated the effect of secondary flow in a meandering channel.

Wilson et al. (2003) developed and validated a numerical code to perform three-dimensional numerical modeling in a meandering channel. Wilson et al. (2003) solved the RANS equations with the standard k-ε turbulence model. They justified the use of the standard *k-ε* turbulence model based on its wide usage. For the validation of the numerical modeling, they used experimental data obtained from a flume study. The plan view and picture of the flume is presented in Figure 2.22 and Figure 2.23, respectively.

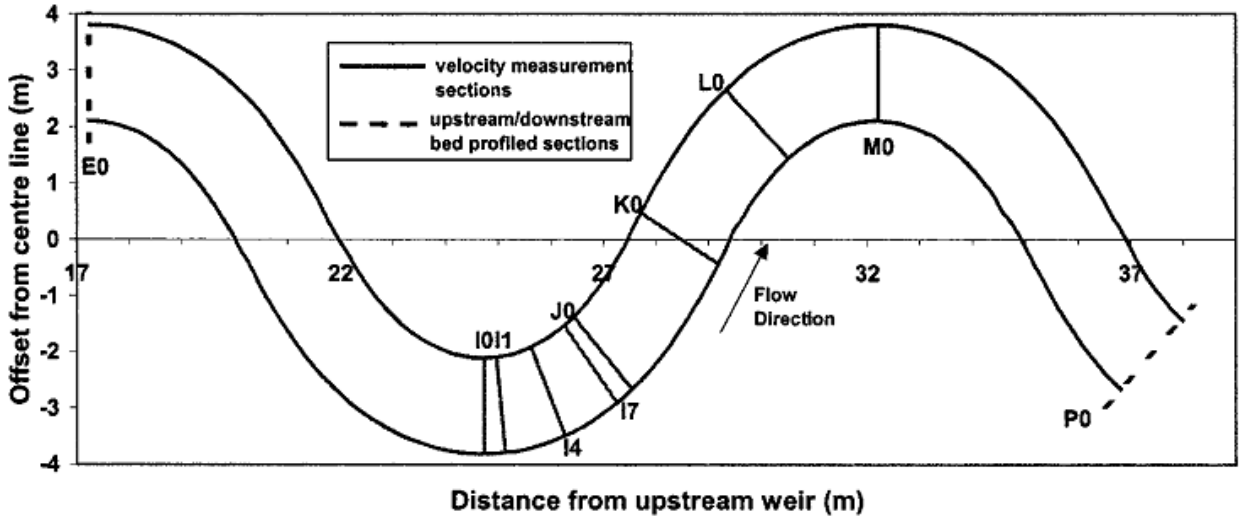

Figure 2.22 Plan view of the flume (from Wilson et al. 2003).

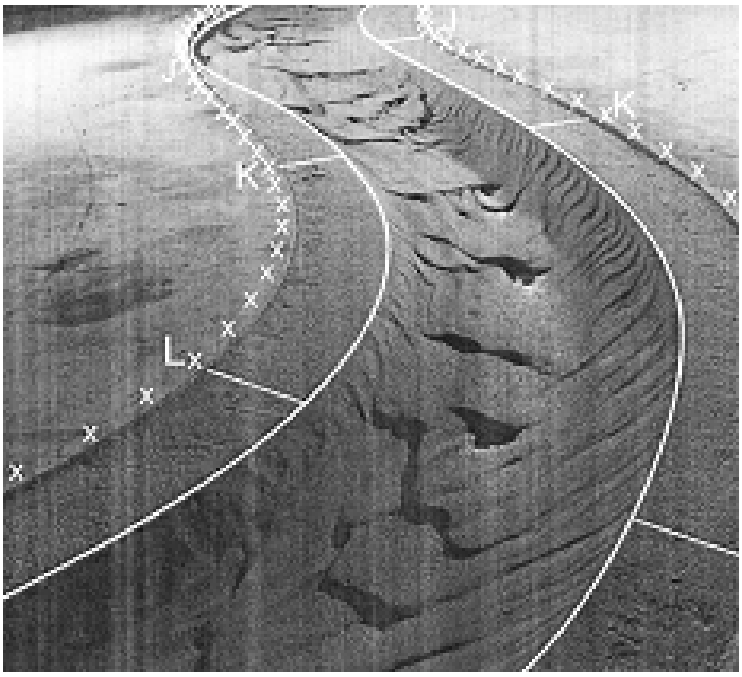

Figure 2.23 Picture of the flume (from Wilson et al. 2003).

Wilson et al. (2003) used three-dimensional finite volume program named SSIIM (Sediment Simulation In Intakes with Multiblock option) that was developed by Olsen of the Norwegian University of Science and Technology (Olsen 2000). The SIMPLE (Semi-Implicit Method for Pressure-Linked Equations) method was used for the coupling of pressure and velocity (Schlichting 1979). This code uses a structured, three-dimensional and non-orthogonal mesh (Wilson et al. 2003). Convergence was checked using the following criteria: "The residuals from continuity, momentum and turbulence equations should not be in excess of 10^{-3}".

Wilson et al. (2003) conducted their numerical study in two stages. The first stage was to calibrate roughness coefficient. The calibration yielded the averaged Manning's coefficient of 0.0137. The second stage was to simulate the presence of secondary flow in a meandering channel. The maximum longitudinal flow velocity was observed at the apex section in cross section I0 due to higher momentum caused by the secondary current. The numerical modeling

results show the presence of the secondary flow in a meandering channel quite well. The simulation result for cross section L0 is shown in Figure 2.24.

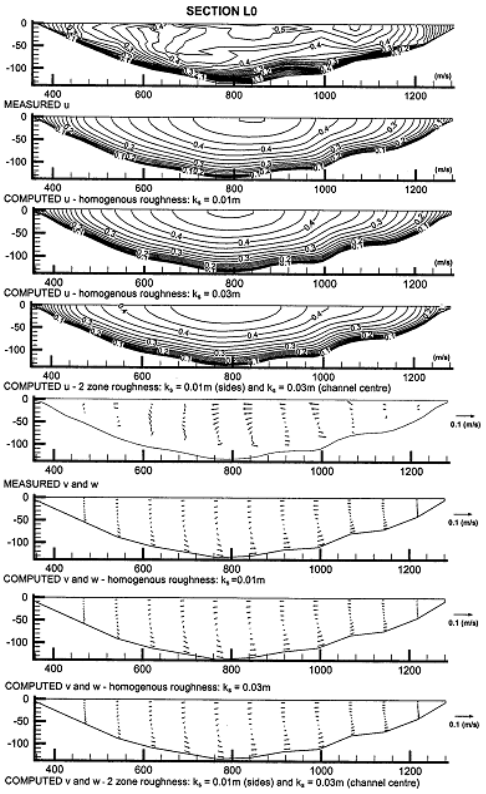

Figure 2.24 Simulation result for cross section L0 (from Wilson et al. 2003).

Rameshwaran and Naden (2005) also conducted three-dimensional numerical modeling of meandering channel flow by solving the three-dimensional Reynolds-averaged continuity and Navier-Stokes equations with the k-ε turbulence model for steady flow. To solve the model equations, a finite volume code was used. The main focus of their study was consideration of free surface flow in a meandering channel. The experimental data to validate the numerical modeling was collected at UK Flood Channel Facility at HR Wallingford. The sketch of the flume is presented in Figure 2.25. The flow rate was 0.0326 m^3/sec. Point gage and Preston tube was used to measure water surface elevation and bed shear stress, respectively. For the measurement of horizontal velocity, miniature propeller meter was used.

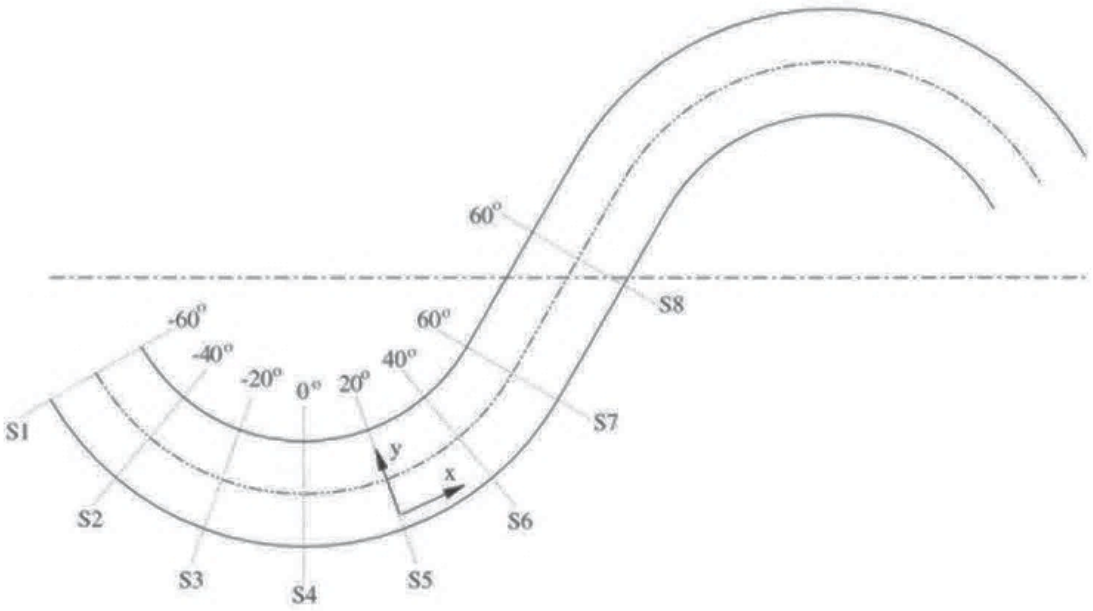

Figure 2.25 Sketch of flume geometry showing channel cross sections (from Rameshwaran and Naden 2005).

To consider super-elevation in a meandering, Rameshwaran and Naden (2005) used pressure distribution at the water surface. Equation 2.13 shows the free surface elevation.

$$\Delta h = \frac{P_f - P_a}{\rho g}, \tag{2.13}$$

where Δh = free surface elevation; P_f is the pressure at surface; and P_a is the atmospheric pressure. The pressure and velocity coupling was done using SIMPLEST algorithm. The numerical simulation result of the free surface profile is shown in Figure 2.26.

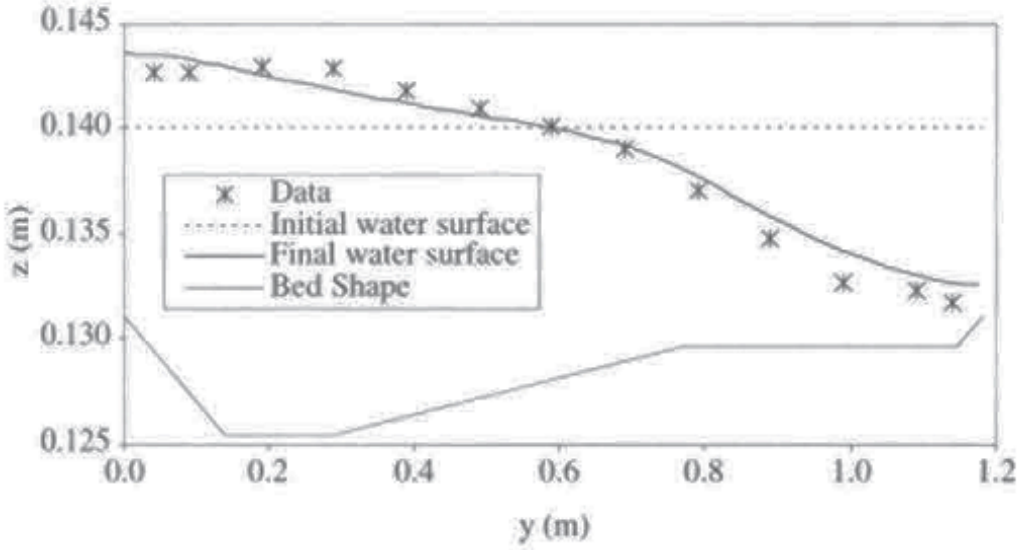

Figure 2.26 Transverse free surface profile at apex cross section (from Rameshwaran and Naden 2005).

Figure 2.26 indicates that the free surface elevation was in good agreement between experimental data and simulation results. That means the consideration of super-elevation of Rameshwaran and Naden (2005) has merit. Furthermore, the bed shear stress presented in Figure 2.27 also shows good agreement between predicted results and measurements. In the Figure 2.27, FST means free surface treatment. The FST for the bed shear stress caused error of bed shear stress about 13.8% with planer surface assumption and 6.2% with the porosity method (Rameshwaran and Naden 2005). They also simulated streamwise flow velocity and transverse velocity. The comparison between the predicted values and measured values is presented in Figure 2.28 and Figure 2.29. The authors argue that the discrepancy was attributed to: a) use of an isotropic turbulence model; and b) measurement error.

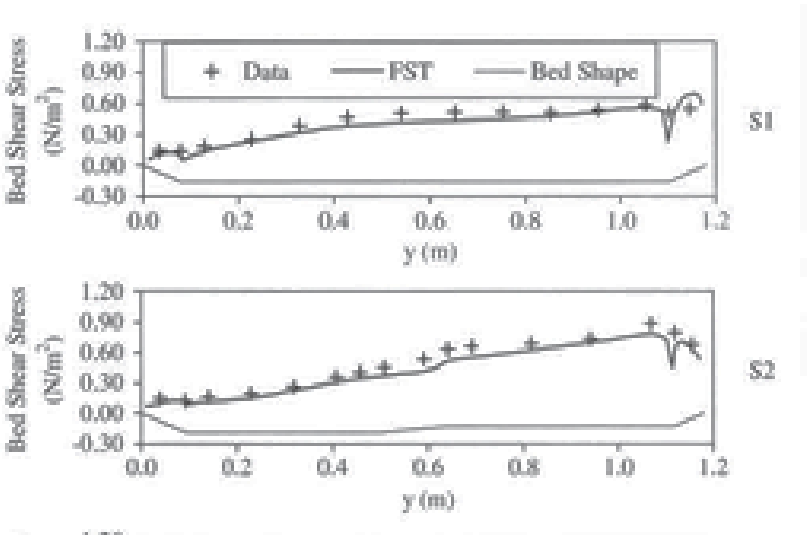

Figure 2.27 Comparisons of bed shear stresses for XS s1 and s2 (from Rameshwaran and Naden 2005).

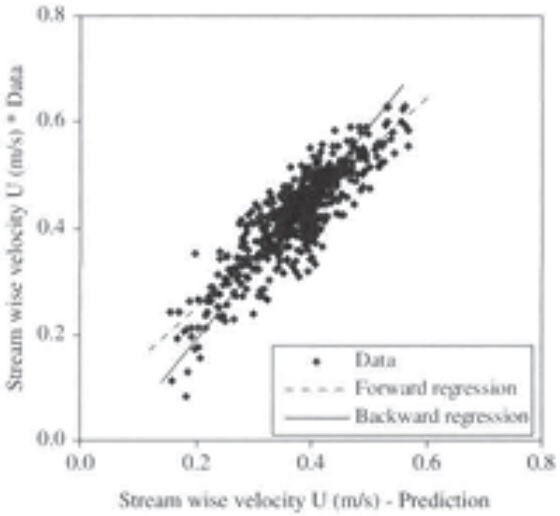

Figure 2.28 Comparisons of streamwise velocity (from Rameshwaran and Naden 2005).

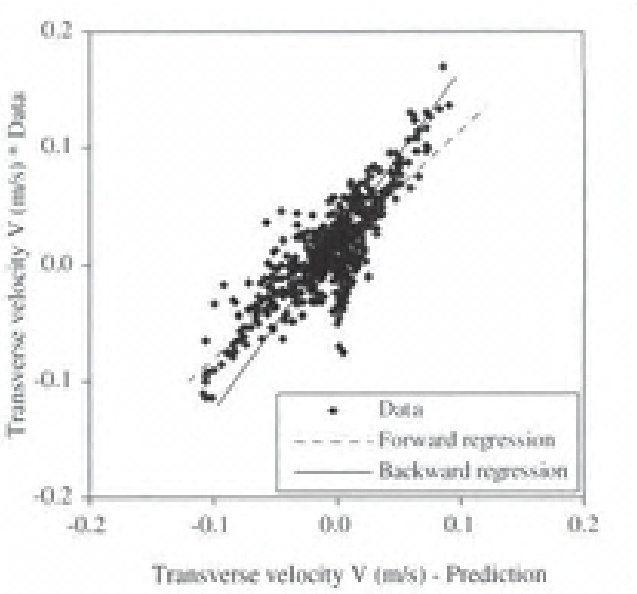

Figure 2.29 Comparisons of transverse velocity (from Rameshwaran and Naden 2005).

Khosronejad et al. (2007) carried out the numerical modeling of flow and sediment transport in channel bend using a laboratory flume. They selected both three-dimensional low-Reynolds number k-ω turbulence model and a standard k-ε turbulence model. To validate the numerical modeling, Khosronejad et al. (2007) used the experimental data of Ghanmi (1999). The plan view of the flume used by Ghanmi (1999) is presented in Figure 2.30. Figure 2.31 and Figure 2.32 show simulation results for the longitudinal and transverse flow velocity components, respectively. Circular dot, solid line and dash line in Figure 2.31 and Figure 2.32 indicate measured value, k-ω model and k-ε model, respectively. These results show that the simulation results using the low-Reynolds number k-ω model has better agreement with experimental data than those obtained from standard k-ε model (Khosronejad et al. 2007). The authors attributed the reason of the higher accuracy of low-Reynolds number k-ω model to its ability to capture wall turbulence better than standard k-ε model. Also, Khosronejad et al. (2007) successfully observed secondary flow using low-Reynolds number k-ω model. Finally, they concluded that low-Reynolds number k-ω model is superior to standard k-ε model.

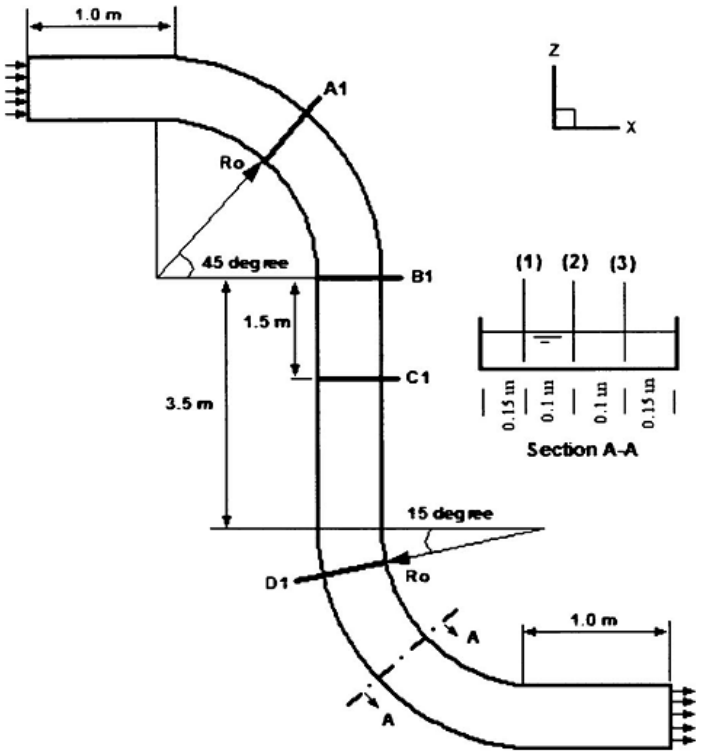

Figure 2.30 Plan view of flume study of Ghanmi (1999) (from Khosronejad et al. 2007).

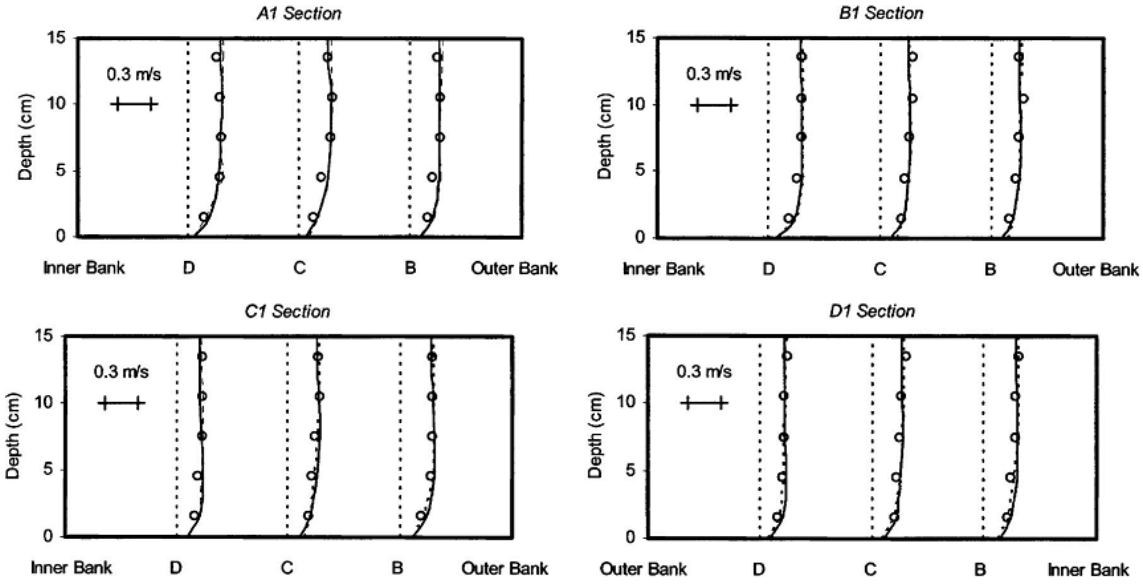

Figure 2.31 Comparison between simulation results and observed values regarding longitudinal flow velocity (from Khosronejad et al. 2007).

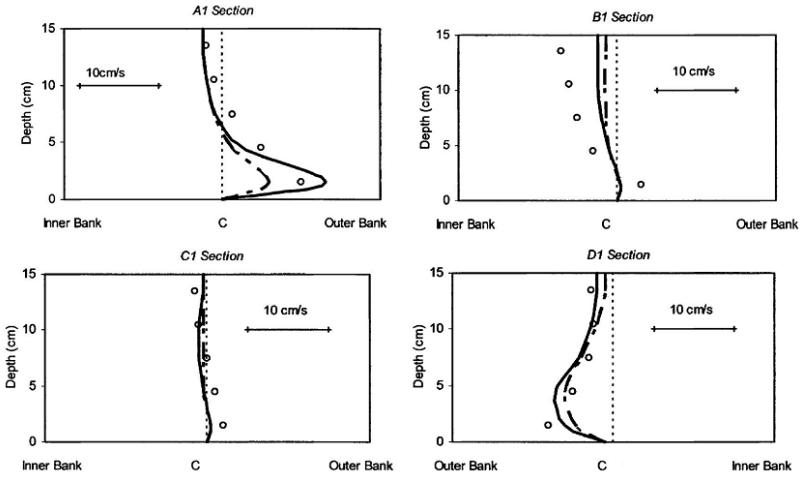

Figure 2.32 Comparison between simulation results and observed values regarding transverse flow velocity (from Khosronejad et al. 2007).

Blanckaert et al. (2009) performed field study, laboratory study and numerical simulation using three-dimensional LES and RANS CFD codes in a curved channel. Additionally, they performed one-dimensional modeling to understand the velocity distribution in a sharp bend. First, they conducted field study at Ledra River presented in Figure 2.33. Three-dimensional ADV (Acoustic Doppler Velocimeter) was used to measure velocity at the six cross sections shown in Figure 2.33 in Ledra River. They then performed an experimental study using a mobile sand bed as well as a fixed sand bed. (Blanckaert et al. 2009) The sketch of the flume for the laboratory study is presented in Figure 2.34. As shown in Figure 2.35, the secondary flow in the bend flow was observed.

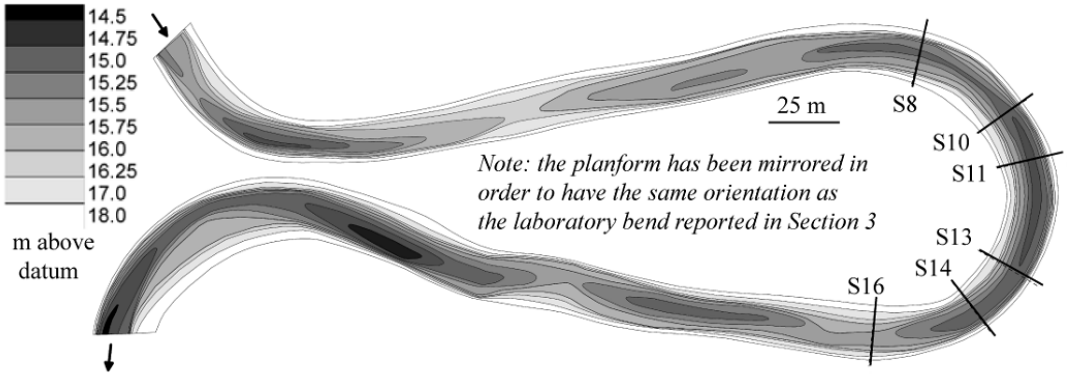

Figure 2.33 Plan view Ledra River (from Blanckaert et al. 2009).

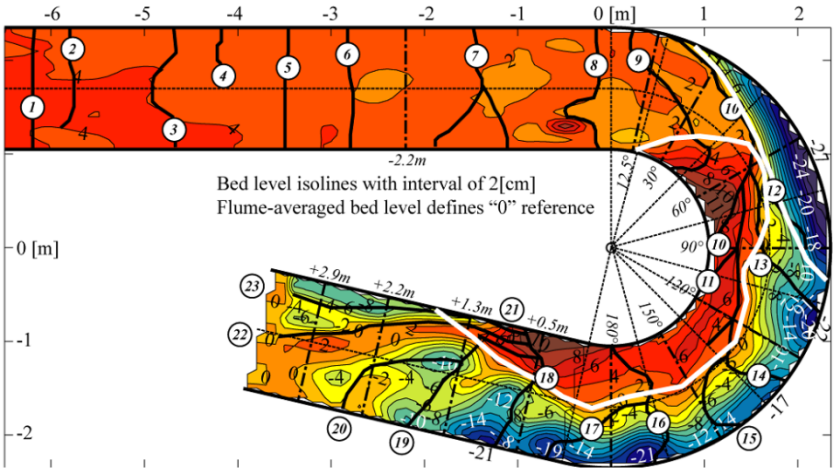

Figure 2.34 Plan view and bed elevation of the flume (from Blanckaert et al. 2009).

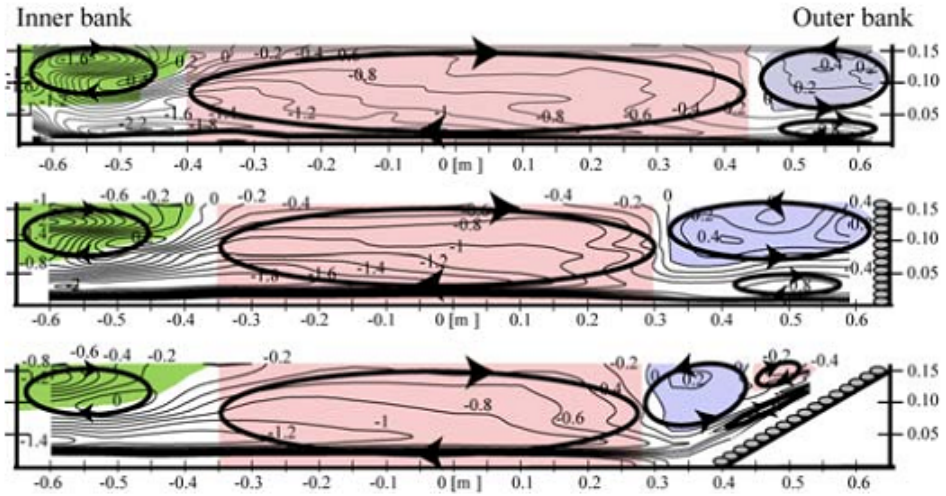

Figure 2.35 Secondary flow in a bend of the flume (from Blanckaert et al. 2009).

The numerical simulation results based on a three-dimensional LES code are reported by van Balen et al. (2009). The numerical results were validated with experimental data of Booij (2003) et al. (The experimental study was introduced in Section 2.2.1.) The validation results are presented in Figure 2.36. Clearly, the LES code shows good agreement with experimental data.

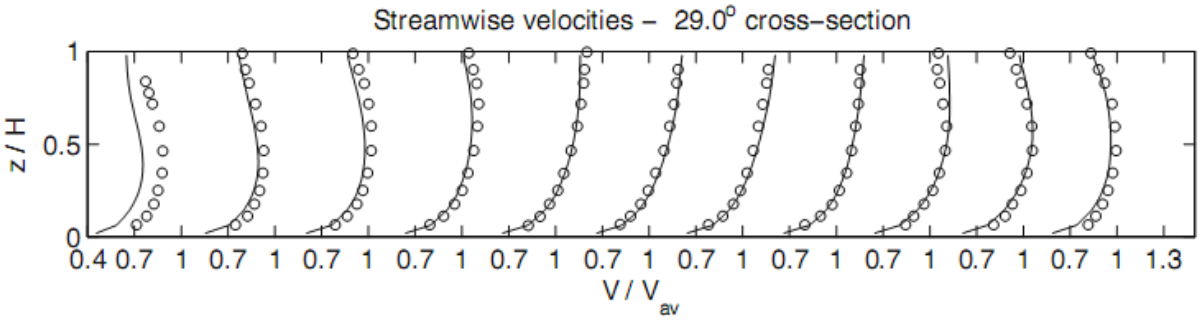

Figure 2.36 Validation of experimental study of Booij et al. (2003) using LES Model (from van Balen 2010).

The measured and simulated velocities are presented in Figure 2.37. The plot on the top, middle and bottom in Figure 2.37 indicate the streamwise, transverse and vertical velocities respectively (Blanckaert et al. 2009). There are notable discrepancies between simulated flow velocities and measured flow velocities because the numerical simulation neglected the effects of dunes in the channel.

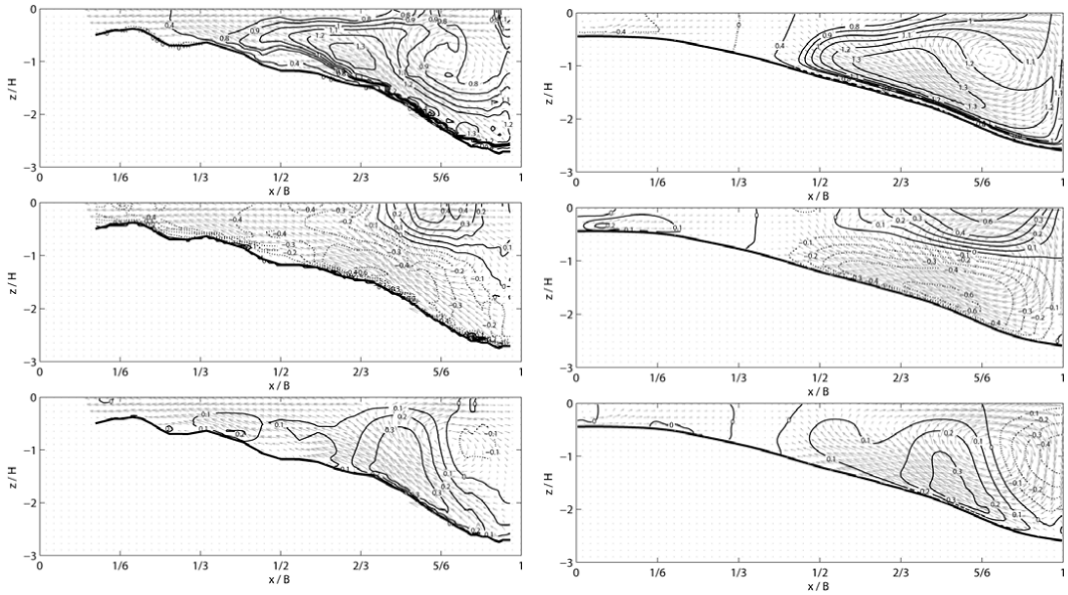

Figure 2.37 Measured flow velocities in 90 degrees in a bend (left) simulated flow velocities using 3D LES codes in 90 degrees in a bend (right) (from van Balen et al. 2009).

Zeng et al. (2010) performed numerical simulation for meandering flow using RANS (Reynolds Averaged Navier-Stokes) model. The simulated properties were flow velocity, water depth, streamwise flow velocity, and bed shear stress. There are two notable points from the work of Zeng et al. (2010). The first point was that the simulations were based on mobile bed topography. Therefore, it was possible to simulate the change in bathymetry. The second notable point was the meandering channel bathymetry used in their simulation was S-shaped channel that is similar to the experimental studies that were conducted at CSU by Heintz (2002). That experimental study prior to that numerical simulation study was performed by Onishi (1972) and Onishi et al. (1976). The schematic sketch of the experimental set up is given in Figure 2.38.

Figure 2.39 shows that the numerical simulation results are in good agreement with the experimental data. (The solid lines are the numerical simulation results in Figure 2.39.) The work of Zeng et al. (2010) proved that the RANS (Reynolds Averaged Navier-Stokes) model can yield good results for simulating meandering flow at a much lower computational cost than LES (Large Eddy Simulations).

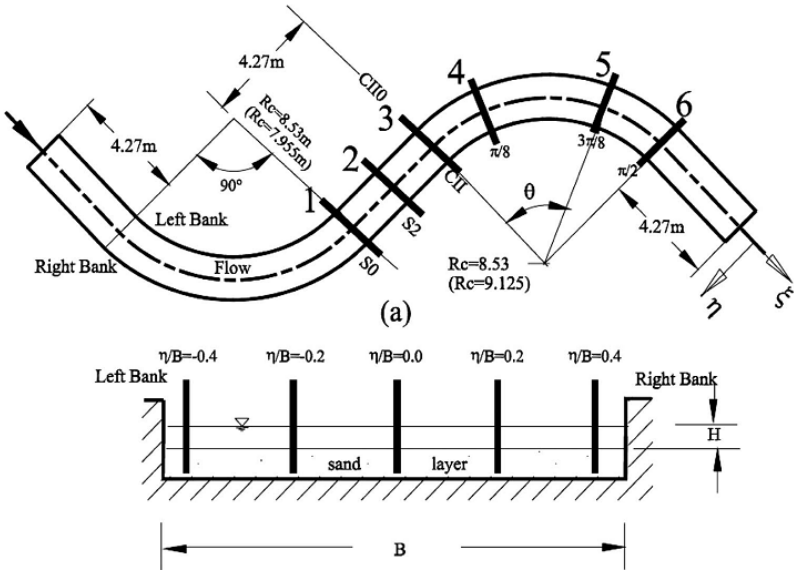

Figure 2.38 Experimental set up for study of Onishi (1972) and Onishi et al. (1976) (from Zeng et al. 2010).

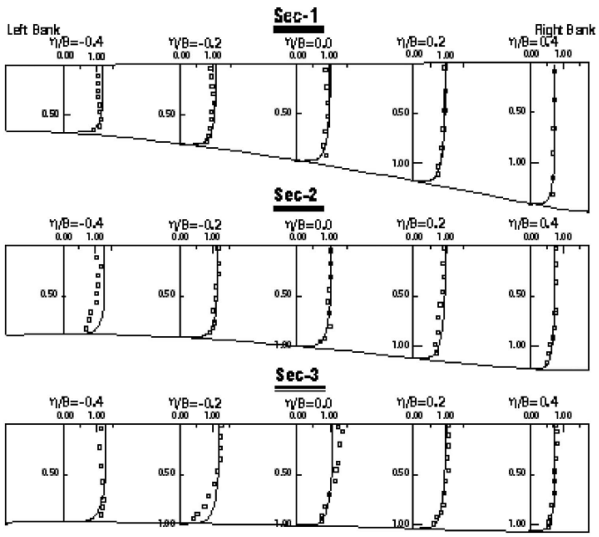

Figure 2.39 Validation of numerical simulation of streamwise flow velocity cross in section 1 through 3 (from Zeng et al. 2010).

Son et al. (2011) performed three-dimensional simulations of meandering flow in natural channel using the RNG (renormalization group theory) k-ε turbulence model. Prior to three-dimensional modeling, Son et al. (2011) conducted two-dimensional numerical simulation using CCHE2D code. The flow domain is portrayed in Figure 2.40. The velocity magnitudes between two-dimensional simulation and measured data at apex sections of the curves; A-A, B-B, and C-C were highly correlated with R^2 values of 0.870, 0.920, and 0.907 respectively.

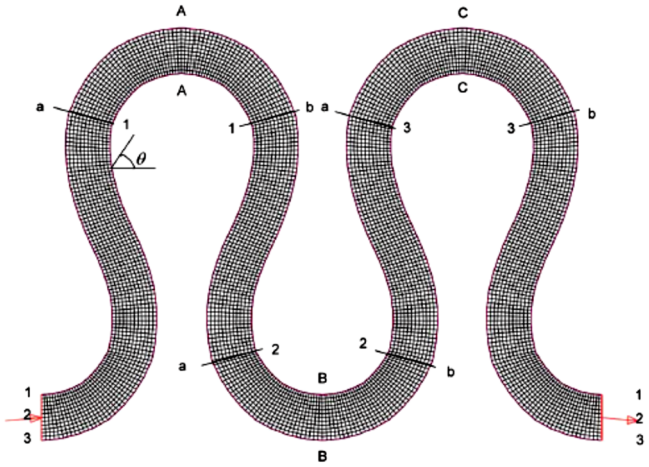

Figure 2.40 Flow geometry for two-dimensional meandering flow simulation (from Son et al. 2011).

Subsequently, Son et al. (2011) performed three-dimensional numerical simulation. They selected the Flow3D CFD code for simulating meandering flow. This is a commercial CFD code that has capacity to simulate free surface change in open channel flow. They performed three-dimensional numerical simulation of meandering flow of a natural channel in South Korea with same boundary conditions with the two-dimensional simulation. Three-dimensional simulation results showed that the flow depths obtained from two-dimensional simulation were higher by up to by 3 percent than three-dimensional simulations.

2.2.2.2 Summary of Numerical Methods

A summary of the relevant numerical studies done previously is presented in Table 2.2.

Table 2.2 Summary table of numerical methods to simulate meandering flow

Researcher	Dimensions of the Model	Model Selection	Simulated Variables	Validation with Field or Laboratory Data
Odgaard (1989)	2D	Numerical	Transverse bed slope	Yes
Jin et al. (1993)	2D	Depth-averaged	Depth-averaged velocity	Yes
Hodskinson and Ferguson (1998)	3D	RNG k-ε model	Flow velocity	Yes
Lien et al. (1999)	2D	Depth-averaged	Velocity ratio across dimensionless channel Width	Yes
Wilson et al. (2003)	3D	Standard k-ε model	Flow velocity	Yes
Rameshwaran et al. (2005)	3D	Standard k-ε model	Transverse free surface profile, bed shear stresses, streamwise velocity and transverse velocity	Yes
Khosronejad et al. (2007)	3D	Low-Reynolds number k-ω model and standard k-ε model	Longitudinal flow velocity, transverse flow velocity, and bathymetry change	Yes
Blanckaert et al. (2009)	3D	LES and RANS Model	Flow velocity, secondary Flow,	Yes
van Balen (2010)	3D	LES	Flow velocity, secondary flow,	Yes
Zeng et al. (2010)	3D	RANS model	Flow velocity, flow depth, change of the bathymetry, bed shear stress	Yes
Son et al. (2011)	2D and 3D	RNG k-ε model	Flow velocity, free surface elevation and shear stress	Yes

2.3 Summary of the Literature Review

Overall, the literature review has shown the promise of using numerical simulations to study meandering flow. However, as pointed out earlier, the effort to understand the interaction between streamwise flow and spanwise flow in meandering channels and their subsequent confluence on boundary shear stresses still remains an open problem. In chapter 3, description of the numerical model and the validation of the model are presented as a first-step towards gaining insights into this complex problem.

Chapter 3. Numerical Model Descriptions and Validations

This chapter presents a description of the numerical framework used in this study together with validation results with an experimental dataset. In particular, details of three-dimensional numerical model for simulating meandering open channel flow will be discussed. This will be followed by a three-dimensional numerical simulation of a previous laboratory scale channel bend flume experiment in order to validate the use of the CFD framework as a suitable tool for the research presented in subsequent chapters.

3.1 Governing Equations

Meandering flow simulation studies are based on fluid flow governing equations (i.e. Navier-Stokes equations) as shown in Equations 3.1 through 3.4. Equation 3.1 describes conservation of mass equation. Equations 3.2 through 3.4 show the momentum equations in the x, y and z directions respectively.

$$\frac{\partial u}{\partial x}+\frac{\partial v}{\partial y}+\frac{\partial w}{\partial z}=0\,, \tag{3.1}$$

$$\frac{\partial u}{\partial t}+u\frac{\partial u}{\partial x}+v\frac{\partial u}{\partial y}+w\frac{\partial u}{\partial z}=g_x-\frac{1}{\rho}\frac{\partial p}{\partial x}+\nu\left(\frac{\partial^2 u}{\partial x^2}+\frac{\partial^2 u}{\partial y^2}+\frac{\partial^2 u}{\partial z^2}\right), \tag{3.2}$$

$$\frac{\partial v}{\partial t}+u\frac{\partial v}{\partial x}+v\frac{\partial v}{\partial y}+w\frac{\partial v}{\partial z}=g_y-\frac{1}{\rho}\frac{\partial p}{\partial y}+\nu\left(\frac{\partial^2 v}{\partial x^2}+\frac{\partial^2 v}{\partial y^2}+\frac{\partial^2 v}{\partial z^2}\right), \tag{3.3}$$

$$\frac{\partial w}{\partial t}+u\frac{\partial w}{\partial x}+v\frac{\partial w}{\partial y}+w\frac{\partial w}{\partial z}=g_z-\frac{1}{\rho}\frac{\partial p}{\partial z}+\nu\left(\frac{\partial^2 w}{\partial x^2}+\frac{\partial^2 w}{\partial y^2}+\frac{\partial^2 w}{\partial z^2}\right), \tag{3.4}$$

where u = the x-axis velocity; v = y-axis velocity; w = z-axis velocity; g_x = acceleration of gravity in x- axis direction; ρ = mass density of fluid; and ν = kinematic viscosity of fluid.

A direct numerical simulation (DNS) of the Navier-Stokes equation is prohibitively expensive for practical engineering problems (Pope 2000). As such, the Reynolds-averaged Navier-Stokes (RANS) equations are widely used to study engineering problems. The RANS equations involve time-averaging of the time-dependent fluctuating velocity and pressure fields using the so-called Reynolds decomposition. The RANS equations are given by in tensor notation:

$$\frac{\partial \overline{u_i}}{\partial x} = 0, \tag{3.5}$$

$$\frac{\partial \overline{u_i}}{\partial t} + \overline{u_j}\frac{\partial \overline{u_i}}{\partial x_j} = -\frac{1}{\rho_o}\frac{\partial \overline{p}}{\partial x_i} + \frac{\partial}{\partial x_j}\left(\nu\frac{\partial \overline{u_i}}{\partial x_j} - \overline{u_i' u_j'}\right), \tag{3.6}$$

where, $\overline{u_i}$ = the time-averaged velocity field; $\overline{p}$ = the average pressure; and $\overline{u_i' u_j'}$ = the Reynolds stress tensor. The Reynolds stresses are additional unknowns for which various so-called turbulence models can provide different levels of closure. The simplest turbulence model is the eddy viscosity model, which is discussed next in the context of the two-equation *k-ε* turbulence model.

3.2 RNG k-ε Turbulence Model

In this study, a comprehensive literature review (presented in Chapter 2) of numerical simulations of meandering channel flow was performed and it was determined that the RNG (The Renormalization Group) *k-ε* turbulence model would be the right choice based on its good performance to simulate meandering flow (see for example studies by Hodskinson et al. 1998 and Son et al. 2011). RNG *k-ε* turbulence model was derived mathematically by Lam (1992). The reader is referred to literature of Lam (1992) and Yahhot et al. (1992) for more details. Equation 3.7 through Equation 3.11 are the RNG *k-ε* model equations (Versteeg et al. (2007)).

$$\frac{\partial(\rho k)}{\partial t}+\nabla\cdot(\rho kU)=\nabla\cdot\left[\alpha_k\mu_{eff}\nabla k\right]+\mu_t S_{ij}-\rho\varepsilon \ , \tag{3.7}$$

$$\frac{\partial(\rho\varepsilon)}{\partial t}+\nabla\cdot(\rho\varepsilon U)=\nabla\cdot\left[\alpha_\varepsilon\mu_{eff}\nabla\varepsilon\right]+C_{1^*\varepsilon}\frac{\varepsilon}{k_t}\tau_{ij}\cdot S_{ij}-C_{2\varepsilon}\rho\frac{\varepsilon^2}{k} \ , \tag{3.8}$$

$$\tau_{ij}=-\rho\overline{u_i'u_j'}=2\mu_t S_{ij}-\frac{2}{3}\rho k\delta_{ij} \ , \tag{3.9}$$

$$\mu_{eff}=\mu+\mu_t \ , \tag{3.10}$$

$$\mu_t=\rho C_\mu\frac{k^2}{\varepsilon}, \tag{3.11}$$

where C_μ =0.0845, $\alpha_k = \alpha_\varepsilon$ =1.39, $C_{1\varepsilon}$ =1.42, $C_{2\varepsilon}$ =1.68, $C_{1^*\varepsilon}=C_{1\varepsilon}-\frac{\eta(1-\eta/\eta_0)}{1+\beta\eta^3}$,

$\eta=\frac{k}{\varepsilon}\sqrt{2S_{ij}\cdot S_{ij}}$, and $\beta=0.012$.

3.3 Wall Functions of Ansys Fluent

A key issue for wall-bounded turbulent flows is sufficient grid resolution in the near-wall region to ensure that the large velocity gradients in velocity are accurately captured. Figure 3.1 shows the subdivisions of the near–wall region. The nondimensional wall normal distance is usually expressed as y^+ value given by:

$$y^+\equiv\frac{\rho u_* y}{\mu}, \tag{3.12}$$

where, ρ = mass density of fluid, u_* is shear velocity defined as $\sqrt{\frac{\tau}{\rho}}$, and τ is shear stress.

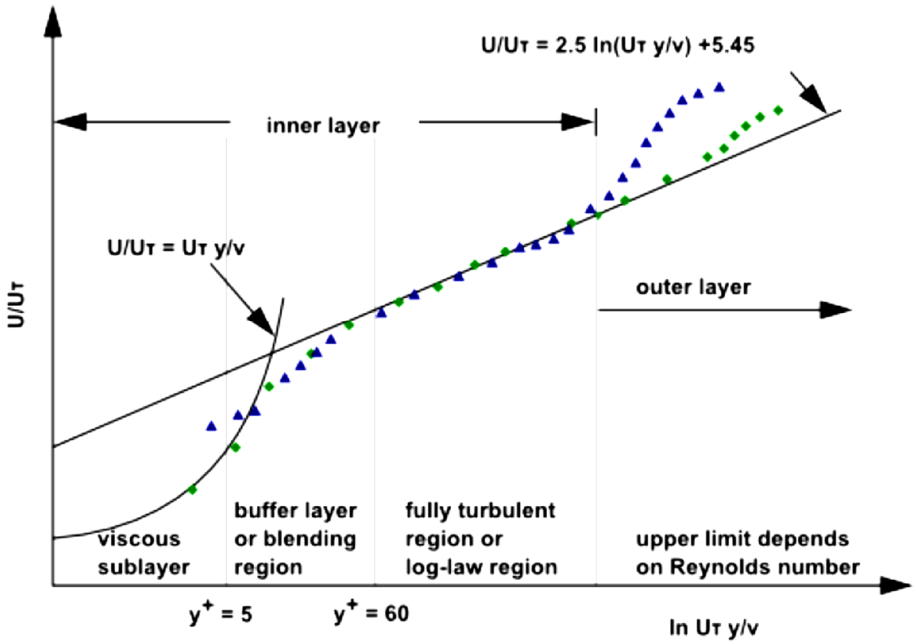

Figure 3.1 Subdivision of the Near-Wall Region (from Ansys 2012).

When wall functions are used in conjunction with the logarithmic law (law-of-the-wall), the value of y^+ must be greater than 15 to ensure that the simulations start in the logarithmic region of the boundary layer and obtain accurate prediction of wall shear stress (Ansys 2012). The minimum number of cells recommended in the boundary layer for accurate modeling of the turbulence model is about 10 but a higher value of say 20 is better in order to obtain desirable simulation results (Ansys 2012a).

Ansys Fluent provides the following options to select wall functions: 1) standard, 2) scalable, 3) non-equilibrium, 4) enhanced wall functions, and 5) user defined wall functions. This study selected standard wall functions for turbulence modeling. More details on wall functions are provided in the text by Pope (2000). Fluent uses log-law function when y^+ value is greater than 11 and Fluent employs laminar stress-strain relationship when y^+ value is less than 11. y^+ and U* value are defined using Equation 3.13 and Equation 3.14 in Fluent.

$$y^{+} \equiv \frac{\rho C_{\mu}^{1/4} k_p^{1/2} y_p}{\mu}, \tag{3.13}$$

$$U^{*} \equiv \frac{U_p C_{\mu}^{1/4} k_p^{1/2}}{\tau_w / \rho}, \tag{3.14}$$

where ρ = mass density of fluid; k_p = turbulence kinetic energy at the near-wall node P; y_p = distance from point P to the wall; μ = dynamic viscosity of fluid; U_p = mean velocity of the fluid at the near-wall node P; and τ_w =shear stress.

3.4 Free Surface Model of Fluent: VOF (Volume of Fluid) Model

Ansys Fluent provides the free surface simulation tool known as VOF (Volume of Fluid). The VOF model has a capacity to simulate multiple types of fluids. In this study, the VOF technique will be used to simulate both water and air in order to simulate open channel flow in curved channels. Equation 3.15 is the volume fraction equation:

$$\frac{1}{\rho_q}\left[\frac{\partial}{\partial t}\left(\alpha_q \rho_q\right) + \nabla \bullet \left(\alpha_q \rho_q \vec{v}_q\right) = S_{\alpha_Q} + \sum_{p=1}^{n}\left(\dot{m}_{pq} - \dot{m}_{qp}\right)\right], \tag{3.15}$$

where, $\dot{m}_{pq}$ = the mass transfer from phase q to phase p, and $\dot{m}_{qp}$ = the mass transfer from phase p to phase q. The default value of the term, S_{α_Q} is zero (Ansys 2012a).

3.5 Numerical Schemes for Numerical Simulations

Selecting proper schemes for discretizing and solving the Reynolds-averaged Navier-Stokes (RANS) equations is important in order to obtain accurate results from numerical simulations. For the pressure and velocity coupling, the 'SIMPLE' (Semi-Implicit Method for Pressure-Linked Equations) algorithm was selected. This algorithm was suggested by Patankar

and Spalding (1972) and shown to yield good convergence. Versteeg et al. (2007) explained "the SIMPLE algorithm is guess-and-corrected procedure for the calculation of pressure on the staggered grid arrangement". The reader is referred to Versteeg et al. (2007) for more details of the SIMPLE scheme.

For discretization of spatial gradients, Ansys Fluent provides three different options; 1) Green-Gauss Cell-Based; 2) Green-Gauss Node-Based; and 3) Least Squares Cell-Based. For this research, 'Least Squares Cell-Based' method was selected due to its best performance. For discretization of pressure, two options are available if VOF technique was used for simulating open channel flow; 1) PRESTO! (PREssure Staggering Option) scheme; and 2) body force weighted scheme. In this study, the body force weighted scheme was selected for simulating curved channel flow. To discretize spatially momentum, volume fraction, turbulent kinetic energy, and turbulent dissipation rate, 'QUICK' (Quadratic Upstream Interpolation for Convective Kinetics) method was used all of the other spatial discretization methods because Ansys (2012a) explained that "the QUICK scheme will show the better performance if the grid is structured aligned with the flow direction. The reader is also referred to Versteeg et al. (2007) and Ansys (2012a) to access the details of the QUICK scheme.

3.6 Optimizing Under Relaxation Factors

Under relaxation factors were set to guarantee convergence of the numerical model. Versteeg et al. (2007) explained that excessive value of the under relaxation factor causes the divergence of numerical model. On the other hand, too small a value can result in the demand of high computational cost (Versteeg et al. (2007)). Optimization of under relaxation factor is dependent on the particular flow case (Versteeg et al. (2007)). As a result, trial and error method

was used for negotiating stability of the numerical model and computational cost. The optimized under relaxation factors are summarized in Table 3.1.

Table 3.1 Summary of optimized under relaxation factors

	Pressure	Density	Body Forces	Momentum	Turbulent Kinetic Energy	Turbulent Dissipation Rate	Turbulent Viscosity
Default Value	0.3	1	1	0.7	0.8	0.8	1
Optimized Value	0.25	1	1	0.3	0.4	0.4	1

3.7 Initial and Boundary Conditions

The mass flow inlet boundary condition was selected at the inlet of the computational domain. The mass flow rate of water was 0.057 m^3/s (2 ft^3/s) and mass flow rate for air was calculated by subtracting the area of water flow from the whole cross section of the channel inlet. The pressure outlet boundary condition was chosen at the outlet in order to define the static pressure using the free surface elevation. The turbulence intensity was specified at the inlet and outlet of the flow domain based on recommendations in Ansys (2012b) and are calculated using Equation 3.16 through Equation 3.18.

$$DH = \frac{4A}{P}, \tag{3.16}$$

$$\mathrm{Re}_{DH} = \frac{DH \times V}{\nu}, \tag{3.17}$$

$$I \equiv \left(0.16 \times \left(\mathrm{Re}_{DH}\right)^{\frac{-1}{8}}\right) \times 100(\%), \tag{3.18}$$

where, DH = hydraulic diameter (ft), A = flow area (ft^2), P = wetted perimeter (ft), Re_{DH} = Reynolds number at the depth of hydraulic diameter, ν = kinematic viscosity of water (1.06×10^{-5} ft^2/sec), and I = turbulent intensity (%).

The boundary condition at the bed of the channel was assumed as a no-slip boundary condition and specified as solid walls. To set bed roughness, Fluent provides an option to set roughness height. Moody (1944) was referred for setting roughness height on the bed of the channel. Ippen et al. (1962a) explained that the Manning's roughness coefficient in their flume study was measured as 0.01 and hence corresponds to 'very smooth' concrete finish. According to the recommendation of Moody (1944), the roughness height of 'very smooth' concrete for designing duct flow was 0.04 mm. Therefore, roughness height of 0.04 mm was used for setting roughness of the channel bed. At the top of the flow domain, a symmetry boundary condition was used to establish an impermeable plate. The initial condition was assumed to quiescent flow. Every initial value was set as zero except for the longitudinal flow velocity to start simulation.

3.8 Validations of the Numerical Model

Before embarking on a detailed investigation, a careful validation of the CFD simulation is necessary. To this end, the experimental flume study of Ippen et al. (1962a) on meandering flow at MIT (Massachusetts Institute of Technology) was used. This study has a well-documented dataset of flow velocity, water surface elevation and shear stress.

3.8.1 Description of Flow Geometry

The flume geometry of Ippen et al. (1962a) is portrayed in Figure 3.2. The flume composed of two straight concrete sections and a curved concrete section. The length of the straight section from the inlet to curved section is 5.334 m (17.5 ft) (cross section 1 through 3) and four cross sections are located in curved section (cross section 4 through 7). The downstream straight section is 10 ft (3.048 m) (from cross section 8 through 10 and outlet). A Sluice gate at the outlet was installed to control flow at the outlet (Ippen et al. 1962a). The cross sectional

shape is trapezoidal and the side slope of the channel cross section was 1:2 (vertical to horizontal). The bottom width of the channel was 0.61 m (2 ft) and the depth of the channel was 20.32 cm (8 in). The bed slope of the flume was surveyed and documented as 0.00064 m/m. The Manning's roughness coefficient was 0.010 (Ippen et al. (1962a)).

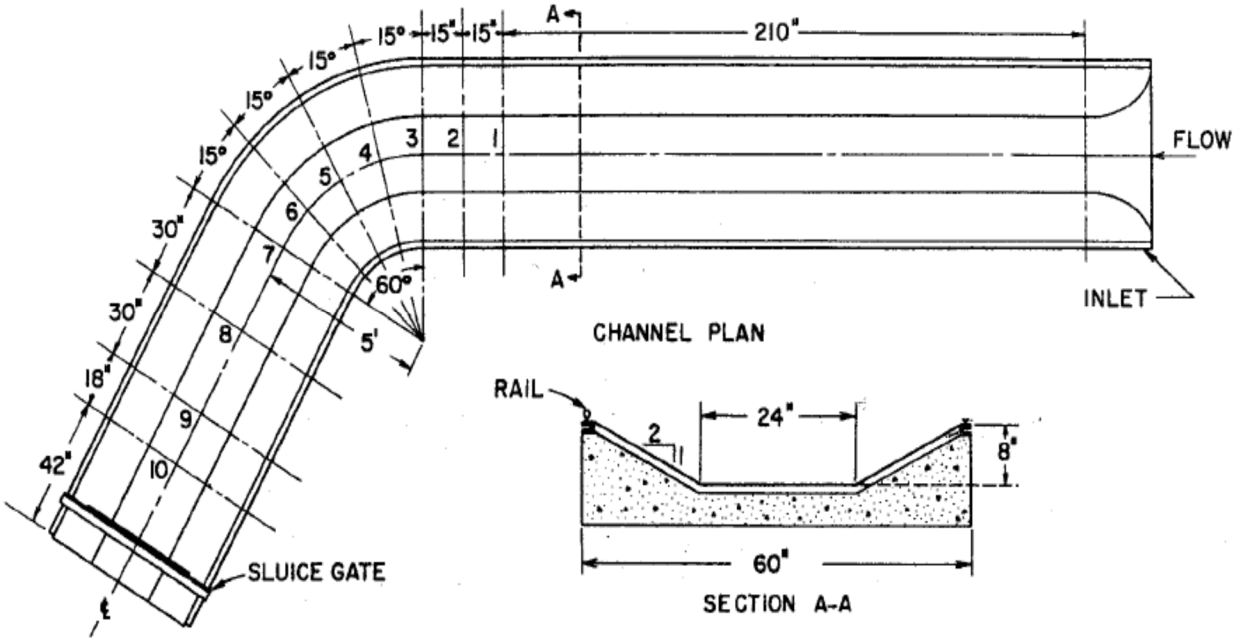

Figure 3.2 Sketch of Ippen et al. (1962a) flume for experimental study (from Ippen et al. (1962a)).

3.8.2 Instrumentation and Data Collections

Ippen et al. (1962a) collected the following data during experimental study; 1) flow velocity data; 2) water surface elevation; and 3) shear stress. To measure flow velocity, 0.794 cm (5/16 in) diameter Prandtl tube was used (Ippen et al. (1962a)).

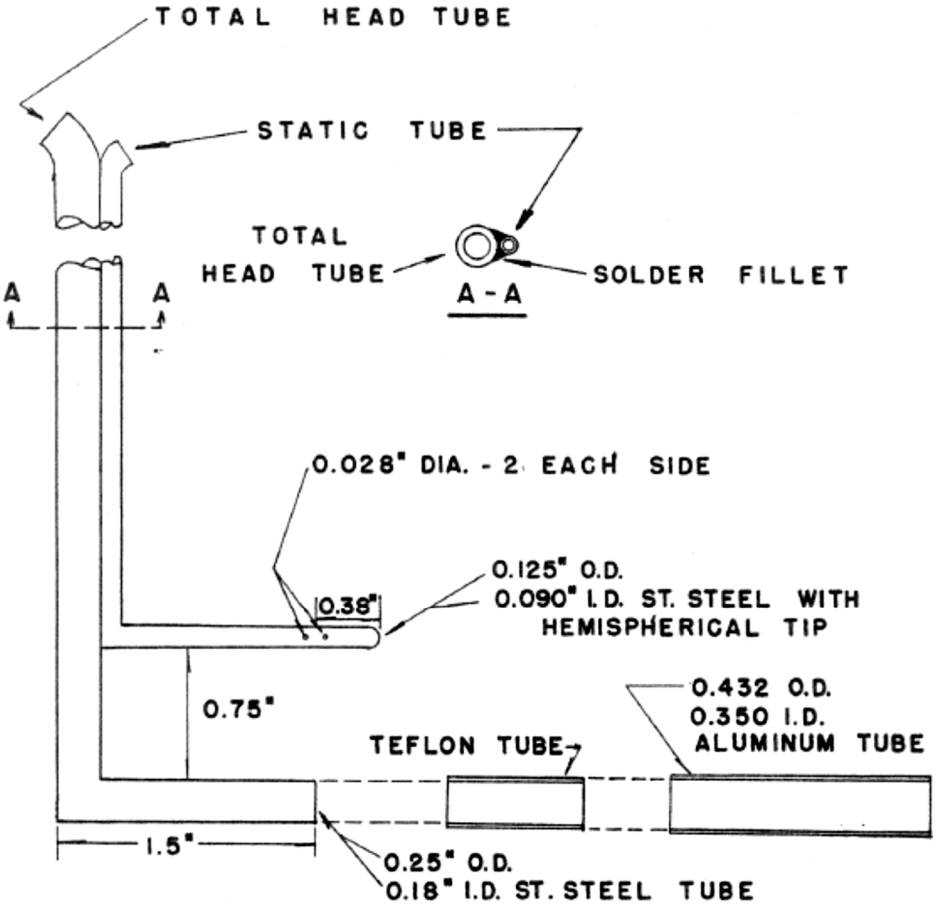

Figure 3.3 The sketch of Pitot tube used for data collection (from Ippen et al. 1962a).

For water surface elevation measurement, a point gauge was used. Ippen et al. (1962a) used surface Pitot tube measurement technique based on the change of dynamic pressure on the channel bed developed by Preston (1954) to measure the bed shear stress.

3.8.3 Mesh Generation

Ansys Design Modeler software was used for mesh generation. The coordinates of the four vertices in each cross section were calculated for all of the cross sections including inlet and outlet of the flume. After creation of the vertices, lines and surfaces were created by connecting vertices. Finally, the volume mesh was generated. To check mesh quality, skewness of each mesh was checked. Ansys (2009) defined the skewness as "Skewness is a measure of the relative distortion of an element compared to its ideal shape". The skewness ranges between zero to one and the maximum acceptable value of skewness is 0.95. If skewness value is close to zero, the quality of mesh is excellent and vice versa. The maximum skewness value for the mesh generated for this validation study was 0.799. The number of cells used was 388,236 and were hexahedral (structured) in shape. The other criterion to judge mesh quality is aspect ratio that is defined as the ratio of the longest side of the grid to the shortest side of the grid. Ansys (2009) recommended the maximum aspect ratio should be less than 40. The maximum value of aspect ratio for this validation study was 29.88.

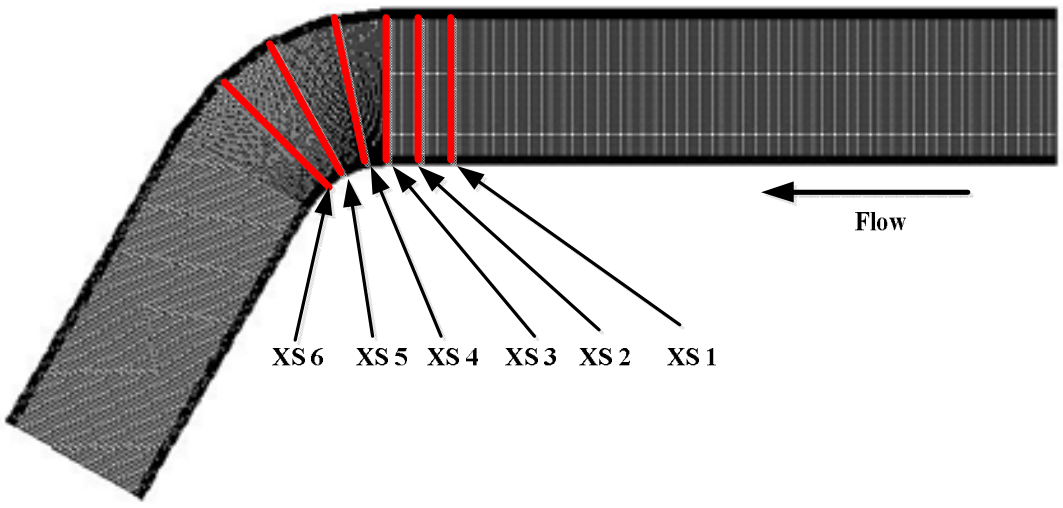

Figure 3.4 Mesh for validating data of Ippen et al. (1962a) (flow: from right to left).

3.8.4 Validations using Experimental Data

The total simulation flow time was 120 seconds. A time step size of 0.01 second was used. The reason for selecting such a small time step size was to ensure that numerical simulation was stable and the duration of flow simulation was selected to satisfy the conservation of mass. The numerical simulation results of flow velocity and shear stress were compared with experimental data of Ippen et al. (1962a) as shown in Figure 3.5.

The three cross sections (XS 4, 5, and 6) in the curved bend were selected for the validation because that is the main interest for this study. The flow velocity comparisons shown in the left panel of Figure 3.5 indicate very good agreement with the experimental data. The right panels ((d), (e), and (f)) in Figure 3.5 show the comparison of the shear stress data with numerical simulation results. There are some discrepancies between the numerical simulation and experimental data.

Table 3.2 summarizes the magnitude of maximum shear stress obtained from experimental data and numerical simulation. The magnitudes between experimental data and numerical simulation results are reasonably close with a maximum difference of 17%.

Table 3.2 Summary of maximum shear stress (Pa)

Cross section	Maximum shear stress (Pa) from experimental data	Maximum shear stress (Pa) from numerical simulation	Percentage differences (%)
4	0.613	0.735	-16.60
5	0.613	0.695	-11.80
6	0.674	0.640	5.31

The water surface elevations results are portrayed in Figure 3.6. The red line in Figure 3.6 is the measured water surface elevation using a point gauge and the blue line in Figure 3.6 is the simulated water surface elevation. Figure 3.6 clearly shows the simulated water surface elevation

agrees well with measured water surface elevation data within 3 percent. Figure 3.6 also shows that numerical simulation captures the super-elevation that is a key characteristic of curved flow.

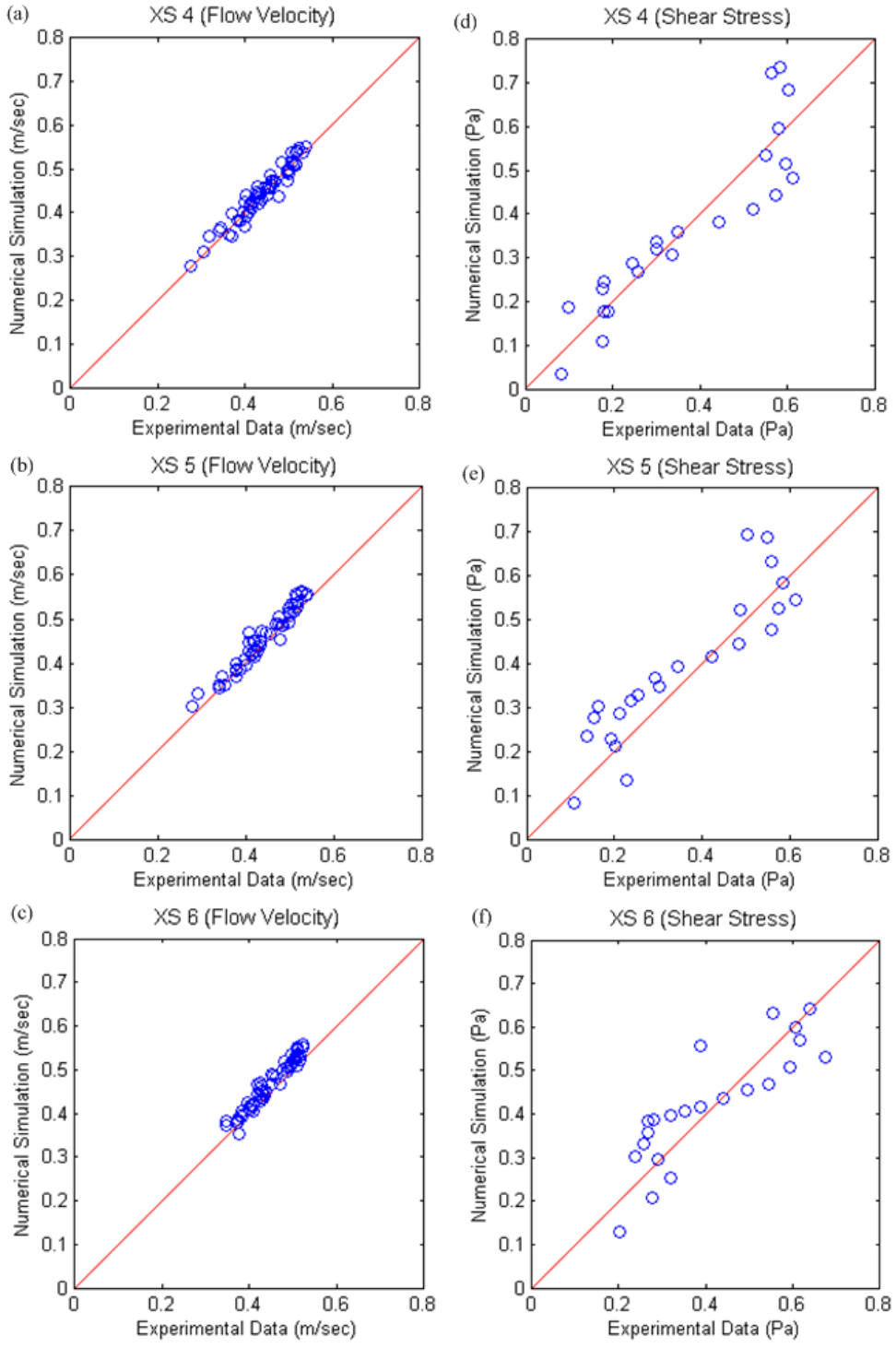

Figure 3.5 Ippen et al. (1962) validation results (flow velocity magnitude (m/sec) ((a), (b), and (c)) and shear stress (Pa) ((d), (e), and (f)).

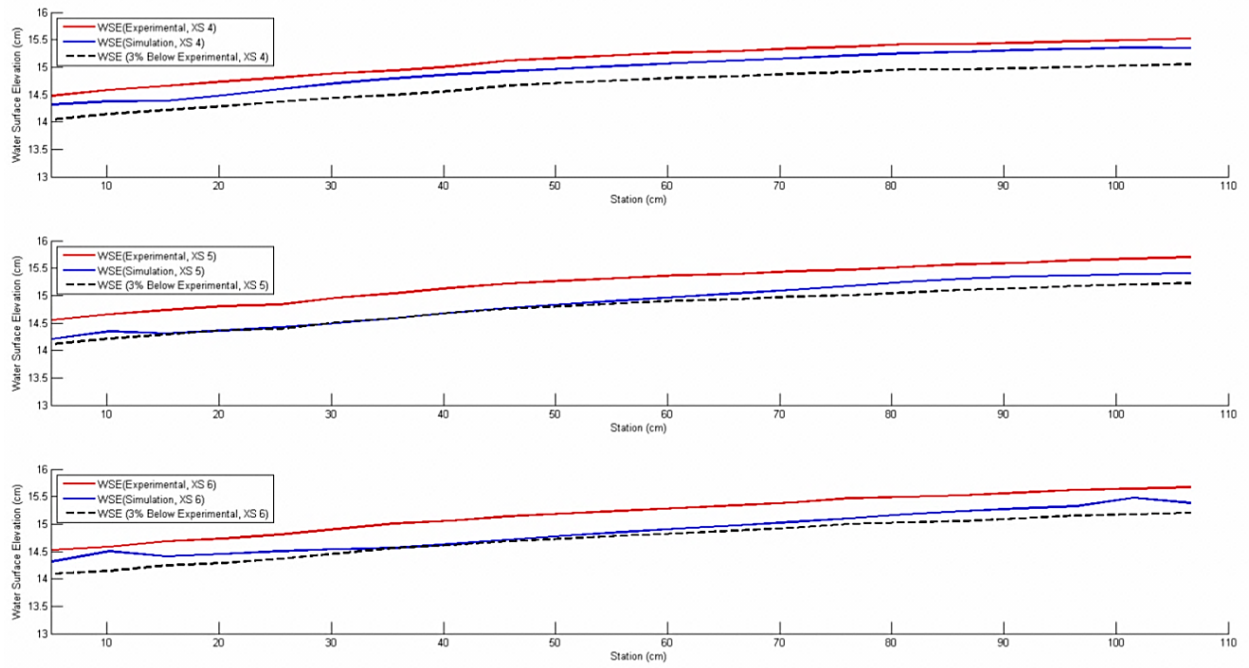

Figure 3.6 Ippen et al. (1962) validation of water surface elevations (cm) (a): water depth of cross section 4, (b): water depth of cross section 5, and (c) water depth of cross section 6).

3.8.5 Reproduction of the Secondary Flow

A key phenomenon in meandering flows is the occurrence of secondary circulation. Secondary flow results from the imbalance between centrifugal force and differential hydrostatic force. The net balance between centrifugal force and hydrostatic force is higher at the bed of the channel and lower close to the water surface. As a result, a circular flow is generated in channel bends. Figure 3.7 shows the secondary flow was observed at the outer bank of cross section 4.

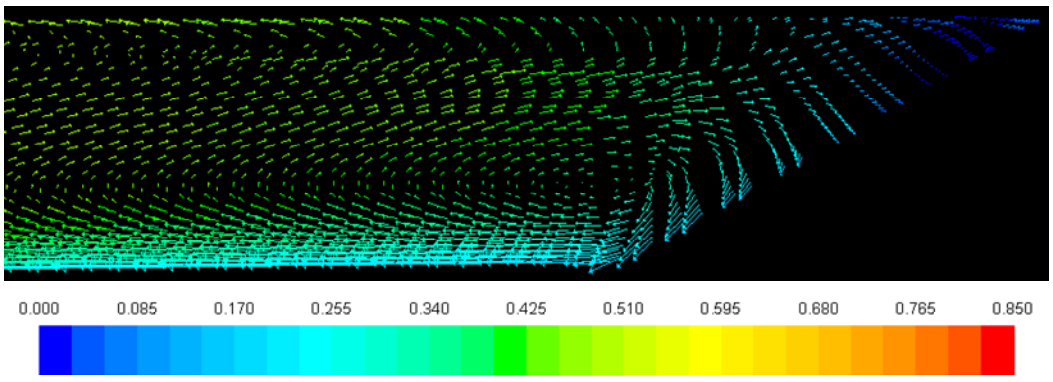

Figure 3.7 Flow velocity vector (m/sec) plot outer bank of cross section 4 shows secondary current (flow: directed to the wall).

3.8.6 Distribution of Y Plus Value

As described in section 3.3, it is important to that the y^+ values are in the proper range in order to obtain good numerical simulation results. Figure 3.8 shows the contour plot of y^+ distribution obtained from numerical simulation. As shown in Figure 3.8, the maximum y^+ value was about 38 and lower y^+ value ranged above 15. This result shows that the mesh used for the numerical simulation was appropriate.

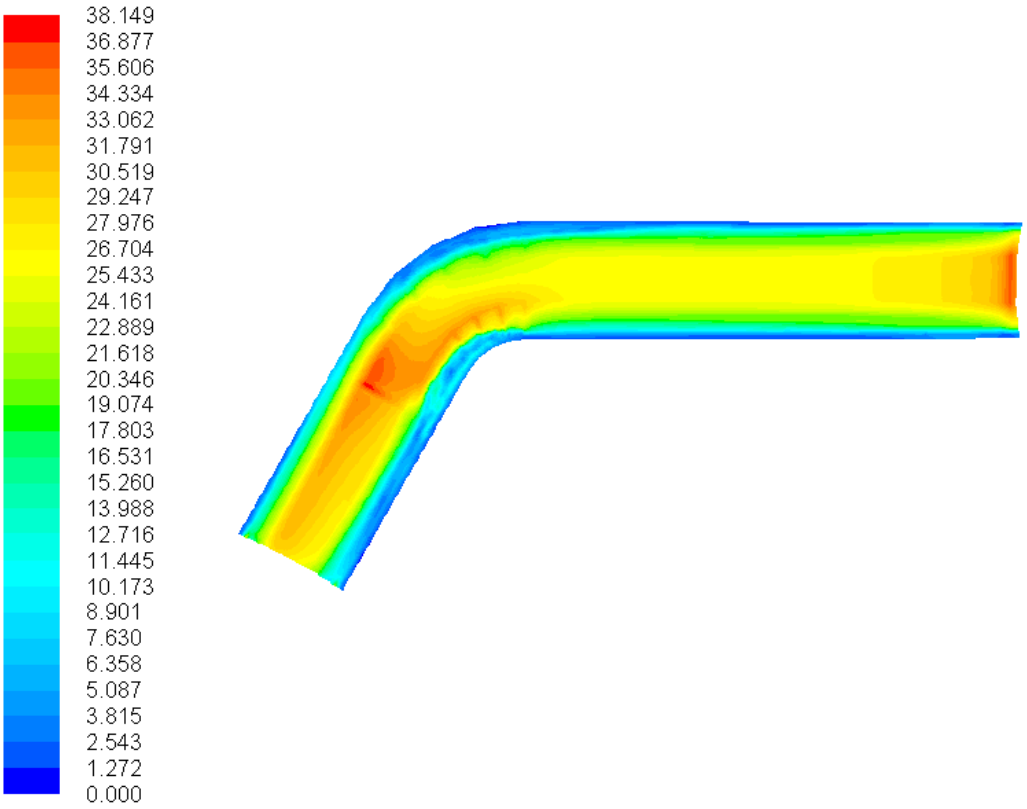

Figure 3.8 Contour of y^+ value (dimensionless) from numerical modeling.

3.9 Summary of Chapter 3

This chapter described the governing equations of three-dimensional numerical simulation for meandering flow and validation. The RNG k-ε turbulence model was selected due to its superior performance for rotational flows compared to the standard k-ε turbulence model based on previous studies. The Ansys Fluent CFD code was selected to study flow around bends based on its ability to capture key physics of meandering flow such as the super-elevation effect and secondary flow in curved channels.

A validation was conducted using the dataset of Ippen et al. (1962b). The validation results showed that the numerical simulation results are in good agreement the experimental data for flow velocity and water surface elevation. Some slight discrepancies were observed for the shear stress comparisons. The numerical model also successfully reproduced the secondary flow that is one of the most representative phenomena in curved channel flows.

The next chapter will focus on elucidating the effect of the free surface in a curved channel flow and highlight the drawback of using the rigid-lid assumption in CFD simulations.

Chapter 4. Implications for Neglecting Free-Surface Effects in Numerical Simulations of Flow in Curved Channels[1]

4.1 Introduction

Understanding the flow dynamics in curved channel bends is important given the ubiquitous presence of meanders in rivers. Studying flow characteristics in a curved channel is a complex problem mainly due to the high level of turbulence and the associated structure of the flow field (van Balen et al. 2009). To this end, numerous studies ranging from laboratory experiments to field observations to numerical simulations have been performed over the last few decades to provide insights into the secondary flow and associated cross-stream circulation (Zeng et al. 2010).

Numerical modeling of flow in curved bends is a complex problem due to the three-dimensional nature of the flow dynamics. There are various approaches that have been employed by different researchers for simulating flow in bends. These include the framework for modeling turbulence and the free-surface effects. For example, the study of Zeng et al. (2010) involved the use of a full three-dimensional Reynolds-averaged Navier-Stokes (RANS) model to investigate the flow and sediment dynamics in curved bends. In addition, Son et al. (2011) performed three-dimensional RNG (renormalization group theory) k-ε turbulence modeling for simulation of meandering flow in natural channel. Other recent studies have used the LES (Large Eddy Simulation) technique with high grid resolution in combination with the rigid-lid assumption

[1] This chapter will be submitted in substantial part as a manuscript entitled "Implications for neglecting free surface effects in numerical simulations of flow in curved channels", by K. Sin, S. K. Venayagamoorthy, and C. I. Thornton, to the *Journal of Hydraulic Research,* International Association for Hydro-environment Engineering and Research (IAHR).

based on arguments that such a technique captures the turbulence characteristics of the flow better (van Balen et al. 2009).

In the last two decades, there has been a proliferation in numerical modeling studies of flow in curved channels that make use of the rigid-lid assumption. Hodskinson and Ferguson (1998) simulated flow separation in a sharply curved meandering channel by using a rigid lid model and obtained satisfactory agreements with measured flow velocity data. Blanckaert et al. (2009) performed a study involving field measurements, laboratory experiments and numerical simulations in a curved channel. They used three-dimensional LES and RANS (Reynolds Averaged Navier-Stokes) CFD codes in a curved using rigid lid assumption. The numerical simulation results were shown to agree well with experimental data of Booij et al. (2003) even though the effect of free surface was neglected. A summary of some recent CFD studies on flow in curved channels is shown in Table 4.1 to highlight the number of CFD studies that make use of the rigid-lid assumption.

Table 4.1 The summary of usage of free surface model from the previous studies

Researcher	Simulation of Free-Surface Change
Odgaard (1989)	Yes
Jin et al. (1993)	No
Hodskinson and Ferguson (1998)	No
Lien et al. (1999)	Yes
Wilson et al. (2003)	Yes
Rameshwaran and Naden (2005)	Yes
Khosronejad et al. (2007)	No
Blanckaert et al. (2009)	No
van Balen (2010)	No
Zeng et al. (2010)	Yes
Son et al. (2011)	Yes

However, to the best knowledge of the author, there has not been a comprehensive study that has been performed to evaluate the consequences for neglecting free surface effects in numerical models. Such a study is necessary in order to clarify when it is appropriate to make use of the rigid-lid assumption since the computational cost associated with performing a proper free-surface modeling study can be quite high. The focus of the work presented in this chapter is to highlight the implications for neglecting free surface effects in simulations of flow in curved channels. This study is accomplished through a broad parametric study to assess the differences between free-surface flow simulations and rigid-lid simulations. In order to assess the differences between a free-surface model and a rigid lid model, it is imperative to use a common turbulence modeling framework. Furthermore, the need to explore a broad parametric space for determining thresholds necessitates the use of a RANS turbulence modeling framework due to the prohibitive computational costs associated with LES models.

Specifically, the goal of this study is to quantify the errors associated with the rigid-assumption based on key non-dimensional parameters for using the rigid lid simulation. In what follows, a validation study where comparisons between the free-surface simulation, a rigid-lid simulation and experimental measurements performed by Ippen et al. (1962a) are shown. This is followed by a presentation of the key results from the parametric study to highlight the limitation of the rigid-lid model assumption.

4.2 Comparison of Free Surface Model and Rigid-lid Model

The major difference between a free surface model and a rigid-lid model is how the free surface is modeled i.e. a free surface model considers both air and water flow and this allows for a distorted interface whereas a rigid-lid model only simulates water flow in a manner analogous to closed conduit flow. The CFD code using the free surface model was already validated as

discussed in Chapter 3. The validation results showed good agreement with experimental data. However, no validation was performed using a version of the CFD code with the rigid-lid assumption and hence is presented here using the data of flow velocity and shear stress from the study by Ippen et al. (1962b).

The mesh for rigid lid model was generated without the portion of air pocket that was used in the free surface model. The elevation of rigid lid was determined based on the measured central free surface elevation from the bottom of the flume at cross section 1 at the inlet (0.152 m) and cross section 10 (0.151 m) at the outlet, respectively because these values are the closest (representative) values of the free surface elevation at the inlet and outlet. The number of cells for rigid lid model was 290,004 cells and the cell type was also hexahedral. The type of inlet boundary condition for rigid-lid modeling is the same as the free surface model. The outlet boundary condition was set using hydrostatic pressure. Wall boundary condition was used for the channel bed in a similar manner to the free surface model discussed in Chapter 3.

Figure 4.1 shows a comparison of flow velocity magnitude from numerical simulation results with experimental data using both free surface and rigid lid model. The left column in Figure 4.1 is the comparison of flow velocity from free surface model and experimental data and the right column shows the comparison of flow velocity from rigid lid model and experimental data. It appears that the simulated flow velocity for both the free surface and rigid lid models agree well with the experimental data.

Vertical velocity profiles are shown in Figure 4.2. Both free surface and rigid lid model show good agreements with experimental data. The left most column in Figure 4.2 is the left bank of the channel and right hand column of Figure 4.2 indicates the right bank of the channel.

Figure 4.3 shows the validation of shear stress data which also shows reasonable agreement with experimental data for both free surface and rigid lid models.

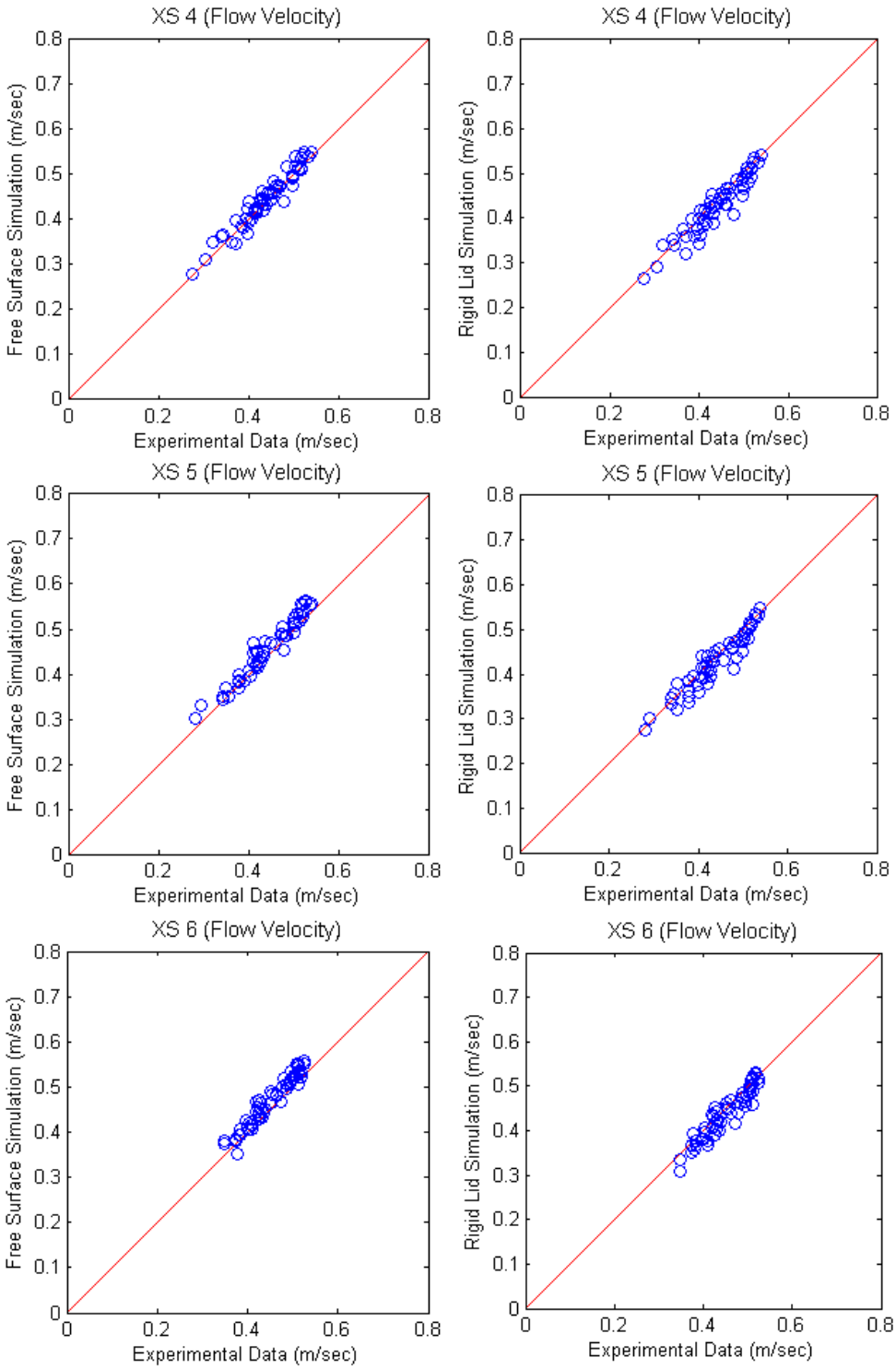

Figure 4.1 Ippen et al. (1962b) validation results for the flow velocity (m/sec) from free surface model (left column panels) and rigid-lid model (right column panels).

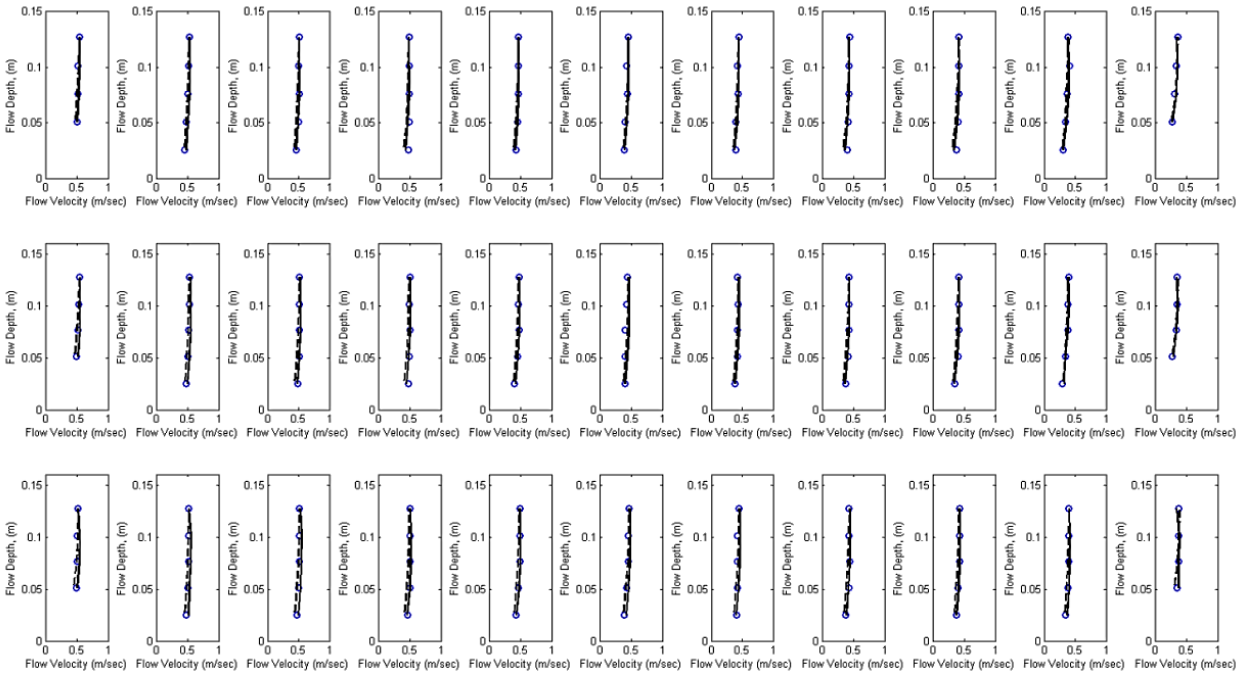

Figure 4.2 Validation of velocity data (m/sec) of Ippen et al. (1962b) from experimental study with numerical simulation (XS 4: top XS 5: middle XS 6: bottom) (circle: flow velocity from experimental study, solid line: flow velocity from free surface simulation and dash line: flow velocity from rigid lid simulation).

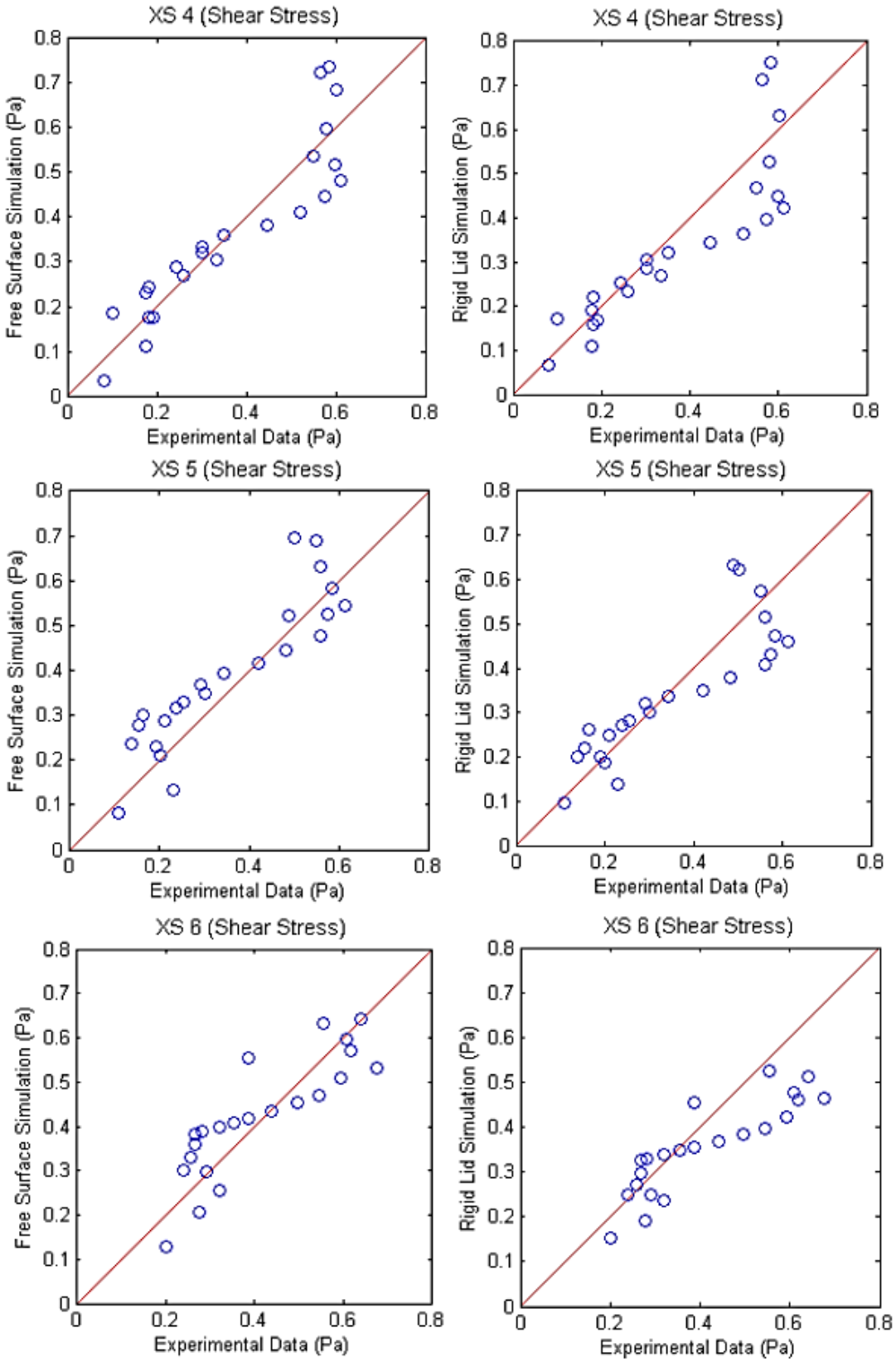

Figure 4.3 Ippen et al. (1962b) validation results for the shear stress (Pa) from free surface model (left column panels) and rigid-lid model (right column panels).

4.3 Modification of Flow Conditions

In order to investigate the differences between the free surface and rigid lid models, a broad parametric study is necessary. This is accomplished by altering two relevant parameters in curved channel flow namely: 1) the upstream Froude number; and 2) the curvature of the channel expressed as a ratio of the arc length L_c to the bend radius R_c. The Froude number was varied by making the original channel bed slope (0.00064 m/m). used by Ippen et al. (1962a) steeper by 25 percent and 50 percent. The curvature of the channel was varied by changing the maximum bend angle of the channel from 60 degrees to 90 degrees, 120 degrees, and 160 degrees, respectively.

4.3.1 Configurations of the Numerical Simulations

A total of 24 different numerical simulation runs were performed to investigate the difference between the two models. Table 1 provides a summary of the configuration of the 24 simulations. The elevation of the rigid lid were specified by using the water surface elevations at the inlet and outlet of the channel as obtained from the free-surface model runs in order ensure consistency with the free surface simulations. A constant slope was used for the rigid lid between the inlet and outlets. The initial and boundary conditions are identical with the validation cases presented earlier.

Table 4.2 The configurations of simulation cases

Case number	Bed slope (m/m)	Maximum bend angle (degrees)	Model type	Water surface elevation at inlet (m)	Water surface elevation at outlet (m)
1	0.00064	60	Free Surface	0.152	0.151
2	0.00064	60	Rigid Lid	N/A	N/A
3	0.00064	90	Free Surface	0.152	0.151
4	0.00064	90	Rigid Lid	N/A	N/A
5	0.00064	120	Free Surface	0.152	0.151
6	0.00064	120	Rigid Lid	N/A	N/A
7	0.00064	160	Free Surface	0.152	0.151
8	0.00064	160	Rigid Lid	N/A	N/A
9	0.0008	60	Free Surface	0.119	0.119
10	0.0008	60	Rigid Lid	N/A	N/A
11	0.0008	90	Free Surface	0.119	0.119
12	0.0008	90	Rigid Lid	N/A	N/A
13	0.0008	120	Free Surface	0.119	0.119
14	0.0008	120	Rigid Lid	N/A	N/A
15	0.0008	160	Free Surface	0.119	0.119
16	0.0008	160	Rigid Lid	N/A	N/A
17	0.00096	60	Free Surface	0.113	0.113
18	0.00096	60	Rigid Lid	N/A	N/A
19	0.00096	90	Free Surface	0.113	0.113
20	0.00096	90	Rigid Lid	N/A	N/A
21	0.00096	120	Free Surface	0.113	0.113
22	0.00096	120	Rigid Lid	N/A	N/A
23	0.00096	160	Free Surface	0.113	0.113
24	0.00096	160	Rigid Lid	N/A	N/A

4.3.2 Mesh Generations for Modified Flow Conditions

A total of 24 numerical meshes were generated using Ansys Design Modeler. Table 4.3 summarizes the mesh details that show relevant mesh quality parameters. Note that the number of cells is less for rigid-lid model runs than those for the free surface model runs since the portion of air pocket are not required. Figure 4.4 shows a subset of mesh geometries used for the free surface model runs with increasing bend angles.

Table 4.3 The summary of mesh quality for extensive simulations

Case number	Type of cells	Number of cells	Maximum skewness	Maximum aspect ratio
1	Hexahedral	388,236	0.80	29.88
2	Hexahedral	291,847	0.84	29.50
3	Hexahedral	494,066	0.84	21.06
4	Hexahedral	357,330	0.87	24.62
5	Hexahedral	503,806	0.79	20.76
6	Hexahedral	359,928	0.83	27.67
7	Hexahedral	522,860	0.79	28.32
8	Hexahedral	552,494	0.83	20.54
9	Hexahedral	388,236	0.80	29.88
10	Hexahedral	239,636	0.90	28.57
11	Hexahedral	460,581	0.79	20.82
12	Hexahedral	321,224	0.89	28.28
13	Hexahedral	503,806	0.80	21.96
14	Hexahedral	381,204	0.89	25.87
15	Hexahedral	522,860	0.81	28.32
16	Hexahedral	325,850	0.89	26.90
17	Hexahedral	388,236	0.81	29.87
18	Hexahedral	239,603	0.91	27.36
19	Hexahedral	460,581	0.79	20.81
20	Hexahedral	329,897	0.91	26.55
21	Hexahedral	539,214	0.85	18.99
22	Hexahedral	294,298	0.90	25.94
23	Hexahedral	522,860	0.81	28.32
24	Hexahedral	326,612	0.90	26.17

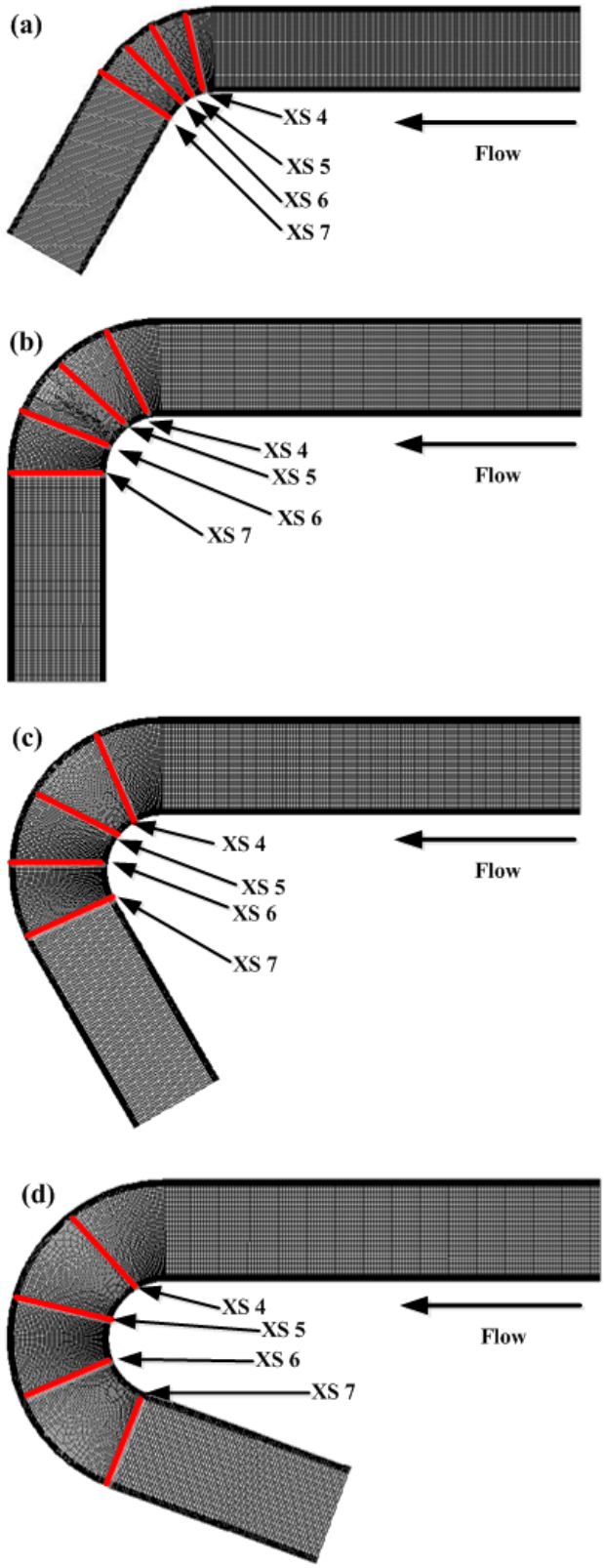

Figure 4.4 Ippen et al. (1962) mesh for free surface simulation (60 degrees maximum bend angle (a), 90 degrees maximum bend angle (b), 120 degrees maximum bend angle (c), and 160 degrees maximum bend angle (d) (flow direction: from right)).

4.3.3 Grid Independence Checks

Grid independence checks were performed to ensure that the results are independent of the grid size. The checks were performed by comparing flow velocity profiles for the extreme bend (160^{o}, case 7) with three different grid resolution (311,700 cells, 522,860 and 1,043,621 cells cells). As shown in Figure 4.5, the flow velocity profiles agreed well for the three different grid resolutions. A similar analysis was performed for the rigid lid model for case 8 with the results shown in Figure 4.6. These results confirm that the medium grid resolution (as shown for all the cases in Table 4.3) is sufficient to ensure that the simulations results are grid independent.

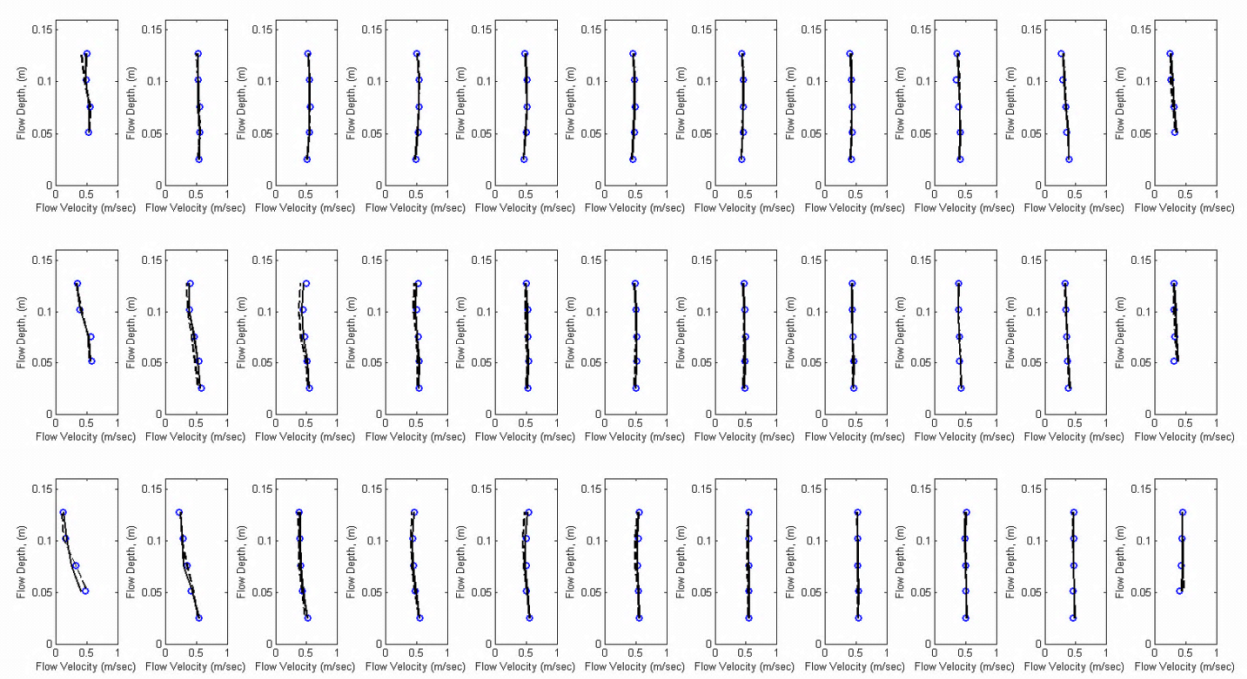

Figure 4.5 Flow velocity (m/sec) profiles for checking grid independence case 7 (XS 5: top XS 6: middle XS 7: bottom, circle: flow velocity from coarse grid, solid line: flow velocity from median grid, and dash line: flow velocity from dense grid).

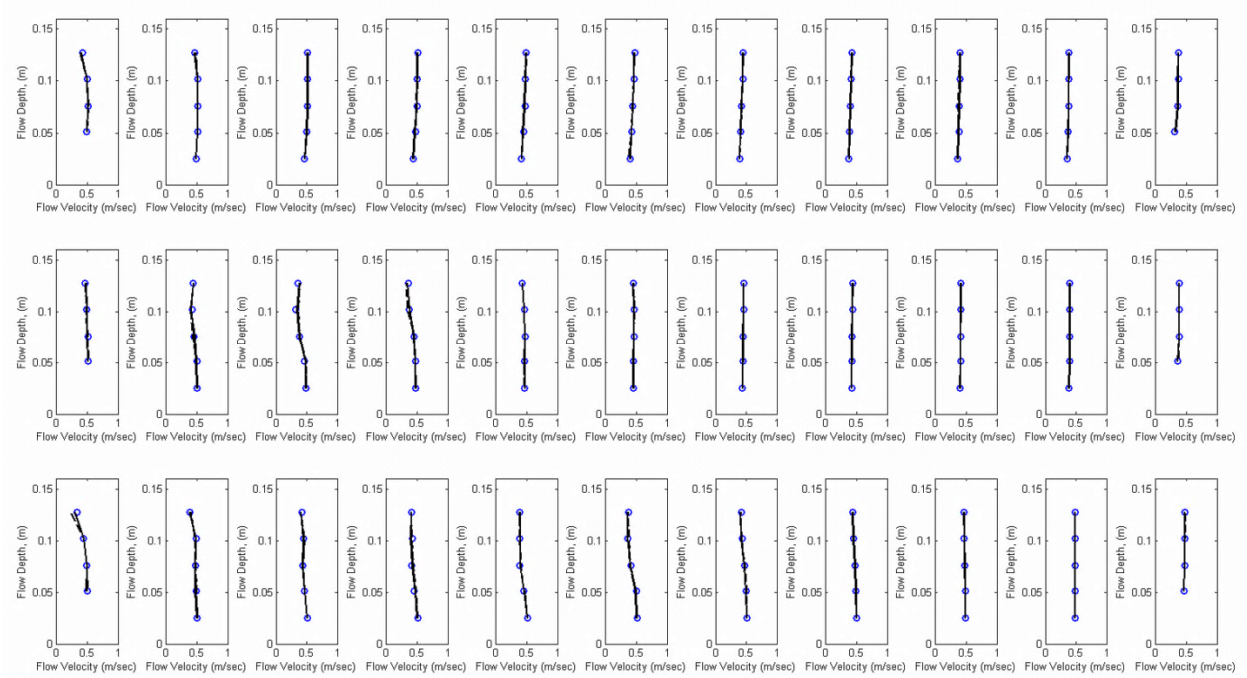

Figure 4.6 Flow velocity (m/sec) profiles for checking grid independence from case 8 (XS 5: top XS 6: middle XS 7: bottom, circle: flow velocity from coarse grid, solid line: flow velocity from median grid, and dash line: flow velocity from dense grid).

4.4 Simulation Results for Modified Flow Conditions

This section will describe the difference between free surface model and rigid-lid model results. Table 4.4 summarizes the super-elevations (cm) observed in the most curved cross sections from the free surface model runs (cross section 7). The positive sign indicates that the water depth is higher than the water depth at the center of channel and the negative sign indicates vice versa. Based on these results, the following can be observed: 1) increasing the maximum bend angle for a given constant bed slope results in higher super-elevations and 2) increasing the upstream Froude number (i.e. bed slope) for a given bend angle of the channel also appears to result in an enhanced super-elevation.

These results indicate that both the Froude number and maximum bend angle of the channel are important factors that control free surface effects in flow around channel bends.

Table 4.4 The summary of super-elevation from free surface modeling.

Case Number	Maximum bend angle (degrees)	Cross Section	Super-elevation, inner bank (cm)	Super-elevation, outer bank (cm)	Froude number at the inlet
1	60	7	-0.396	+0.366	0.53
3	90	7	-0.244	+0.427	0.53
5	120	7	-0.457	+0.488	0.53
7	160	7	-0.213	+0.488	0.53
9	60	7	-0.610	+0.823	0.59
11	90	7	-0.640	+0.884	0.59
13	120	7	-0.732	+0.732	0.59
15	160	7	-0.671	+0.975	0.59
17	60	7	-0.427	+1.067	0.64
19	90	7	-0.792	+0.975	0.64
21	120	7	-0.945	+0.762	0.64
23	160	7	-0.823	+1.036	0.64

To study the differences in the flow characteristics between the free surface model and rigid-lid model, contour plots of the depth averaged velocity field viewed from the top of the channel are presented in Figure 4.7 (Case 17 through Case 24). The depth averaged flow velocity is obtained using the one-point method which uses the flow velocity at the top 60% of the flow depth from water surface elevation. As shown in Figure 4.7, the differences in flow velocity magnitudes using free surface model and rigid lid model are qualitatively evident.

To highlight the differences in the flow structures between the two models, contour plots of the turbulence intensity is portrayed in Figure 4.8. The turbulence intensity is defined turbulence as the ratio of the root mean square of the velocity fluctuations to the mean flow velocity. As shown in Figure 4.8, the differences between the two models increase with increasing curvature. The largest differences in turbulence intensities were observed for Cases 23 and 24 for which the bend angle of the channel is 160^{o} (see Figure 4.8 (g) and (h)). Moreover, Figure 4.8 shows that the free surface effect was stronger at the inner bank of the curved channel.

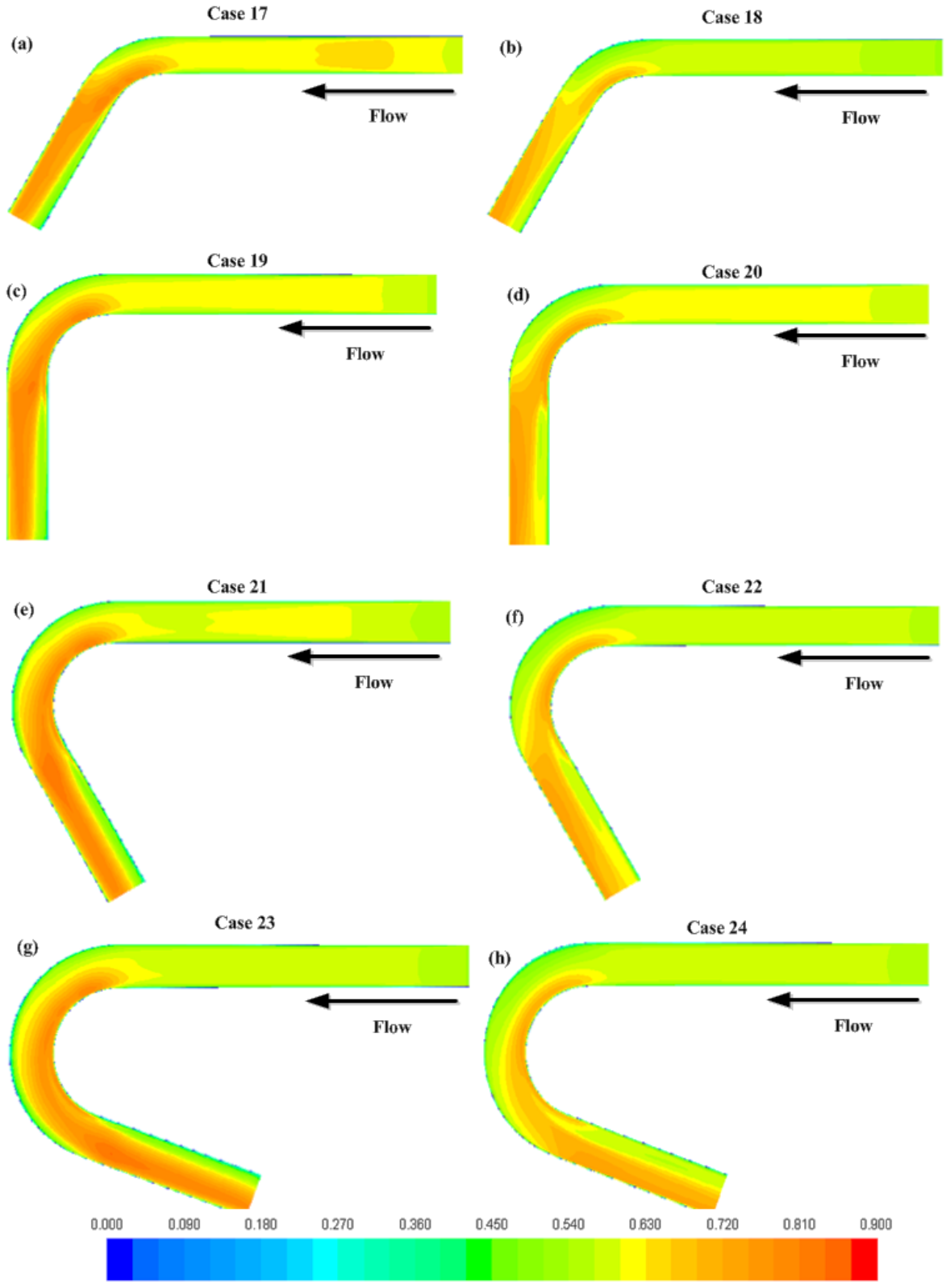

Figure 4.7 Contour map of flow velocity magnitude (m/sec) view of 60% depth down from free surface (left column: free surface model right column: rigid lid model, bed slope = 0.00096 m/m).

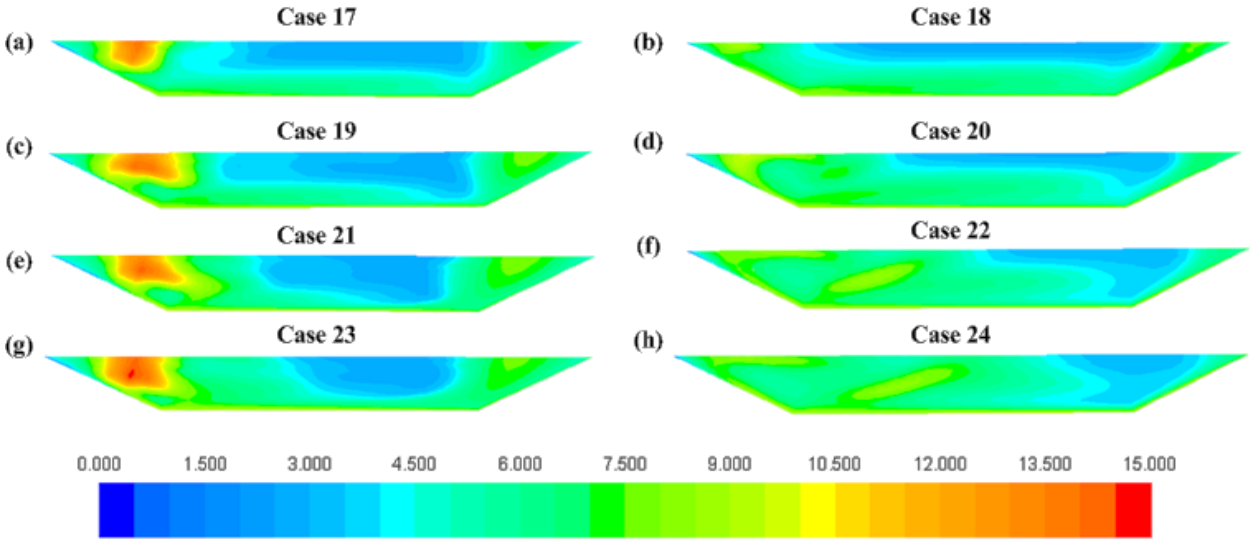

Figure 4.8 Contour map of turbulence intensity (%) cross section at maximum bend angle (left column: free surface model right column: rigid lid model, bed slope = 0.00096 m/m).

Figure 4.9 and Figure 4.10 show the comparisons of free surface model and rigid lid model for flow velocity and shear stress respectively. Moving views from the first column to the fourth column indicates the change in the curvature of the channel from 60^{o} to 160^{o} respectively. Shifting view from the first row to the third row indicates the change from the lowest bed slope (0.00064 m/m) to the highest bed slope (0.00096 m/m) respectively.

What is immediately obvious from the results shown in both Figures 4.9 and 4.10 is how the agreement between the two models rapidly deteriorates as the curvature of the channel is increased for a given bed slope (i.e. observe the results across the columns for a given row). Furthermore, the discrepancies are even more pronounced (increased scatter) at the higher curvature bends with higher bed slopes. This indicates that both the Froude number and the curvature are important parameters that govern the basic flow dynamics around bends. The data points that exhibit the most scatter come from the inner bank of the curved channel that was previously shown in Figure 4.8. This is because, for the sharp bends (i.e. with $R_c/T_w < 2$) simulated here, the maximum velocities and shear streeses occur on the convex (inner) side of the bend.

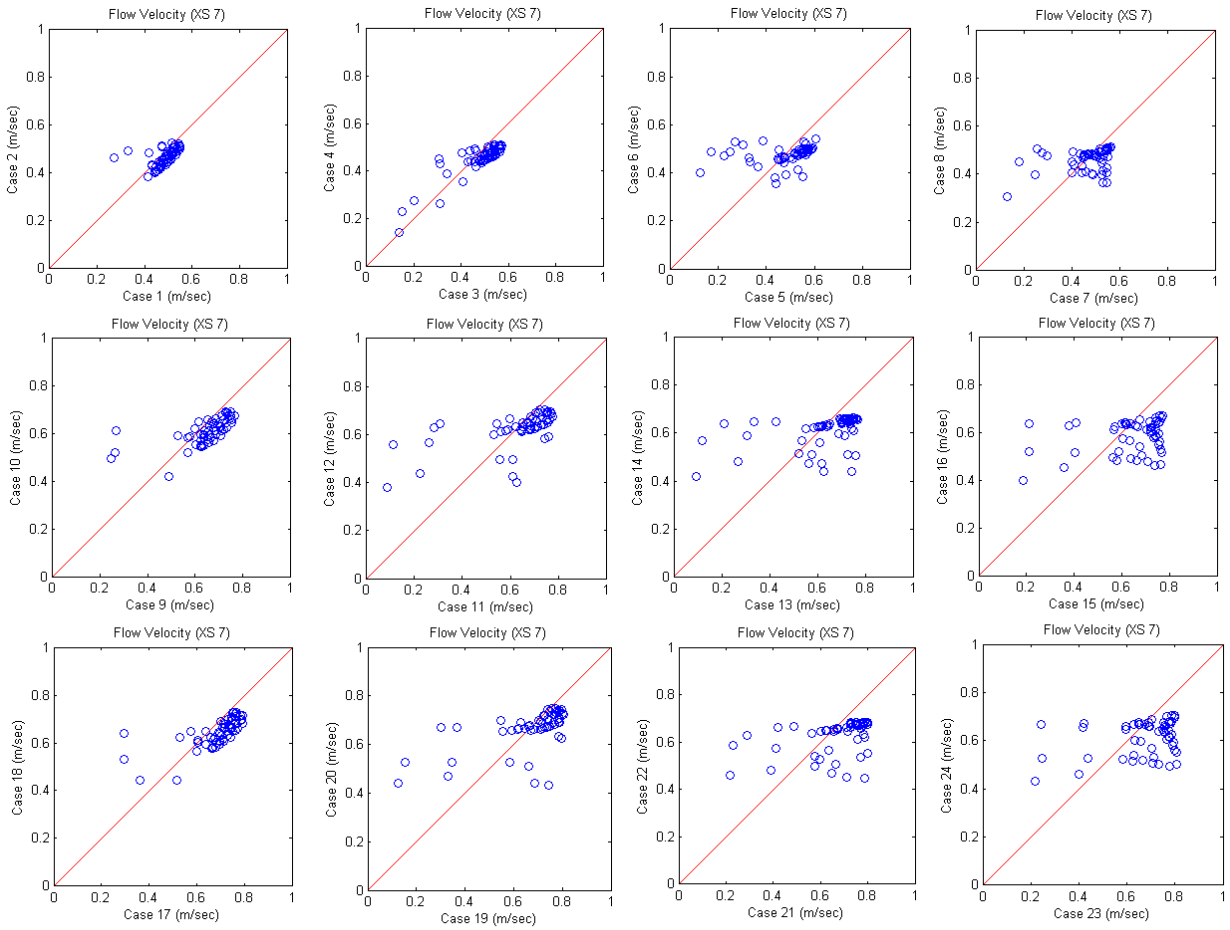

Figure 4.9 Comparisons of flow velocity (m/sec) from free surface simulation (horizontal axis) and rigid lid model (vertical axis). From Top row to bottom row: increasing bed slope of the channel, and from left column to right column: increasing bend angle of the channel.

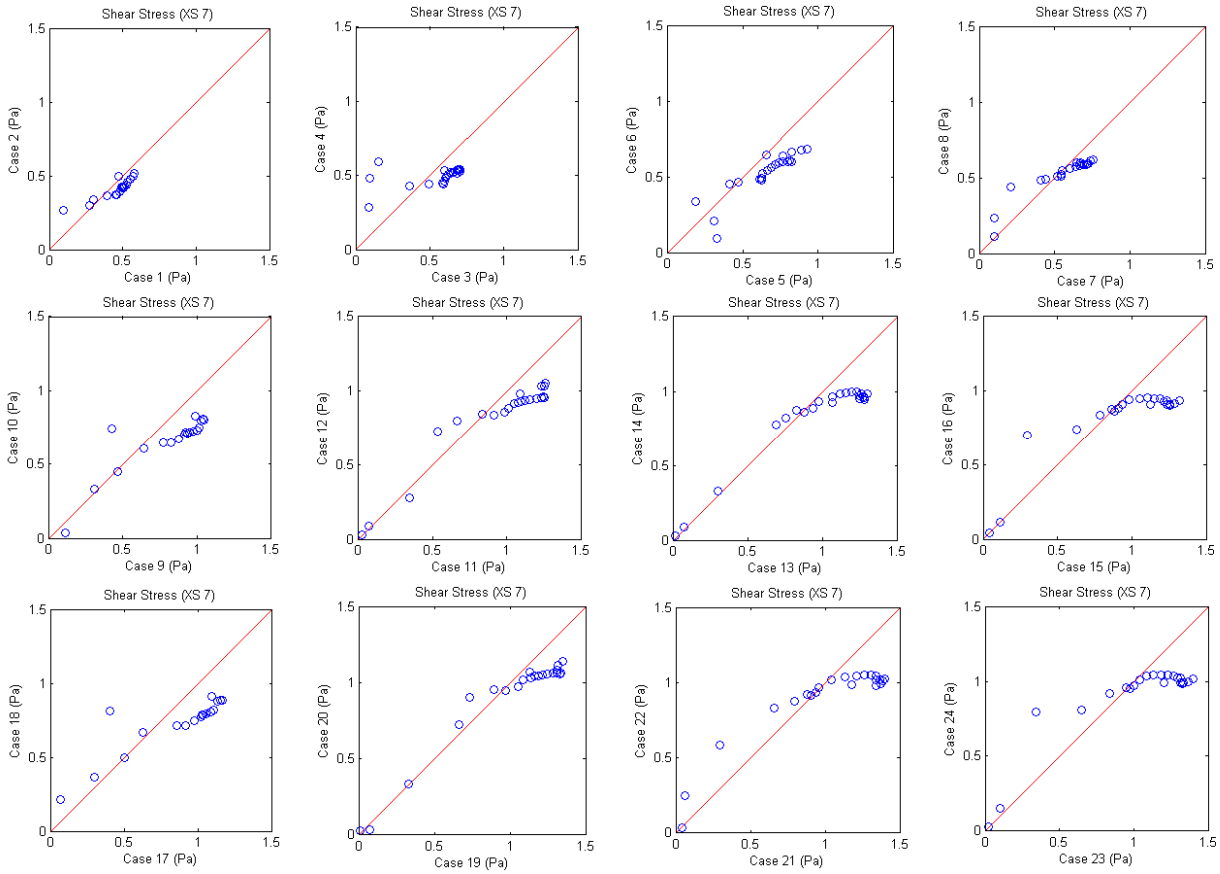

Figure 4.10 Comparisons of shear stress (Pa) from free surface simulation (horizontal axis) and rigid lid model (vertical axis). From Top row to bottom row: increasing bed slope of the channel, and from left column to right column: increasing bend angle of the channel.

Figure 4.11 shows the flow velocity profiles across the channel in the bend to highlight the differences between the two models for all the four different bend angles (rows in figure 4.11). The columns in Figure 4.11 show the flow velocity profiles at the inner bank (the first column) to center of the channel (the second column) to the outer bank of the channel (the third column). Figure 4.11 shows that the velocity profiles at the outer bank of the bend cross section showed the best agreement and that the agreement gets worst at the inner bank of the cross section. This is especially severe for strongly curved flows (rows 2 through 4) indicating the consistent story with Figure 4.8 higher discrepancies between free surface model and rigid lid model observe in the inner bank of the channel.

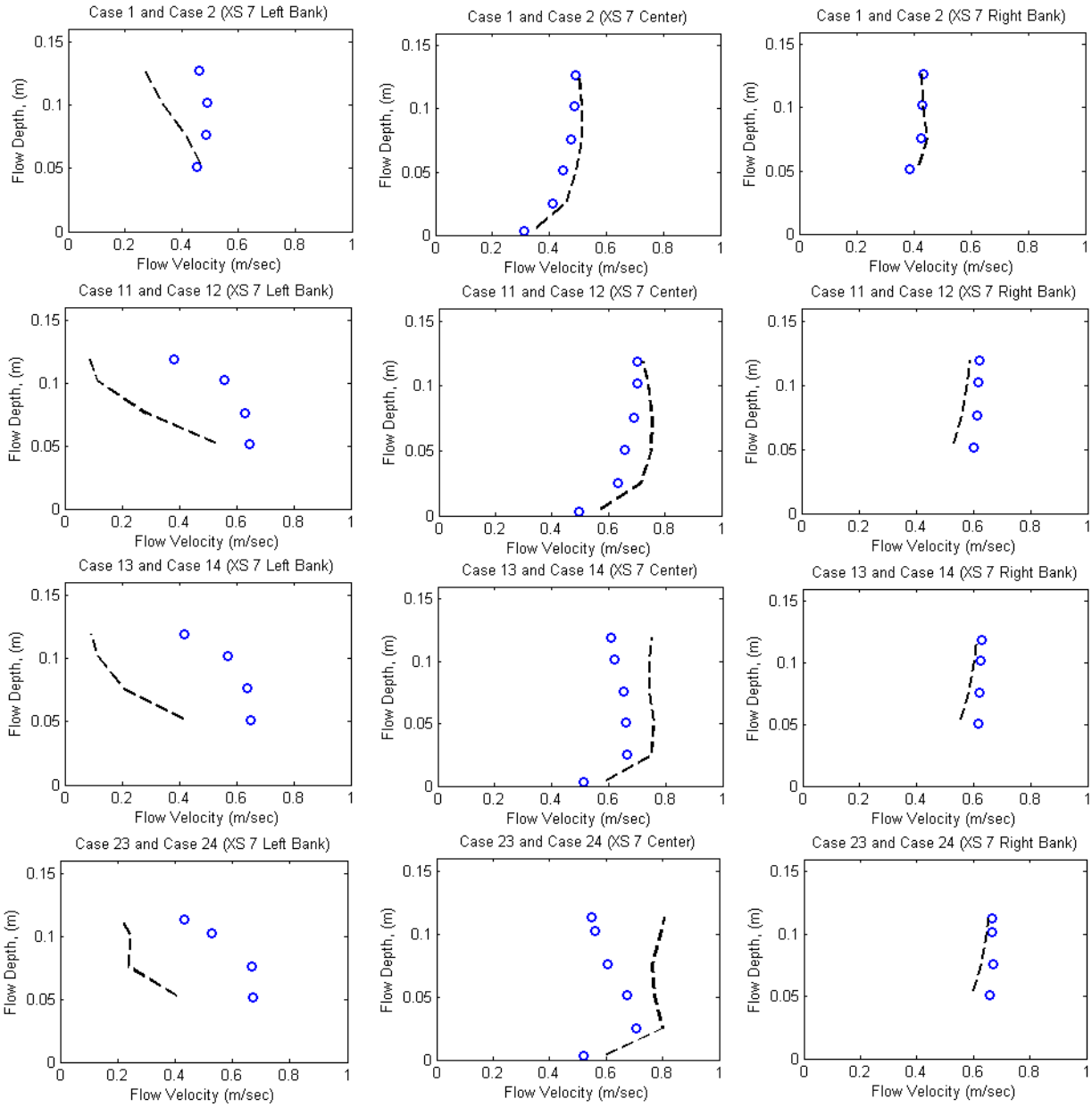

Figure 4.11 Comparison of flow velocity (m/sec) profiles of cases 1 & 2 (60^{o}, low bed slope), cases 11 & 12 (90^{o}, medium bed slope), cases 13 & 14 (120^{o}, medium bed slope) and cases 23 & 24 (160^{o}, high bed slope); (dash line: flow velocity from free surface simulation, circle: flow velocity from rigid lid simulation).

4.5 Error analysis between Free Surface Model and Rigid Lid Model

The preceding discussion showed in a somewhat qualitative sense that the rigid lid model appears to produce similar results as the free surface model as long as the curvature expressed in terms of L_c/R_c is small and that the Froude number should also be low (as implied by a low bed slope). However, the results between the two models begin to differ as L_c/R_c increases. Here, a quantitative analysis is presented using error analysis of the differences in flow velocities, in order to determine thresholds in L_c/R_c beyond which the use rigid lid model is questionable.

4.5.1 Differences in Normalized Flow Velocity

Figure 4.12 shows the ratio of the maximum flow velocity in the bend to the averaged flow velocity M_v as a function of L_c/R_c. The averaged flow velocity was computed from the Manning's formula using the normal depth. It is clear that as L_c/R_c becomes larger than $\pi/2$ (> 90^o) and medium bed slope (0.00080 m/m), the difference in M_v become larger. Based on the results presented here and the preceding section, it appears that the bend effects are more pronounced. From an intuitive standpoint, this makes sense since a more pronounced flow separation is likely to occur as the bend angle increases.

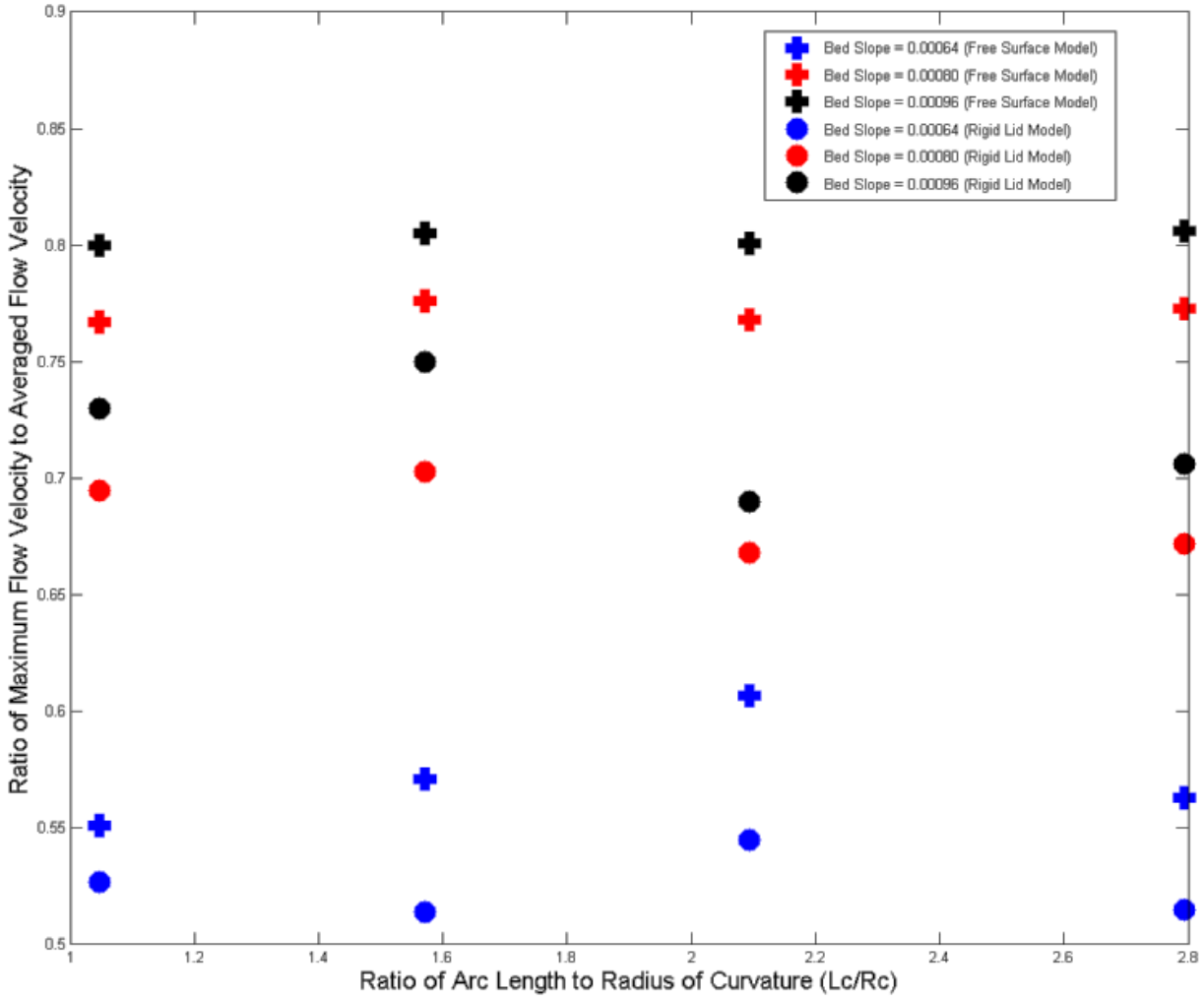

Figure 4.12 Plot of M_v values, ratio of maximum flow velocities to averaged flow velocities with change of curvature.

4.5.2 Maximum RMSE value of Flow Velocity

The RMSE (Root Mean Square Error) of flow velocity between free surface and rigid lid model was performed. The RMSE values are calculated using Equation 4.1.

$$RMSE = \sqrt{\frac{1}{n} \times \sum_{i=1}^{n} (F - R)^2} \tag{4.1}$$

where n = the number of the data samples; F = simulation results from free surface model and R = simulation results from rigid lid model.

Table 4.5 shows the summary of RMSE for the flow velocity. The RMSE between the free surface and rigid lid models increased consistently with increasing bend angle.

It is evident that both the Froude number (expressed here as a function of the bed slope) and the curvature (expressed here as L_c/R_c) of the channel are key parameters that control the dynamics of flow around bends but curvature is stronger parameter than Froude number. Figure 4.13 shows a plot of the dimensionless maximum RMSE of flow velocity as a function of L_c/R_c. The actual RMSE were nondimensionalized using the averaged flow velocity. The Froude number for each bed slope was calculated using the corresponding normal depth. The Froude numbers for the three different bed slopes of 0.00064 (m/m), 0.00080 (m/m), and 0.00096 (m/m) were 0.53, 0.59, and 0.64 respectively.

Table 4.5 The summary of RMSE at cross section 7 (flow velocity, m/sec)

Case	XS	RMSE (m/sec)	Case	XS	RMSE (m/sec)
1 and 2	7	0.050	13 and 14	7	0.152
3 and 4	7	0.058	15 and 16	7	0.154
5 and 6	7	0.112	17 and 18	7	0.091
7 and 8	7	0.094	19 and 20	7	0.129
9 and 10	7	0.095	21 and 22	7	0.140
11 and 12	7	0.134	23 and 24	7	0.155

Figure 4.13 also indicates that when $L_c/R_c \geq \pi/2$, the errors are quite significant. A key point is that the errors between free surface and rigid lid models dramatically increased with Froude number based on the bed slope of 0.0008 (m/m) and $L_c/R_c \geq \pi/2$. This indicates that L_c/R_c appears to be the right parameter to use to signify the free surface effect than perhaps the Froude number of the channel, especially for sharp bends ($R_c/T_w < 2$). However, this observation is tentative and requires further investigation. Regardless, a key finding from the statistical analysis is that rigid lid models should not be used to simulate flow in channel bends when $L_c/R_c \geq \pi/2$ for sharp bends with $R_c/T_w < 2$.

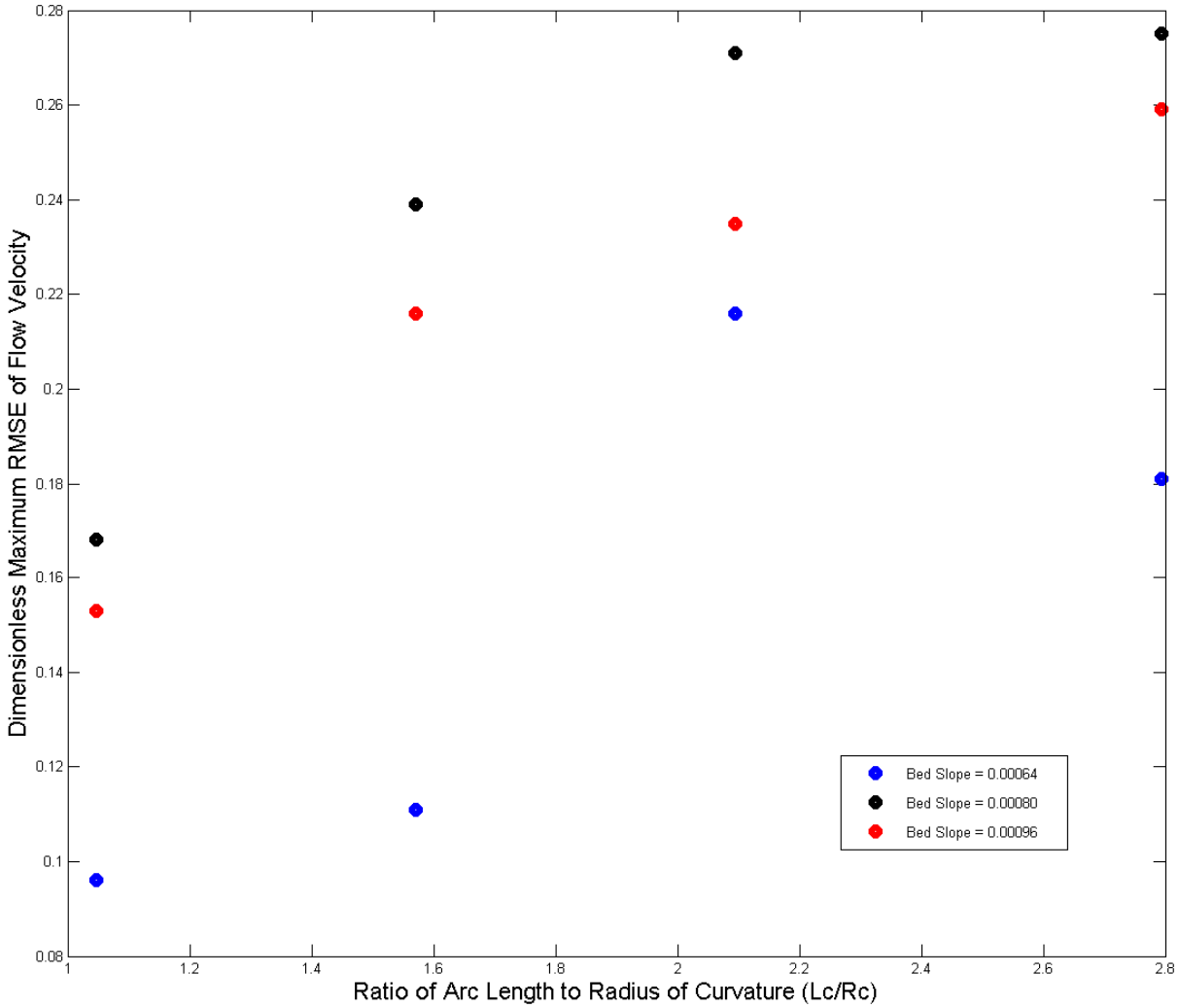

Figure 4.13 Plot of dimensionless maximum RMSE values (flow velocity, m/sec).

4.6 Summary and Conclusions of Chapter 4

This chapter focused primarily on results from a broad parametric study consisting of 24 numerical simulation runs to highlight the need for a free surface model for flow in strongly curved channel bends. Two relevant parameters namely the nondimensional channel bend length (L_c/R_c) and the Froude number, were chosen to quantify the differences between simulations that capture the effects of the free surface versus simulations that make use of the rigid lid assumption. The flow conditions were modified by varying the two relevant parameters. The following main conclusions can be drawn:

- The numerical simulations results show that the discrepancy between the free surface and rigid lid models are more pronounced at the inner bank of the channel bend than the outer bank of the channel for sharp bends.
- The flow dynamics in a bend is dependent on both the Froude number and the maximum bend angle of the channel.
- The maximum bend angle of the channel is the more sensitive variable that controls the free surface effect than the Froude number of the channel.
- When $L_c/R_c < \pi/2$, the error between the two models is simply dependent on the Froude number (i.e. increases with Fr). When $L_c/R_c \geq \pi/2$, the parametric studies results show that the curvature effects begin to dominate the dynamics and the error dramatically increases regardless of the value of the Froude number.

Chapter 5. Parameterization of Shear Stress in Curved Channels[2]

5.1 Introduction

As described in Chapter 1, the conventional approach for parameterizing shear stress in curved channels is to express K_b as a function of R_c/T_w. Here, K_b is the ratio of the maximum shear stress in a channel bend to the averaged approach shear stress in a straight channel, R_c radius of curvature and T_w is the channel top width. The work presented in this chapter proposes that K_b might not necessarily be only a function of a single parameter and should be parameterized as a function of other geometric parameters such as the bend angle given by L_c/R_c in conjunction with the Froude number.

The first step in this study is to revisit the conventional approach of quantifying K_b as a function of R_c/T_w. This is followed by presentation of shear stress results from numerical simulations performed as part of this study results in terms of R_c/T_w. Finally, the variations of the shear stress are investigated as a function of both L_c/R_c and the Froude number.

5.2 Description of Conventional Approach

The conventional approach for parameterizing shear stress is based on R_c/T_w values (the ratio of radius of curvature to the top width). The main hypothesis of this approach is that R_c/T_w is a strong indicator of the rate of channel erosion rate. As described in Chapter 2, the field studies performed by Hickin et al. (1975) showed that the R_c/T_w had a consistent relationship with the channel migration rate. Kilgore and Cotton (2005) selected this approach for parameterizing shear stress in curved channels. Kilgore and Cotton (2005) quantified K_b

[2] This chapter will be submitted in substantial part as a manuscript entitled "Parameterization of shear stress in curved channels", by K. Sin, S. K. Venayagamoorthy, and C. I. Thornton, to *Journal of Hydraulic Research,* International Association for Hydro-environment Engineering and Research (IAHR).

empirically in terms of R_c/T_w as:

$$K_b = 2.00 \quad R_c/T_w \leq 2, \tag{5.1}$$

$$K_b = 2.38-0.206(R_c/T_w)+0.0073(R_c/T_w)^2 \quad 2< R_c/T_w <10\ , \tag{5.2}$$

$$K_b = 1.05 \quad 10 \leq R_c/T_w, \tag{5.3}$$

where, R_c = radius of curvature of the bend to the channel centerline, m (ft); and T_w = channel top (water surface) width, m (ft).

Sin (2010) performed experimental data analysis of shear stress data collected in curved channels at Colorado State University (CSU). Table 5.1 is a summary table of the K_b values and R_c/T_w values obtained from conventional experimental studies. Figure 5.1 shows the distribution of the K_b values of the composite experimental data and the recommendations of HEC-15. The experimental data from the study of Sin (2010) showed a more conservative envelope of up to about 30 percent over the recommendation of HEC-15. However, the main point to note from Figure 5.1 is the scatter in the K_b values of up to a factor of 2 to 3 for low values of R_c/T_w (i.e. for strongly curved flows). This raises doubt on the conventional approach of parameterizing K_b solely as a function of R_c/T_w.

Table 5.1 Summary of K_b values from previous experimental studies

Researchers	Channel Width (ft)	R_c/T_w	K_b	Side Slope (H:V)
Ippen et al. (1962)	2.00	1.67	2.00	2:1
	2.00	1.52	1.78	2:1
	2.00	1.50	1.78	2:1
	2.00	1.35	2.20	2:1
	2.00	1.35	2.20	2:1
	2.00	1.25	2.40	2:1
	2.00	1.25	2.40	2:1
	1.00	3.49	1.59	2:1
	1.00	2.91	1.60	2:1
	1.00	2.51	1.76	2:1
	2.00	1.47	2.51	2:1
	2.00	1.22	2.80	2:1
	2.00	1.52	2.22	2:1
	2.00	1.25	2.40	2:1
	2.00	1.52	2.86	2:1
	2.00	1.25	3.00	2:1
USBR (1964)	2.00	3.76	1.35	1.5:1
Yen (1965)	6.00	4.18	1.20	1:1
	6.00	4.00	1.30	1:1
	6.00	3.99	1.30	1:1
	6.00	3.98	1.30	1:1
	6.00	3.73	1.30	1:1
CSU (2010)	10.20	2.82	1.79	3:1
	6.00	6.91	1.78	3:1
	10.20	2.62	1.78	3:1
	6.00	6.20	1.88	3:1
	10.20	2.48	1.94	3:1
	6.00	5.72	1.99	3:1
	10.20	2.41	2.00	3:1
	6.00	5.44	1.68	3:1

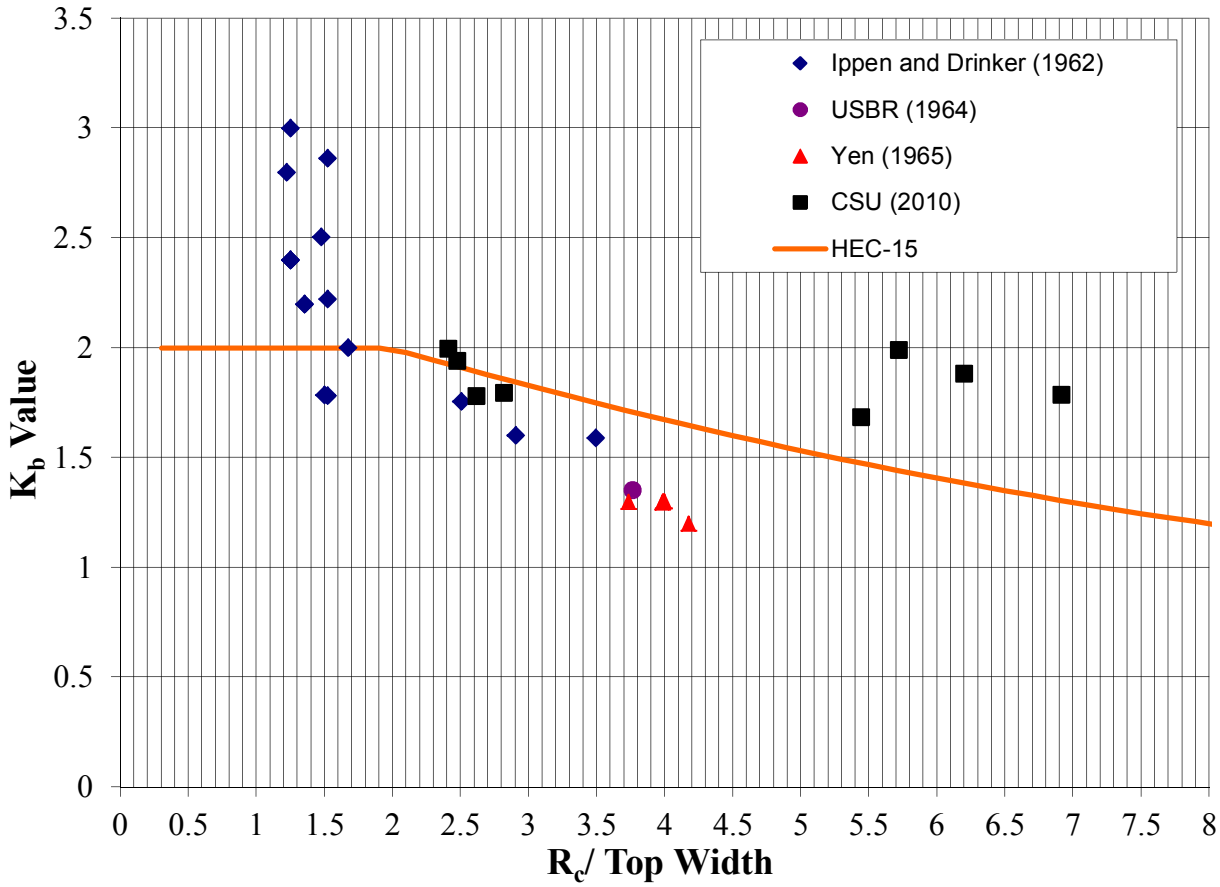

Figure 5.1 Plot of distribution of K_b values as a function of R_c/T_w (from Thornton et al. 2012).

5.3 Dimensional Analysis to Determine Dependency of Shear Stress on Pertinent Nondimensional Parameters

The relevant variables that influence the distribution and magnitude of the shear stress in a channel bend are as follows:

$$\tau = f\,(V, D, L_c, R_c, S_o, \varepsilon, g, \rho, \nu), \tag{5.4}$$

where V is the uniform velocity at the upstream end (straight section of the channel), D is the hydraulic radius of the channel cross-section at the upstream end, L_c is the length of channel bend, R_c is the radius of curvature, S_o is the bed slope, ε is the channel bed roughness, g is the acceleration due to gravity, ρ is the density of the fluid, and ν is the kinematic viscosity.

Using V, D and ρ as the pertinent scaling (repeating variables), invoking the Buckingham Pi theorem yields the following relationship (in nondimensional form): where Fr = $V/(gD)^{1/2}$, $Re = VD/\nu$.

$$\frac{\tau}{\rho V^2} = \varphi\left(\frac{L_c}{D}, \frac{R_c}{D}, Fr, Re, S_o, \frac{\varepsilon}{D}\right), \tag{5.5}$$

Given that Re >>1 in natural river flows, the shear stress should become independent of Reynolds number. Hence, the key parameters that directly affect the shear stress are namely the following: the bend geometric parameters L_c/D; and R_c/D; the flow parameter Froude number and the bed slope S_o and roughness ε/D. To simplify the analysis, for a given bed slope, bed roughness, and Froude number, the two most relevant geometric parameters are the nondimensional bend length L_c/D; and nondimensional bend radius R_c/D;. We note that quite often in literature, the channel top width T_w is used in lieu of D. These two scales can be used interchangeably.

5.4 Additional Validation of the Numerical Model

5.4.1 Flow Geometry of USBR (1964)

In order to strengthen the applicability of the CFD framework employed in this study, an additional validation was performed against the experimental data of USBR (1964). The data of USBR (1964) was selected because the flume constructed by USBR (1964) had a similar geometry to that used by Ippen et al. (1962a). Table 5.2 provides a comparison of the flow conditions of USBR (1964) and Ippen et al. (1962a).

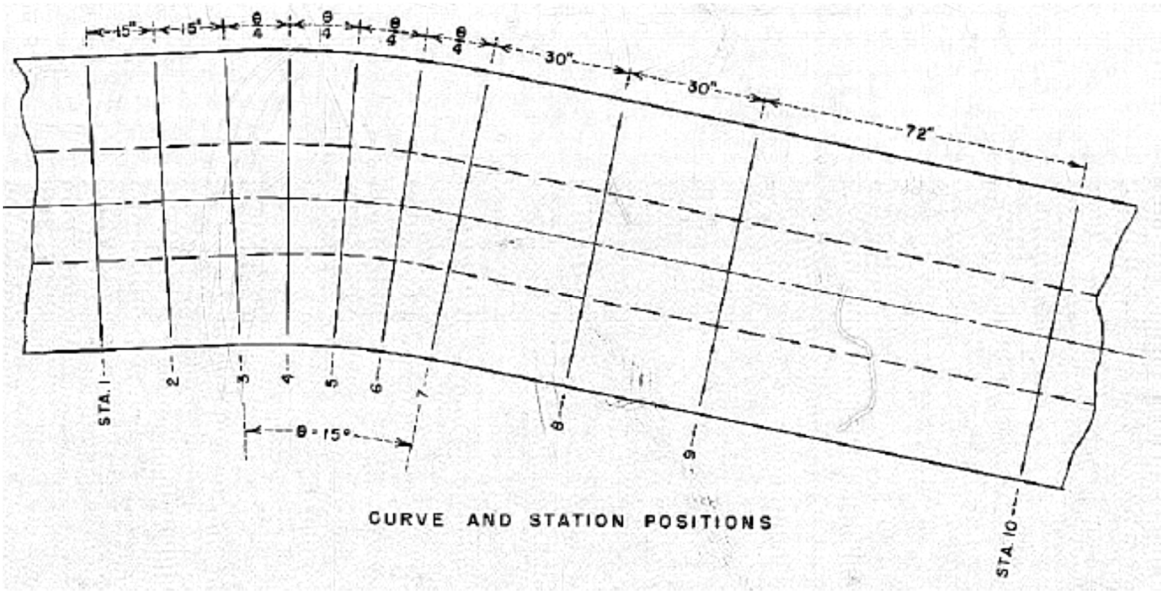

Figure 5.2 Sketch of the curved area of USBR (1964) flume (flow: from left to right).

Table 5.2 Comparison of flow conditions of Ippen et al. (1962) vs USBR (1964)

	Ippen et al. (1962)	USBR (1964)
Discharge (cms)	0.057	0.081
Flow Depth (m)	0.152	0.23
Channel Height (m)	0.203	0.343
Side Slope (H:V)	2:1	1.5:1
Maximum Bend Angle (Degrees)	60	15
Bed Slope (m/m)	0.00064	Horizontal (zero slope)
Radius of Curvature (m)	1.52	4.88

5.4.2 Initial and Boundary Conditions

Similar initial and boundary conditions were chosen for simulating the USBR (1964) flow to those used for the Ippen et al. (1962) study presented in Chapter 3. That is, mass inlet boundary condition was selected at the inlet of the channel and the pressure outlet boundary condition was chosen at the outlet. Wall boundary condition was used at the channel bed. USBR (1964) described that the channel bed was constructed of metal lath covered with mortar and troweled to a very smooth finish. That description implies that channel bed can be assumed to be a smooth surface. Hence, the roughness height was set as 0.04 mm.

5.4.3 Validation Results

The simulation was performed for a flow through time of 200 seconds to ensure conservation of mass. Figure 5.3 shows the water surface elevation for both the simulation results (blue color) and the USBR experiment (black line), Please note that though the water surface from numerical simulation exhibits some fluctuations, the vertical scale is quite small and the water surface elevations agreed within 1.5 mm.

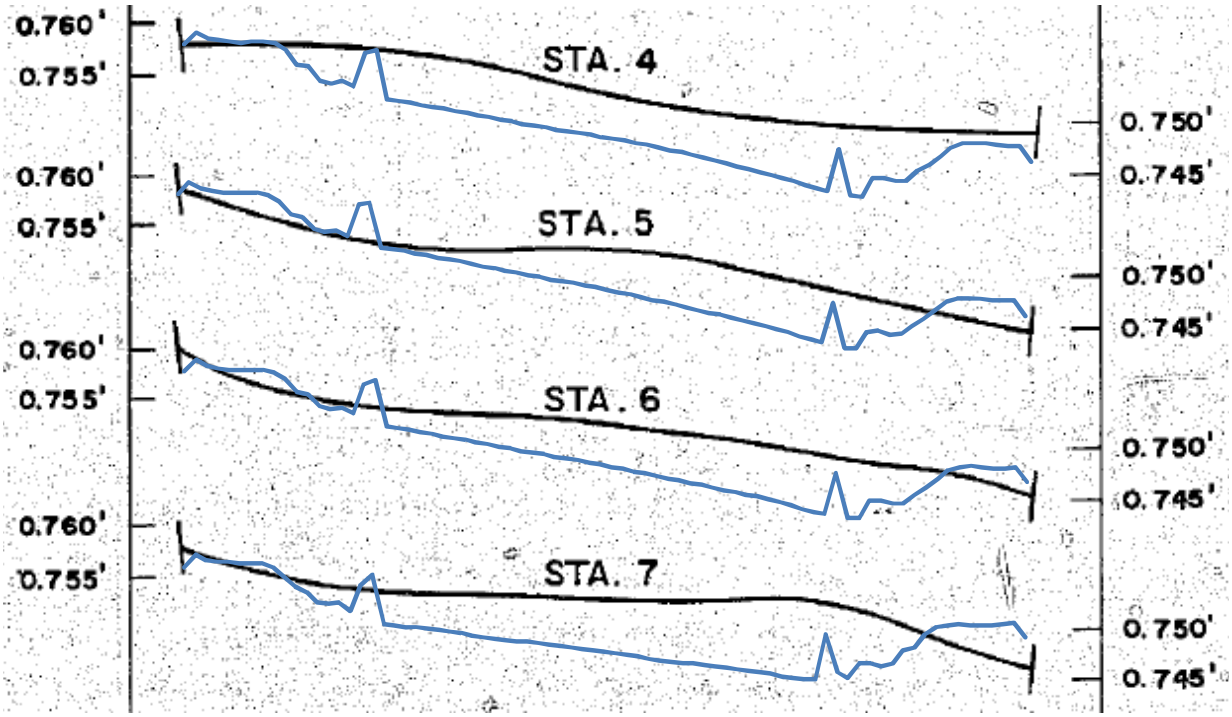

Figure 5.3 Validation of water surface elevations (ft) from data of USBR (1964).

Figure 5.4 and Figure 5.5 show the distributions of the bed shear stress from the flume study and numerical simulation study, respectively. Due to lack of availability of the quantitative dataset, the validation was limited but the two contour plots qualitatively show that the trends of shear stress maxima distribution are very similar. As per Figure 5.4, the maximum shear stress value from the experiment was 0.35 Pa (0.0073 psf). Figure 5.5 shows that the shear stress maximum from the numerical simulation was 0.32 Pa (0.0067 psf). This translates to a 9% discrepancy which can be considered to be acceptable given the nature of errors and uncertainties in both the measurements and simulations.

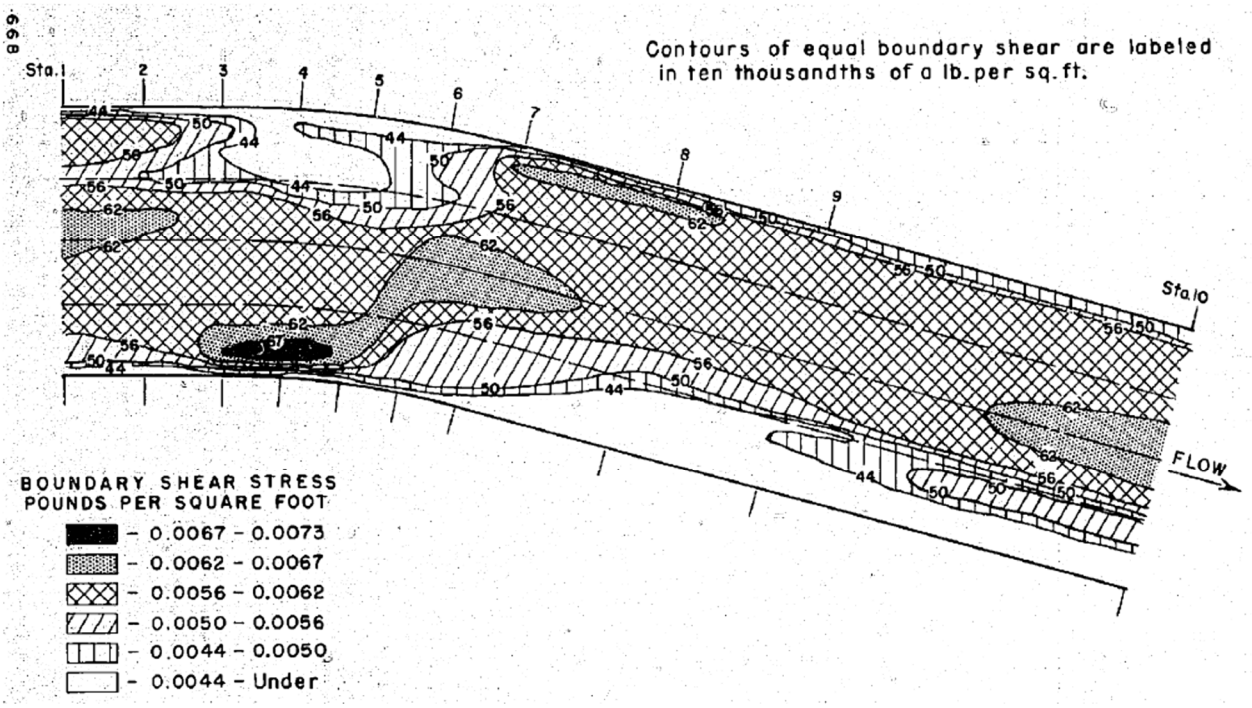

Figure 5.4 Contour plot of shear stress (psf) from USBR (1964) data (from USBR 1964) (Flow: from left to right).

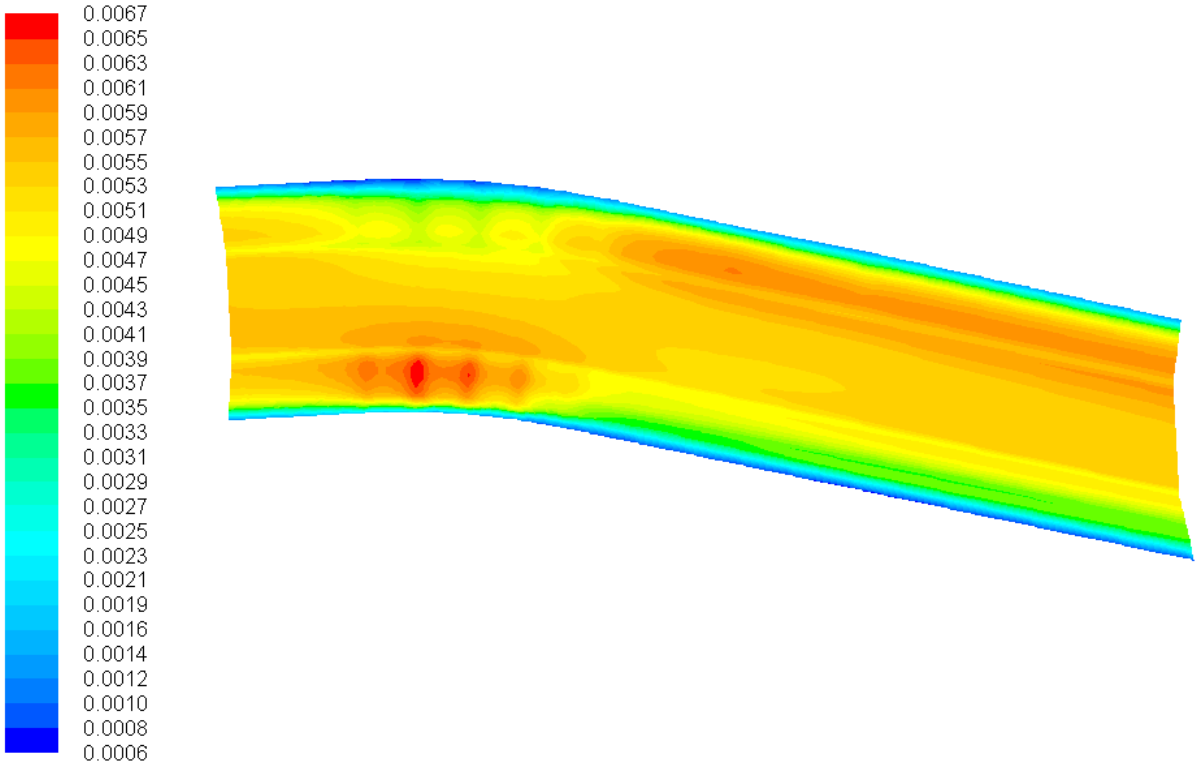

Figure 5.5 Contour plot of shear stress (psf) from numerical simulation in curved area (Flow: from left to right).

5.5 Shear Stress Distributions from Numerical Simulations

5.5.1 Summary of Numerical Simulations

Table 5.3 summarizes the numerical simulations that were performed for this study. A total of 15 numerical simulation runs were done of which 12 are taken from the free surface modeling previous study discussed in Chapter 4 (i.e. Scenarios 1 through 12). Three additional numerical simulations were performed (Scenario 13 through Scenario 15). Scenarios 13 and 14 are the simulation cases where the radius of curvature were increased from 1.52 m (5 ft) to 3.04 m (10 ft) and 6.10 m (20 ft) in order to explore the sensitivity of the K_b value as a function of R_c/T_w values. Scenario 15 is a case where the flow rate was reduced by a factor of two from the flow rates used for all the other scenarios presented in Table 5.3.

Table 5.3 Configurations of numerical simulation scenarios

Scenario number	Bed slope (m/m)	Maximum bend angle (degrees)	Radius of curvature (m)	Notes
1	0.00064	60	1.52	
2	0.00064	90	1.52	
3	0.00064	120	1.52	
4	0.00064	160	1.52	
5	0.0008	60	1.52	
6	0.0008	90	1.52	
7	0.0008	120	1.52	
8	0.0008	160	1.52	
9	0.00096	60	1.52	
10	0.00096	90	1.52	
11	0.00096	120	1.52	
12	0.00096	160	1.52	
13	0.00096	160	3.04	R_c was increased to 3.05 m
14	0.00096	160	6.1	R_c was increased to 6.1 m
15	0.00096	160	1.52	Flow Rate = 0.028 cms (1 cfs)

5.5.2 Shear Stress Distributions in Curved Channels

Figure 5.6 shows the bed shear stress distributions from Scenario 9 through Scenario 14 for different maximum bend angles of the channel for the maximum constant bed slope (0.00096 m/m). It is evident that higher shear stresses occur at the inner (convex) bank of the curve for scenarios 9 through 12 due to the enhanced flow velocities at the inner half of the channel bend. Note that these scenarios depict sharp bends with R_c/T_w <2. On the other hand, for scenario 13 (with R_c/T_w = 2.89), the higher shear stresses shift towards the centre of the bend. Scenario 14 (with R_c/T_w = 5.82), the maximum shear stresses shift further toward the outer (concave) bank of the channel bend.

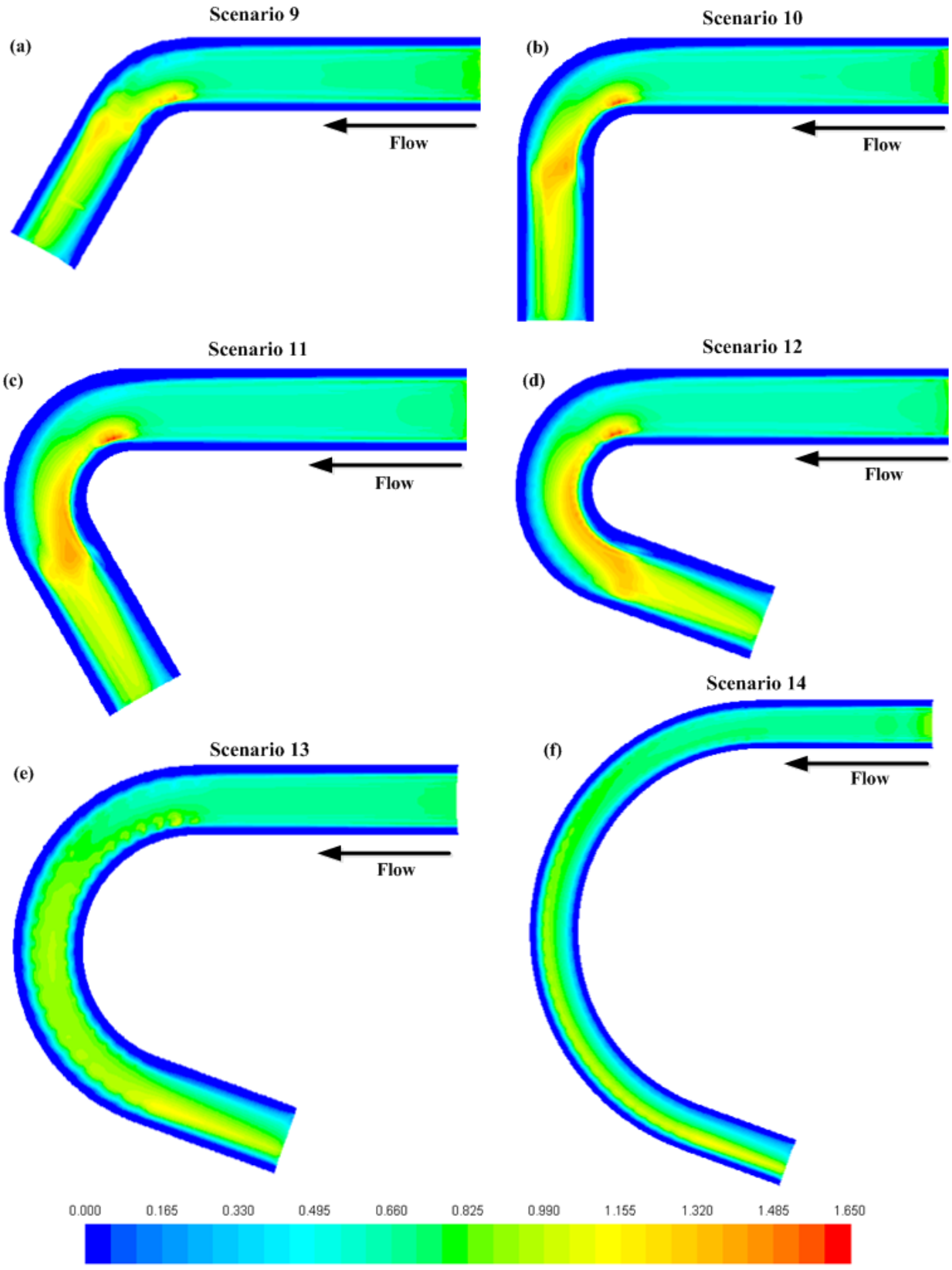

Figure 5.6 Contour plot of shear stress (Pa) from numerical simulation (Scenario 9 ~ Scenario 14).

5.5.3 Shear Stress in Curved Channels as a Function of R_c/T_w

The K_b values were calculated by normalizing the maximum shear stress in the bend by the averaged approach shear stress. In order to ensure that the normalization value is unambiguous, it was decided that the average shear stress should be calculated based on uniform upstream flow conditions given by:

$$\tau_o = \gamma \times R \times S_f, \tag{5.6}$$

where τ_o = averaged shear stress (Pa), γ = specific weight (kg/m^3), R = hydraulic radius (m), and S_f = friction slope. The hydraulic radius was calculated using the normal (uniform) depth for each simulation scenario. It was assumed that the flow is steady and uniform so that the bed slope can be used to calculate τ_o. The summary of the averaged shear stresses for all 15 scenarios are presented in Table 5.4. The corresponding K_b values are presented in Table 5.5.

Table 5.4 Summary of τ_o values from normal depth

	Normal Depth (m)	R (from normal depth (m))	S_o	$\tau_o = \gamma R S_o$ (Pa)
Scenario 1	0.126	0.093	0.00064	0.58
Scenario 2	0.126	0.093	0.00064	0.58
Scenario 3	0.126	0.093	0.00064	0.58
Scenario 4	0.126	0.093	0.00064	0.58
Scenario 5	0.119	0.088	0.00080	0.69
Scenario 6	0.119	0.088	0.00080	0.69
Scenario 7	0.119	0.088	0.00080	0.69
Scenario 8	0.119	0.088	0.00080	0.69
Scenario 9	0.113	0.085	0.00096	0.80
Scenario 10	0.113	0.085	0.00096	0.80
Scenario 11	0.113	0.085	0.00096	0.80
Scenario 12	0.113	0.085	0.00096	0.80
Scenario 13	0.113	0.085	0.00096	0.80
Scenario 14	0.113	0.085	0.00096	0.80
Scenario 15	0.077	0.062	0.00096	0.58

Table 5.5 Summary of K_b values from numerical simulations

	Maximum bend angle (degrees)	Rc/T_w	Maximum shear stress (Pa)	τ_o (Pa)	K_b value (dimensionless)
Scenario 1	60	1.50	0.74	0.58	1.26
Scenario 2	90	1.27	0.75	0.58	1.30
Scenario 3	120	1.28	0.93	0.58	1.60
Scenario 4	160	1.28	0.79	0.58	1.37
Scenario 5	60	1.42	1.26	0.69	1.82
Scenario 6	90	1.45	1.45	0.69	2.09
Scenario 7	120	1.44	1.42	0.69	2.05
Scenario 8	160	1.44	1.44	0.69	2.08
Scenario 9	60	1.45	1.43	0.80	1.79
Scenario 10	90	1.53	1.56	0.80	1.96
Scenario 11	120	1.47	1.64	0.80	2.06
Scenario 12	160	1.46	1.59	0.80	1.99
Scenario 13	160	2.89	1.04	0.80	1.30
Scenario 14	160	5.82	1.06	0.80	1.33
Scenario 15	160	1.68	0.91	0.58	1.57

Figure 5.7 shows the plot of K_b versus R_c/T_w, where results from previous experiments are also included. Figure 5.7 shows that the range of R_c/T_w values for scenarios 1-12 were somewhat narrow (from 1.27 to 1.53) due to the use of a constant radius of curvature (1.52 m (5 ft)). However, the range of K_b values obtained from the numerical simulations was relatively high with a minimum value of 1.26 and a maximum value of 2.09. Scenarios 13 and 14 use larger radii of curvatures (10 and 20 ft, respectively). It is interesting to note that the K_b values obtained from Scenario 13 and 14 with the higher values of R_c/T_w = 2.89 and 5.82 were 1.30 and 1.33. These values are very close to the K_b values obtained for lower values of R_c/T_w. Based off of these findings, It is clear that the shear stress in the bend may correlate/depend on more than one pertinent parameter.

Figure 5.8 (a) shows the contour plots of shear stress for Scenario 12, 13 and 14, respectively. It is evident from these plots that the location of the maximum shear stress shifts from the inner (convex) bank to the outer (concave) bank of the channel bend as R_c/T_w increases, as previously discussed. Figure 5.8 (b) shows the profiles of the shear stress at cross-section (7) (see Figure 4.4) which was used to obtain the K_b values. The profiles provide a quantitative indication of the shift in the location of the peak shear stress from the inner to outer bank as the radius of curvature increases. It also shows that the magnitude drops significantly as the radius of curvature increases, as one would intuitively expect.

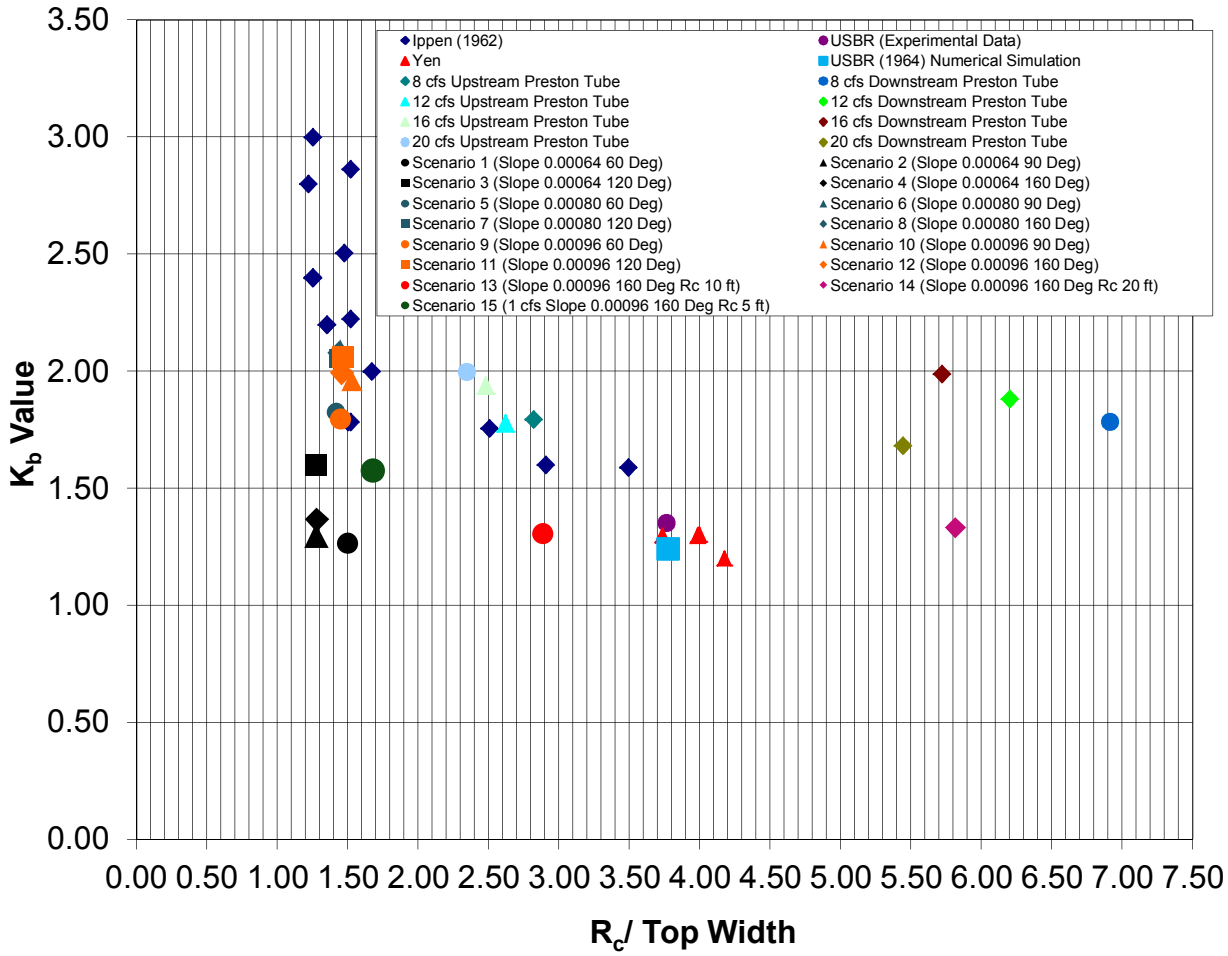

Figure 5.7 Plot of K_b versus R_c/T_w using experimental data and numerical simulations.

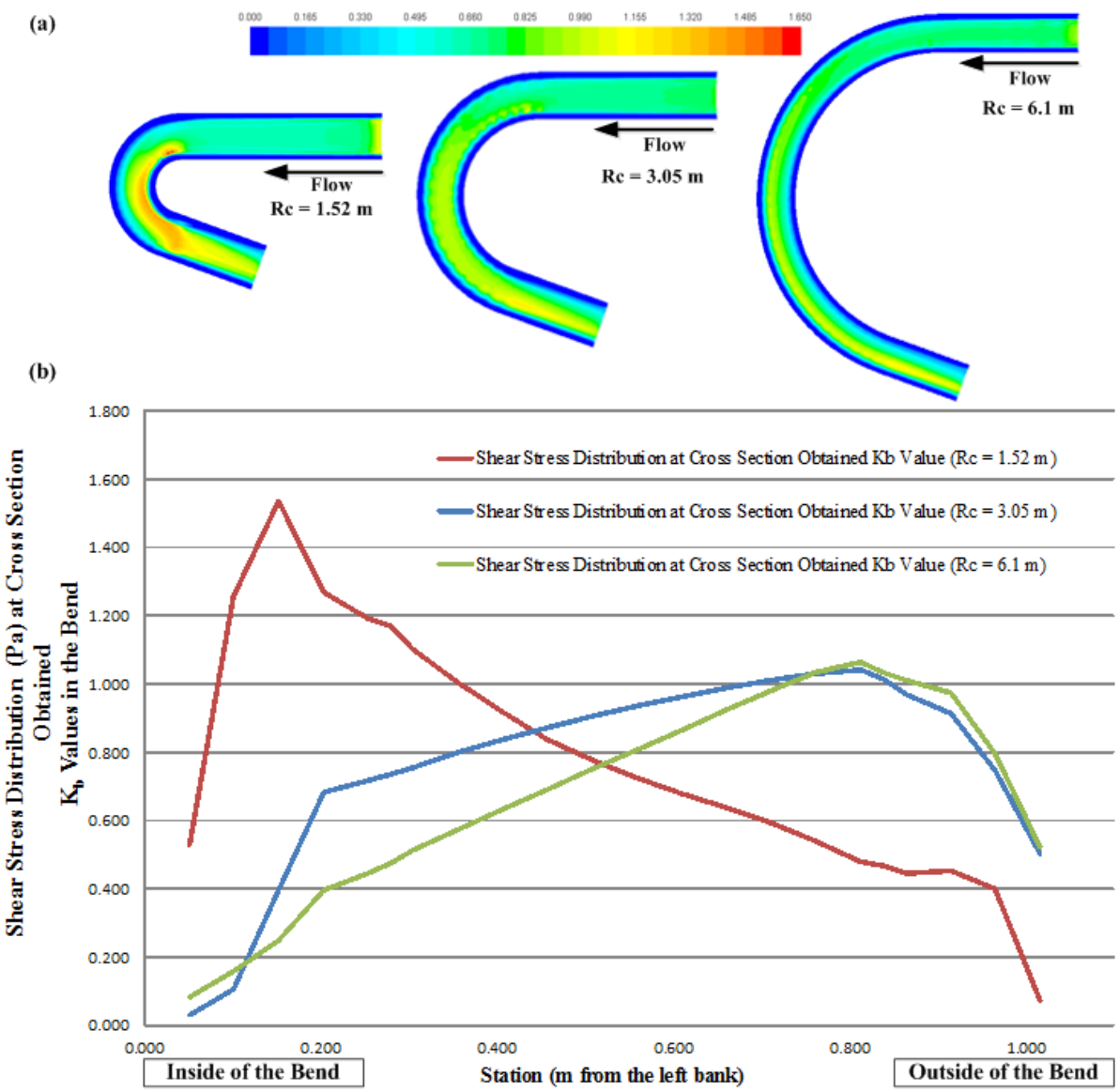

Figure 5.8 (a) Contour plot of shear stress (Pa) from numerical simulation for scenarios 12, 13 and 14; (b) Shear (Pa) distribution at cross section (7) for scenarios 12, 13 and 14 from where the K_b values were computed.

5.6 Shear Stress as a function of L_c/R_c and Froude number

Langbein and Leopold (1966) used a sine function to define the degree of channel meandering that was related to the direction angle and the distance along the channel meander. Based on this motivating concept, the shear stress might be better correlated with the ratio of the arc length of the curve of the channel and the radius of curvature of the bend given by L_c/R_c. Figure 5.9 shows a plot of K_b as a function of L_c/R_c. The plot also includes the K_b value from the simulation of USBR (1964) case that is located at bottom left (blue circle). The corresponding Froude numbers are shown in color with magnitudes indicated by the color bar. The K_b values from Scenario 13, Scenario 14, and Scenario 15 are plotted as with a triangular shape (▼), a rectangular shape (■), and other triangular shape (▲) respectively.

Two things are immediately evident from Figure 5.9. First, it is clear that K_b increases as a function of L_c/R_c and reaches an asymptotic limit as $L_c/R_c \approx \pi/2$, for $R_c/T_w < 2$, especially for the higher Froude cases. Second, the Froude number causes the values to depart for any given value of L_c/R_c. It can be seen that the differences in the K_b values are significant between the low and high Froude simulations. These results show that L_c/R_c may be a better descriptor of the variation of the maximum shear stress in a bend compared to R_c/T_w. These observations are consistent with the findings discussed in Chapter 4 where it was shown that the free surface effects were controlled by both Froude number and the maximum bend angle of the curved channel.

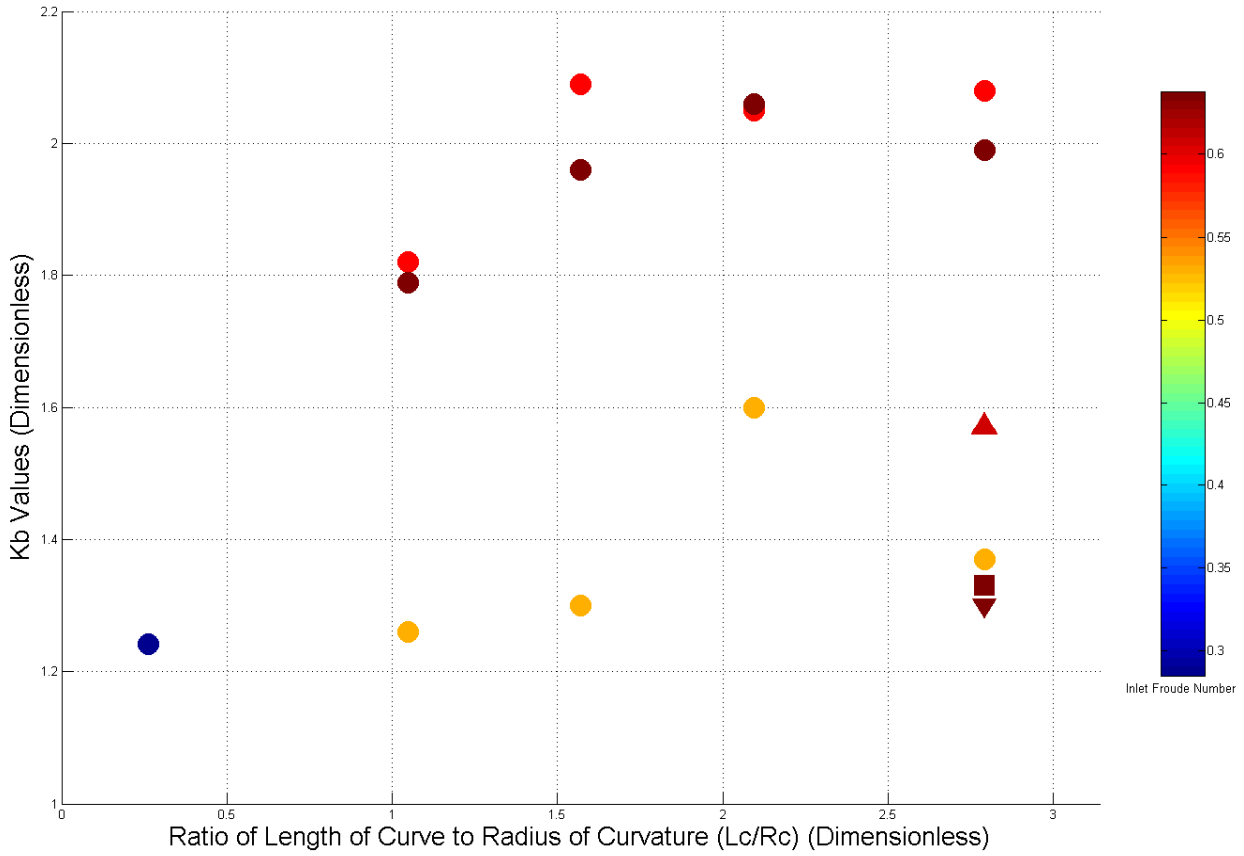

Figure 5.9 The distribution of K_b versus L_c/R_c.

5.7 Summary and Conclusions of Chapter 5

This study investigated two different approaches for possibly parameterizing the shear stress in curved channels. The first approach was the conventional approach where K_b is parameterized in terms of R_c/T_w. This approach is based on the argument from previous research by others that R_c/T_w is directly related with the degree of bank erosion. The new approach that was proposed in this study is to parameterize the shear stress in curved channels as a function of the ratio of the arc length of the curve to the radius of curvature L_c/R_c. This approach was motivated by the theory put forth by Langbein and Leopold (1966). The following main conclusions can be drawn:

- The conventional approach for parameterizing K_b using R_c/T_w appears to be limited because the distributions in the K_b values exhibit significant scatter for small changes in R_c/T_w.
- The numerical simulation results highlight that the R_c/T_w value controls the location of the maximum shear stress in the bend and the L_c/R_c value controls the magnitude of the maximum shear stress in the bend, especially for sharp bends with $R_c/T_w < 2$.
- The new approach shows that it might be promising to parameterize K_b in terms L_c/R_c or alternately a combination of the parameters L_c/T_w and R_c/T_w and the upstream Froude number of the flow.

Chapter 6. Conclusions and Recommendations

6.1 Overview

The focus of this dissertation was on flow around curved channel bends with an emphasis on the use of three-dimensional numerical simulations to provide insights on the flow dynamics in channel bends. The study aimed to provide some guidelines on two main questions namely: 1) when is it appropriate to use the rigid lid assumption for modeling flow around bends?; and 2) what is (are) the most relevant parameters for quantifying the enhanced shear stress in channel bends that can be practically useful? A computational fluid dynamics framework was developed using the Ansys Fluent code and validated using experimental flume data. Following the validation study, a total of 26 simulations were performed and the results analyzed in an attempt to answer the two main questions. The key results of this dissertation are presented in Chapter 3, 4, and 5 respectively. In what follows, the main conclusions and recommendations for the further research are presented.

6.2 Main Conclusions

The following is a brief outline of the key results obtained from this study:

- A validation was conducted using the dataset of Ippen et al. (1962b). The validation results showed that the numerical simulation results were in agreement with the experimental data for flow velocity and water surface elevation. The numerical model also successfully reproduced the secondary flow that is one of the most representative phenomena in curved channel flows. The comparison of the water surface elevations

were within 3% while the maximum percentage error for the shear stress was less than 17%.

- The results parametric study presented in Chapter 4 showed that for sharp bends, when $L_c/R_c < \pi/2$, the errors between the free surface model and the rigid lid model are simply dependent on the Froude number (i.e. increases with Fr). When $L_c/R_c \geq \pi/2$, the parametric studies results show that the curvature effects begin to dominate the dynamics and the error dramatically increases regardless of the value of the Froude number. The results from this study calls for caution to be used when using the rigid lid assumption and a good rule of thumb (guideline) is not to use this assumption for simulating flows when $L_c/R_c \geq \pi/2$, especially for bends with $R_c/T_w < 2$.
- The conventional approach for parameterizing K_b using R_c/T_w appears to have limitation because the distributions in the K_b values exhibit significant scatter for small changes in R_c/T_w i.e. for flow around strongly curved bends.
- The new approach proposed in this research shows that it might be promising to parameterize K_b in terms L_c/R_c (or a combination of L_c/T_w and R_c/T_w) and the upstream Froude number of the flow.
- It is also found that R_c/T_w dictates the location of the maximum shear stresses in the bend as it governs the while L_c/R_c controls the magnitude of the maximum shear stresses as it is directly related to the change in momentum flux along the bend.

6.3 Limitations and Recommendations for Further Research

The main limitation of the work presented in this dissertation revolves around the parameter(s) and associated ranges explores. The emphasis of this study has been mainly on sharp curved bends ($R_c/T_w < 2$). However, the analysis can be readily extended to curved bends with $R_c/T_w > 2$ with

some further work. It is envisaged that such an analysis will lead to a framework for parameterizing K_b in a comprehensive manner that would be useful for practical design guidelines.

The following recommendations will help to further the work presented in this dissertation and lead to practical design guidelines.

- More carefully designed experimental studies are required to supplement available datasets with more refined measurements using the latest instrumentation for measurement of flow variables such as velocity and shear stress.
- The new parameter L_c/R_c proposed in this dissertation for parameterizing shear stress in curved channels showed a more consistent behavior than the conventional parameter (R_c/T_w). In order to be practically relevant, a broader parameter range is required and as such, more numerical simulations are necessary. More importantly, it is necessary to carefully separate the radius of curvature effect which tend to influence the location/distribution of the maximum shear stresses from the change in momentum flux effects which is primarily dictated by the bend angle for a given radius i.e. the length of the bend.
- It is necessary to investigate the back-water effects in subcritical meandering open channel flow. The numerical simulation results indicate that back-water effects are important. It is recommended that a detailed study be conducted to ascertain the minimum length of the upstream straight channel that is required for the flow to be free from the three-dimensional backwater effects of curved channel and hence be at uniform flow conditions.

- This research was limited to investigations of the flow physics in prismatic curved channels with constant bed roughness. In order to develop more comprehensive practical design guidelines, it is necessary to perform numerical simulations for natural meandering channels with varying degrees of roughness and flow conditions.

References

Ansys, Inc . (2009) Ansys Meshing Application Introduction.

Ansys, Inc (2012a) Ansys Fluent 14.5 Theory Guide.

Ansys, Inc (2012b) Ansys Fluent 14.5 User's Guide.

Bathurst, J.C. and Throne, C.R. (1978) Secondary Flow and Shear Stress at River Bends. *ASCE Journal of the Hydraulics Division*, December, 1277-93.

Begin Z. B. (1981) "Stream curvature and bank erosion: a model based on the momentum equation *The Journal of Geology*, Vol. 89, No 4 (Jul., 1981), pp. 497-504

Blanckaert, K., Graf, W. H. (2004) "Mean Flow and Turbulence in Open-Channel Bend". *ASCE Journal of the Hydraulics Engineering*, October, 835-847.

Blanckaert, K., Schnauder, I., Sukhodolov, A., van Balen, and W., Uijttewaal, W.S.J. "Meandering: field experiments, laboratory experiments and numerical modeling" Presented at: River, Costal and Estuarine Morphodynamics (RCEM), Santa Fe, Argentina, September 21-25, 2009.

Booij, R. (2003) "Modeling the Flow in Curved Tidal Channels and Rivers". International Conference on Estuaries and Coasts November 9-11, 2003, Hangzhou, China.

Demuren and Rodi (1986) "Calculation of flow and pollutant dispersion in meandering channels". Journal of Fluid Mechanics, 172, 63-92.

Detrich, W. E., and Smith, J. D. (1983) "Influence of point bar on flow through curved channels". *Water Resources Res*., 19(5), 1173-1192.

DeVriend, H, J. (1976) "A mathematical model of steady flow in curved shallow channels". Part Ⅰ" Report No, 76-1, Dept of Civ. Engineering, Delft University of Technology.

DeVriend, H, J. (1977) "A mathematical model of steady flow in curved shallow channel." *J. Hydr.Res.,* Delft, The Netherlands. 15(1), 37-54.

Federal Highway Administration (FHWA) (2001). River Engineering for Highway Encroachments. Report No. FHWA NHI 01-004 HDS 6.

Heintz, M.L. (2002). Investigation of Bendway Weir Spacing. M.S. Thesis, Colorado State University, Department of Civil Engineering, Fort Collins, CO.

Hickin, E. j. (1974) "The development of meanders in natural river-channels." *Am, Jour. Sci*., v. 274, p.414-442.

Hickin, E. j. and Nanson, G. L. (1975) "The character of channel migration on the Beatton River, Northeast British Columbia, Canada." *Geology Soc*iety of *American Bulletin.*, v. 86, p.487-494.

Hodskinson, A., Ferguson R. I. (1998) "Numerical modeling of separated flow in river bends: Model testing and experimental investigation of geometric controls on the extent of flow separation at the concave bank" *Hydrol. Process*. 12, 1323-1338(1998).

Ippen, A.T., Drinker, P.A., Jobin, W.R and Shemdin, O.H (1962a) "Stream Dynamics and Boundary Shear Distributions for Curved Trapezoidal Channels" *Report No 47.* Massachusetts Institute of Technology January, 1962

Ippen, A.T., Drinker, P.A., Jobin, W.R and Noutsopoulos, G.K (1962b) "The Distribution of Boundary Shear Stresses in Curved Trapezoidal Channels" *Basic Data Supplement to Technical Report No 43.* Massachusetts Institute of Technology October, 1960

Ippen, A.T., and Drinker, P.A. (1962c) "Boundary Shear Stresses in Curved Trapezoidal Channels" *J. Hydr Div*.., ASCE, HY5 143-179.

Jin, Y., Steffler, P. (1993) "Predicting flow in curved open channels by depth-Averaged method". *ASCE Journal of the Hydraulics Engineering*, January, 109-124.

Julien, P.Y. (2002). River Mechanics. Cambridge University Press, New York, NY.

Khosronejad, A., Rennie, C.D., Salehi Neyshabouri, S.A.A., Townsend, R.D. (2007) "3D Numerical Modeling of Flow and Sediment Transport in Laboratory Channel Bends". *ASCE Journal of the Hydraulics Engineering*, December, 1123-1134.

Kilgore, R.T. and Cotton, G.K. (2005). "Design of Roadside Channels with Flexible Linings." *Hydraulic Engineering Circular*-15, Federal Highway Administration, 3rd ed., September.

Knighton, D.A. (1998). Fluvial Forms and Processes. Oxford Press, (Published under license from Arnold Publishing, London), New York, NY.

Lane, E., 1955. Design of Stable Channels. Transactions ASCE, Vol. 120.

Langbein, W.B., and Leopold, L. B (1966), "River meanders – theory of minimum variance". *Geological Survey Professional Paper 422-H,* United States Government Printing Office, Washington.

Lam, S.H (1992), "On the RNG Theory of Turbulence". Physics of Fluids A, 4 , pp. 1007-1017, May 1992

Leopold, L. B., and Wolman, M. G., (1960) "River meanders" *Geology Society America Bulletin.*, vol. 71, p.769-794.

Lien, H.C., Hsieh, T.Y., and Yang, J. C. (1999) "Bend-flow simulation using 2D depth-averaged model". *ASCE Journal of the Hydraulics Engineering*, October, 1097-1109.

Moody, L. F. "Friction Factors for Pipe Flow," *ASME Trans*., vol. 66, pp. 671-684, 1944.

Nouh, M.A. and R.D Townsend (1979). Shear Stress Distribution in Stable Channel Bends. *J. of the Hydraulic Division*, ASCE, Vol. 105, No. HY 10, Proc. Paper 14598, October, pp. 1233-1245.

Odgaard, A.J (1986) "Meander Flow Model. Ⅰ: Development". *ASCE Journal of the Hydraulics Engineering*, December, 1117-1134.

Odgaard, A.J (1986) "Meander Flow Model. Ⅱ: Applications". *ASCE Journal of the Hydraulics Engineering*, December, 1137-1149.

Onish, Y. (1972). "Effects of meandering of sediment discharges and friction factors of alluvial streams." Ph.D. thesis, University of Iowa, Iowa City, IA,USA

Onish, Y., Jain, S.C., and Kenndy, J.F. (1976). "Effects of meandering in alluvial streams." *J.Hydr.Di.,*102 (7), 899-917

Patankar, S. V. and Spalding, D.B (1972). "A Calculation Procedure for Heat, Mass and Momentum Transfer in Three-dimensional Parabolic Flows, *Int.J. Heat Mass Transfer,* Vol. 15, p. 1787.

Pope, S.B (2000). "Turbulent Flows". Cambridge University Press.

Preston, J. H. (1954) "The Determination of Turbulent Skin Friction by Means of Pitot Tubes." *Journal of the Toyal Aeronautical Society*, Vol. 58: 109-121.

Rameshwaran, P. and Naden, P.S. (2004) "Three-dimensional modeling of free surface variation in a meandering channel." Journal of Hydraulic Research, 42:6, 603-615

Rozovskii, I.L. (1961). Flow of Water in Bends of Open Channels. Academy of Sciences of the Ukrainian SSR

Sclafani, P. (2008) "Preston Tube Calibration" Open File Report Colorado State University Engineering Research Center Fort Collins, Colorado.

Sin, K. (2010). Methodology for calculating shear stress in a meandering channel. M.S. Thesis, Colorado State University, Department of Civil Engineering, Fort Collins, CO.

Son, A., Ryu, J., and Han, K. (2011) "A study of Flow Characteristics in Meandering River" *Korean Society of Hazard Mitigation (KOSHAM) Journal of Hazard Mitigation* 11:3 191-200

Steffler, P.M. (1984). "Turbulent flow in a curved rectangular channel," PhD thesis, University of Alberta, Alberta, Canada.

Sturm, T.W. (2009). Open Channel Hydraulics. (Second Edition) McGraw-Hill.

Thorne, C. R., Rais, S., Zevenbergen, L. W., Bradley, J.B., and Julien, P.Y. (1983.) "Measurements of bend flow hydraulics on the Fall River at low stage." WRFSL Report No. 83-9P, Nat. Park Serv., 107C Natural Services, Colorado State University, Fort Collins, Colorado

Thornton, C.I., Sin, K.S., Sclafani, P. and Abt, S.R. "Boundary Shear Stress Along Rigid Trapezoidal Bends (2012)". Project Report prepared for U. S. Bureau of Reclamation (USBR). Colorado State University Engineering Research Center Fort Collins, Colorado.

U. S. Bureau of Reclamation (USBR) (1964). Boundary Shear Distribution Around a Curve in a Laboratory Canal. *Progress Report I, Report No. Hyd-526,* Denver, Colorado, June.

van Balen, W., Uijttewaal, W.S.J., and Blanckaert, K. (2009a). "Large-eddy simulations mildly curved open-channel flow". Journal of Fluid Mechanics, 630, 413-442.

van Balen, W., Blanckaert, K., Uijttewaal, W.S.J (2009). "Large-eddy simulations and experiments of single-bend open-channel flow at different water depths". Journal of Turbulence (submitted for publication).

van Balen, W. (2010). "Curved open-channel flows, A numerical Study". PhD thesis, Delft University of Technology, Delft, Netherlands.

Versteeg, H.K and Malalasekera, W. (2007) An Introduction to Computational Fluid Dynamics The Finite Volume Method. Pearson, UK.

Von Schelling, Hermann (1951). Most frequent particle paths in a plane. *Am. Geophys, Union Trans.,* v.32, p.222-226

Von Schelling, Hermann (1964). Most frequent random works. *Gen. Elec. CO. Rept. 64GL92*, Schenectady, N.Y

Watson, C.C., Biedenharn, D.S., Thorne, C.R. (2005). Stream Rehabilitation. Cottonwood Research, Fort Collins, CO USA.

Wilson, C.A.M.E., Boxall, J. B., Guymer, I., Olsen, N.R.B. (2003) "Validation of a Three-Dimensional Numerical Code in the Simulation of Pseudo-Natural Meandering Flows" *ASCE Journal of the Hydraulics Engineering*, October, 758-768.

Yen, Ben Chie (1965). "Characteristics of a subcritical flow in a meandering channel". Institute of Hydraulic Research, University of Iowa, Iowa City

Young, G.K., et al., (1996). HYDRAIN – Integrated Drainage Design Computer System: Version 6.0 – Volume VI: HYCHL, FHWA-SA-96-064, June.

Zeng, J., Constantinescu, G. and Weber, L. (2010) "3D Calculations of Equilibrium Conditions in Loose-Bed Open Channels with Significant Suspended Sediment Load" *ASCE Journal of the Hydraulics Engineering*, September, 557-571.